STRUCTURAL SYSTEMS

RESEARCH PROJECT

Report No.
SSRP – 2002/09

ELECTRICAL SUBSTATION EQUIPMENT INTERACTION – EXPERIMENTAL FLEXIBLE CONDUCTOR STUDIES

by

André Filiatrault

Christopher Stearns

Final Report to the Pacific Earthquake Engineering Research Center (PEER) for Task 403 of the PEER Lifeline Directed Studies Program

February 2003

Department of Structural Engineering
University of California, San Diego
La Jolla, California 92093-0085

University of California, San Diego
Department of Structural Engineering
Structural Systems Research Project

Report No. SSRP-2002/09

ELECTRICAL SUBSTATION EQUIPMENT INTERACTION – EXPERIMENTAL FLEXIBLE CONDUCTOR STUDIES

by

André Filiatrault
Professor of Structural Engineering

Christopher Stearns
Undergraduate Student Researcher

Department of Structural Engineering
University of California, San Diego
La Jolla, California 92093-0085

February 2003

DISCLAIMER

Opinions, findings, conclusions and recommendations expressed in this report are those of the authors and do not necessarily reflect views of the Pacific Earthquake Engineering Research Center (PEER).

ACKNOWLEDGEMENTS

This project was sponsored by the Pacific Earthquake Engineering Research Center's Program of Applied Earthquake Engineering Research of Lifeline Systems supported by the California Energy Commission, California Department of Transportation, and the Pacific Gas & Electric Company.

This work made use of Earthquake Engineering Research Centers Shared Facilities supported by the National Science Foundation under Award Number EEC-9701568.

We greatly appreciated the input and coordination provided by Dr. Michael Riemer from PEER and Mr. Eric Fujisaki from the Pacific Gas and Electric Company (PG&E) during the development of this research project. The supports of Mr. David Chambers from the California Energy Commission and of Mr. Craig Riker from the San Diego Gas and Electric Company (SDG&E) are also gratefully acknowledged.

Mr. Jean Bernard Dastous from Hydro Quebec and Mr. Rulon Fronk from Fronk Consulting are also gratefully acknowledged for sharing qualification test data with the authors. Finally, the authors extend their sincere appreciation to Mr. Howard Matt, Graduate Student Researcher at UC-San Diego, for his assistance in conducting the shake table tests.

LIST OF SYMBOLS

a	Mode shape constant related to beam properties
a_c	Horizontal acceleration measured at top of an equipment item
a_u	Horizontal acceleration measured at top of equipment during uncoupled seismic test
A_i	Mode shape constants to be determined from boundary conditions
$\left(A^{(1)}\right)$	Fundamental mode shape of equipment item
C_1, C_2, C_3	Constants used in solution of Bernoulli-Euler beam
CF	Correction factor for first modal participation factor of interconnected equipment
d_c	Diameter of a conductor
$d_{i,i+1}$	Distance between adjacent inclinometers i and i+1
d_{si}	Diameter of i^{th} strand in conductor
EI_{ec}	Effective flexural stiffness of conductor
$EI_{\max}$	Maximum possible flexural stiffness of conductor
$EI_{\min}$	Minimum possible flexural stiffness of conductor
f_1	Fundamental frequency of equipment item
F_c	Force measured by load cell at top of equipment item during a coupled seismic test
F_{nh}	Net horizontal force developed during a coupled seismic test
F_u	Force measured by load cell at top of an equipment item during an uncoupled seismic test
g	Acceleration of gravity
F	Concentrated lateral force on a conductor
L	Loaded span of conductor
l	Length of beam
l_c	Total length of Conductor
l_{ch}	Chord length of conductor

$\overline{m}(y)$	Mass per unit length of beam
m_{lc}	Equivalent load cell mass
m_t	Lumped mass at the top of beam
$[m]$	Mass matrix for equipment item
M	Total mass of beam
M_1^*	First modal mass
N_l	Number of strand layers in conductor
N_s	Total number of strands in conductor
R^2	Coefficient of correlation
$S_d(f_1,\xi_1)$	Spectral displacement values of base excitation at fundamental frequency and modal damping ratio ξ_1 of equipment item
s	Slackness of flexible conductor
T	Axial tension in conductor
v	Lateral displacement of conductor
V	Voltage of equipment item
W	Total seismic weight of equipment item
W_1	First modal weight of equipment item
x	Position along a conductor
y	Coordinate along beam span
y_0	Coordinates of attachment point of a conductor
y_{si}	Distance from centroid of the i^{th} strand in conductor to the centroid of the conductor
α	F/T
α_1	First modal participation factor of equipment item
δ	Displacement in ATC-24 loading protocol
δ_y	Yield Displacement in ATC-24 loading protocol
Δ_{max}	Maximum displacement amplitude of equipment item
λ	$\sqrt{T/EI}$

$\ddot{o}_i$	Curvature between two adjacent inclinometers i and i+1
μ	Displacement ductility factor in ATC-24 loading protocol
$\phi(y)$	Mode shape of beam with lumped mass at its top
$\square(y_0)$	Value of the fundamental mode shape of conductor at the attachment point y_0
$\dot{e}_i$	Slope measured by inclinometer i and i+1
$\dot{e}_{i+1}$	Slope measured by inclinometer i and i+1
ζ_1	First modal damping ratio of equipment item

TABLE OF CONTENTS

INTRODUCTION

Electric power distribution and transmission systems are particularly vulnerable to earthquake loading. In North America, most of these systems were constructed in the 1950s and 1960s, and incorporate several pieces of equipment, such as porcelain bushings or poorly anchored transformers that are particularly vulnerable to earthquake damage. Electrical equipment components are typically designed primarily to meet electrical function requirements as opposed to structural performance requirements. Furthermore, electrical bus conductors are used to interconnect substation equipment components, thereby complicating their structural dynamic response. Both rigid and flexible conductors interconnect electrical substation equipment. Flexible bus ("conductors") exert relatively little force, provided that they remain slack and that their flexural stiffness is negligible. Some utilities have implemented slack requirements in flexible conductors to provide flexibility between interconnected pieces of equipment. During recent earthquakes in California, it is believed that significant structural dynamic interaction and equipment damage due to forces transferred through the conductors occurred.

The 1989 Loma Prieta Earthquake caused major damage to the Metcalf, Moss Landing, and San Mateo substations owned by the Pacific Gas and Electric Company (PG&E). Monte Vista and Newark substations, also owned by PG&E, suffered less severe damage. Live-tank circuit breakers were severely damaged. Transformer radiators developed oil leaks, and had damaged bushings. Current transformers failed or developed oil leaks, air disconnect switches were damaged, and transfer buses were damaged (Benuska, 1990). As a result of the damage to the 500-kV switchyard of the Moss Landing power plant, a complete 750 MW unit of the plant remained inoperative for four days after the earthquake. Damage to the San Mateo substation tripped off a portion of the 115-kV power supply running up the peninsula to San Francisco.

Electric power generating and distributing plants sustained relatively minor damage during the 1994 Northridge Earthquake mainly because of their locations (Hall, 1995). Three facilities suffered architectural damage, with isolated instances of equipment damage. Some substation equipment suffered significant damage too (Hall, 1995).

In response to the vulnerabilities exhibited by substation equipment in recent earthquakes, utilities manufacturers, and others closely related with the industry have developed new seismic qualification procedures that are described in the IEEE 693 standard (Institutes of Electrical and Electronics Engineers, 1997). These procedures, however, only qualitatively address interaction between equipment connected by conductors. This is due to the wide variety and complex behavior of equipment used in substations, manufacturer and utility-specific design characteristics of both the equipment and their support structures, and practical considerations of the qualification procedure. For these reasons, electrical equipment items are, in general, seismically qualified in a "stand-alone" condition (i.e. without connection to the adjacent equipment), and the effects of interaction are typically ignored.

This research project is the continuation of an investigation on substation equipment interaction performed in Phase II of the PEER-PG&E program (Filiatrault et al., 1999, Filiatrault and Kremmidas, 2000). Analytical studies performed in the Phase II program suggested that bending properties of flexible conductors might affect the behavior of short jumpers and some "long" conductors. Very limited dynamic interaction experiments involving equipment models interconnected by flexible conductors have been performed to evaluate the importance of this dynamic interaction effect. Also, no method exists for evaluating the bending properties of flexible conductors that can be used in the dynamic analysis of interconnected equipment.

In this project, quasi-static and shake table testing were performed in order to determine the bending conductor properties as a function of typical conductor parameters (length, size, tension, lay, etc.) and experimentally characterize the seismic response substation equipment interconnected by flexible conductors.

Scope of Research

One of thee main objectives of Task 4 (Substation Equipment) of the Lifeline Program of the Pacific Earthquake Engineering Research Center (PEER) is to develop guidelines for the design of flexible bus (conductor) systems in order to minimize or eliminate the seismic interaction between interconnected substation equipment. These guidelines will be formulated in terms of recommended generic conductor configurations and will be based on the results of experimental

studies conducted in this project and analytical studies conducted in another project at the University of California, Berkeley.

This research project consist of 2 main parts:

Part 1: Definition of dynamic properties of substation equipment items;

Part 2: Experimental studies consisting of quasi-static bending testing of flexible conductors and shake table tests of interconnected generic equipment.

Report Layout

Following an introduction to the project, and scope of the current study in this chapter, **Chapter 2** describes the collection of dynamic properties data from various substation equipment items. **Chapter 3** describes the quasi-static bending tests performed on flexible conductor specimens. **Chapter 4** presents the shake table tests performed on five pairs of generic substation equipment connected by three different flexible conductor assemblies incorporating various slackness values. Finally, the report provides conclusions on the results obtained.

PART 1. DYNAMIC PROPERTIES OF SUBSTATION EQUIPMENT

1.1 Introduction

The first part of this report deals with the definition of Single-Degree-of-Freedom (SDOF) properties to model the dynamic behavior of substation equipment. For this purpose, dynamic properties of various substation equipment items were collected from past investigations and available qualification data from various participating utilities.

1.2 Data Collection Procedure

Dynamic properties data from 283 different substation equipment items have been collected. These data were obtained mainly in partnership with Pacific Gas and Electric Company and Hydro-Quebec that graciously collected and provided a significant amount of seismic qualification data. The list of contributors at the time of writing is given in Table 1.1.

Table 1.1 Contributors of Seismic Qualification Data

Name	Organization	Contact E-mail
Jean-Bernard Dastous	Hydro-Quebec	Dastous.Jean-Bernard@ireq.ca
Rulon Fronk	Fronk Consulting	rulonrf@hotmail.com
Eric Fujisaki	Pacific Gas and Electric Company	EMF1@pge.com
Gregory Fenves	Pacific Earthquake Engineering Research Center (PEER)	fenves@ce.berkeley.edu

The physical parameters collected for each equipment item are: the voltage V, the fundamental frequency f_1, the first modal damping ratio ξ_1, the first modal participation factor α_1, the total seismic weight W, and the first modal weight W_1. The first modal participation factor α_1 of an equipment item can be approximated by assuming that the mode shape component at the point of connection (top of the equipment) is equal to unity (Clough and Penzien, 1993):

$$\alpha_1 = \frac{\Delta_{\max}}{S_d(f_1, \xi_1)} \tag{1.1}$$

where Δ_{max} is the maximum displacement amplitude of the equipment and $S_d(f_1,\xi_1)$ is the spectral displacement values of the base excitation at the fundamental frequency f_1 and modal damping ratio ξ_1 of the equipment.

The first modal weight W_1 of an equipment item can be approximated by:

$$W_1 = M_1^* g = \alpha_1^2 \left(A^{(1)}\right)^T [m] \left(A^{(1)}\right) g \qquad (1.2)$$

where M_1^* is the first modal mass, $\left(A^{(1)}\right)$ is the fundamental mode shape of the equipment item, $[m]$ is the mass matrix for the equipment item, and g is the acceleration of gravity.

1.3 Equipment Categories

Table 2-2 presents the various categories for the 283 substation equipment items data collected at the time of writing.

1.4 Computerized Database

A computerized database has been developed in this project to centralize the dynamic characteristics of substation equipment. This database includes in downloadable Excel format all the data collected for the 283 equipment items. The database is accessible from the Internet at the following website: http://seismic.ucsd.edu/peer/substation.html. As shown in Fig. 1.1, the database contains two search tools: a search by equipment category (see Table 1.1) and a search by voltage range. Also, the database allows the insertion of new equipment items. The complete database containing the 283 equipment items collected at the time of writing is printed in Appendix A.

Table 1.2 Categories and Number of Equipment Items Collected.

Equipment Category	Number of Items
Circuit Breakers	74
Disconnect Switches	55
Voltage Transformers	39
Transformer Bushings	38
Current Transformers	19
Lightning Arresters	12
Circuit Switchers	10
Surge Arresters	9
Switch Poles	9
Capacitors	5
Voltage Dividers	4
Air Core Reactor	3
Switch Gears	2
Bypass Breaker	1
Fault Interrupter	1
Shunt Reactor	1
Shunt Inductance	1
Total	283

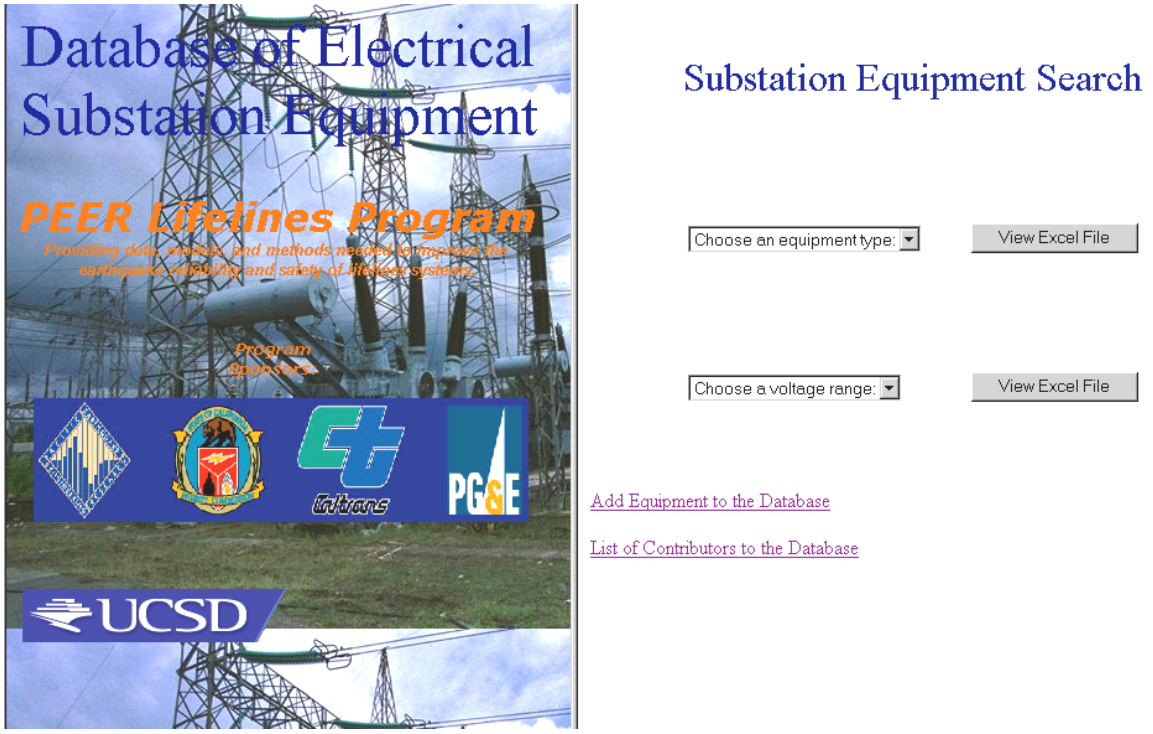

Figure 1.1 Main Page of Substation Equipment Database.

1.5 Correlative Study

Based on the data collected in the database, a preliminary correlative study was performed in order to estimate the relationships between the various dynamic characteristics of substation equipment. The main trends resulting from this study are briefly discussed in this section.

Figure 1.2 presents the semi-logarithmic variations of the fundamental frequency with voltage rating for all equipment categories with voltage from 72 kV to 500 kV (500 kV is the maximum voltage used in California). The range of natural frequencies (under 1 Hz to above 20 Hz) is large. Also, significant scatters in the data can be observed. A least square regression analysis indicates the weak trend (correlation coefficient $R^2 = 0.081$) that the fundamental frequency of substation equipment is reduced as the equipment voltage increases.

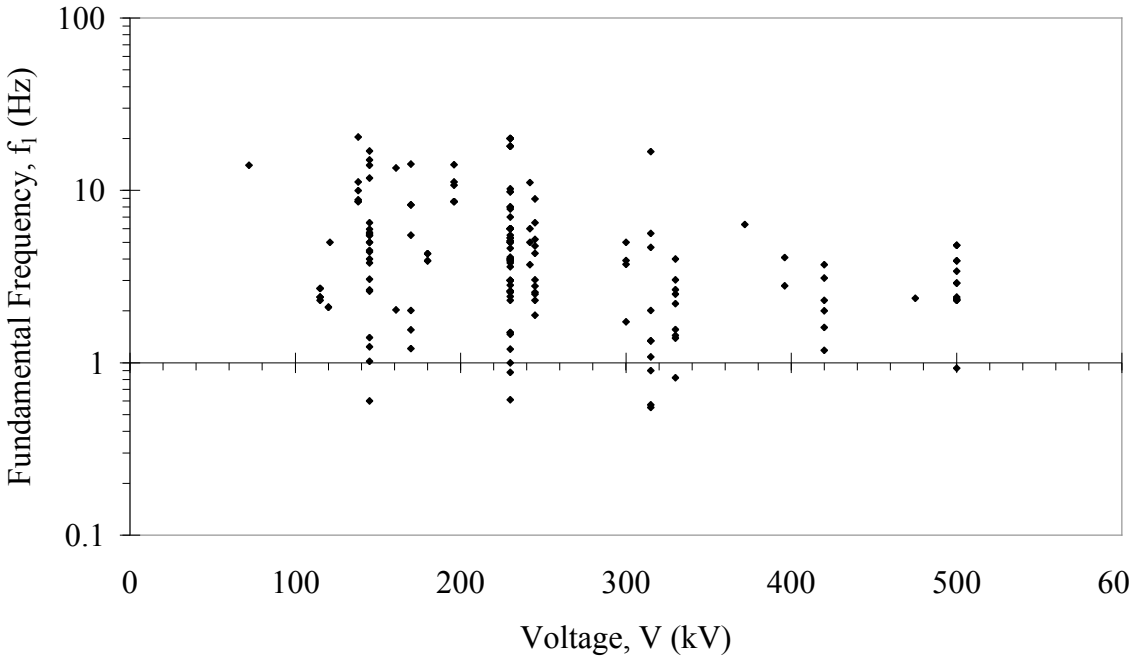

Figure 1.2 Variations of Fundamental Frequency with Voltage, All Equipment Categories with Voltage from 72 kV to 500 kV.

Figure 1.3 presents the semi-logarithmic variations of the fundamental frequency with voltage for each of the four equipment categories containing more than 20 equipment items (see Table 1.1): a) circuit breakers, b) disconnect switches, c) voltage transformers, and d) transformer bushings. All four categories show the same trends: the fundamental frequency equipment is reduced as the equipment voltage increases. Also the correlation coefficients are higher than that in Fig. 1.2 for all equipment categories.

Figure 1.4 compares the resulting least-square regression curves for each of the four most populated equipment categories and for all equipment categories. Although these regression curves were generated from highly scattered data, some trends can still be observed. The lighter transformer bushings exhibit the highest fundamental frequencies for the whole range of voltage. Conversely, the lowest natural frequencies occur for the much heavier circuit breakers.

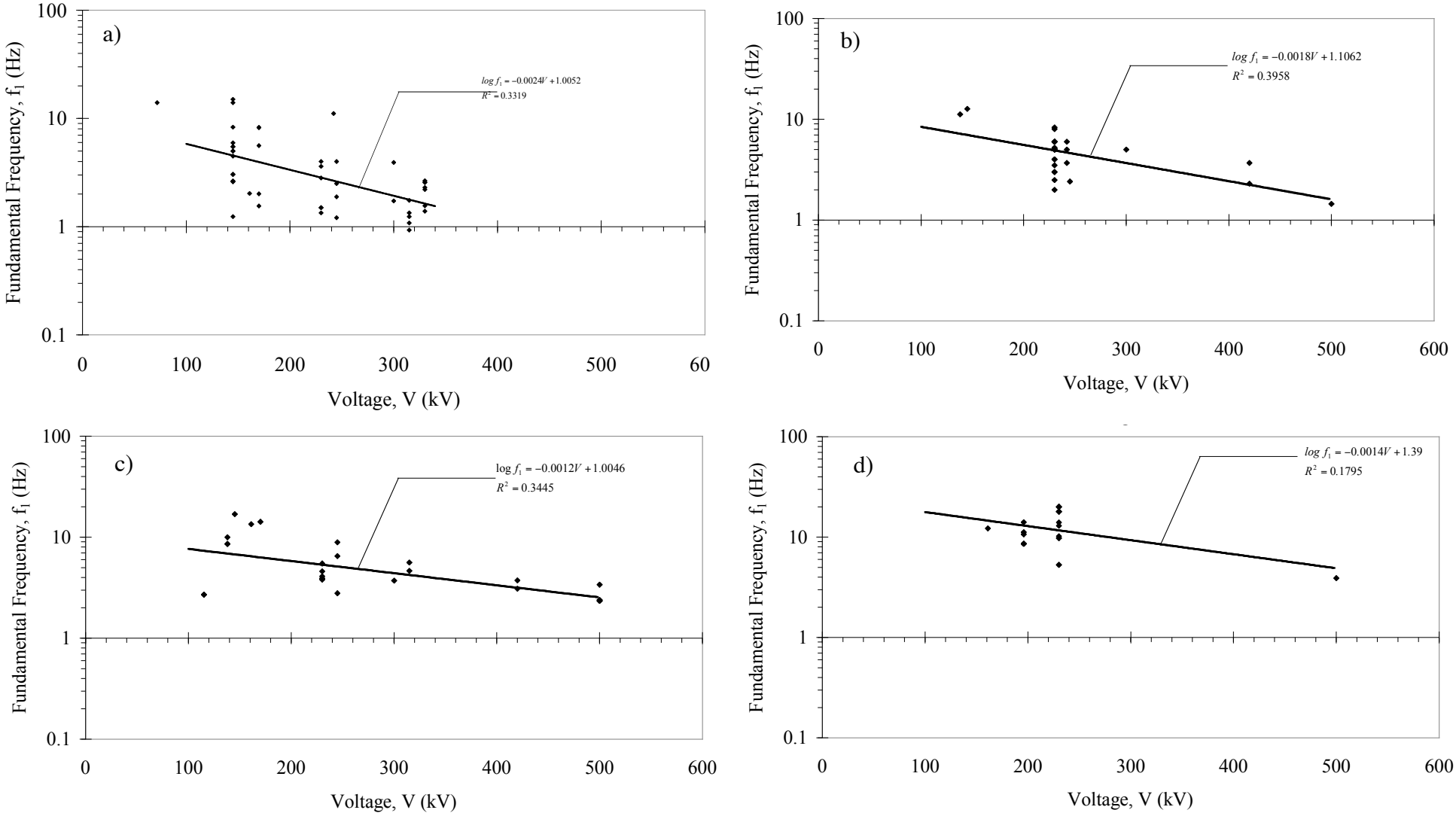

Figure 1.3 Variations of Fundamental Frequency with Voltage: a) Circuit Breakers, b) Disconnect Switches, c) Voltage Transformers, and d) Transformer Bushings.

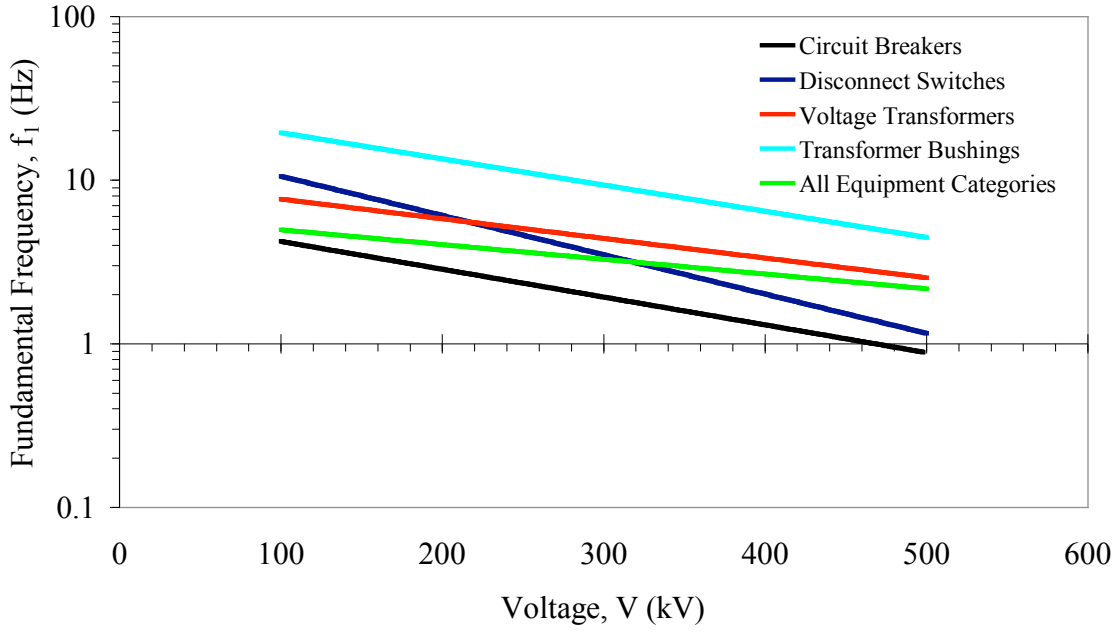

Figure 1.4 Least-Square Semi-logarithmic Regression Curves for each of the Four Most Populated Equipment Categories and for all Equipment Categories.

Figure 1.5 presents the semi-logarithmic variations of the first measured modal damping ratio with voltage for all equipment categories between 115 kV to 500 kV. The first modal damping ratio does not exhibit any correlation with the voltage range. The mean data damping ratio is 3% of critical, which is higher than the 2% value used in seismic qualification testing and analyses (Institutes of Electrical and Electronics Engineers, 1997).

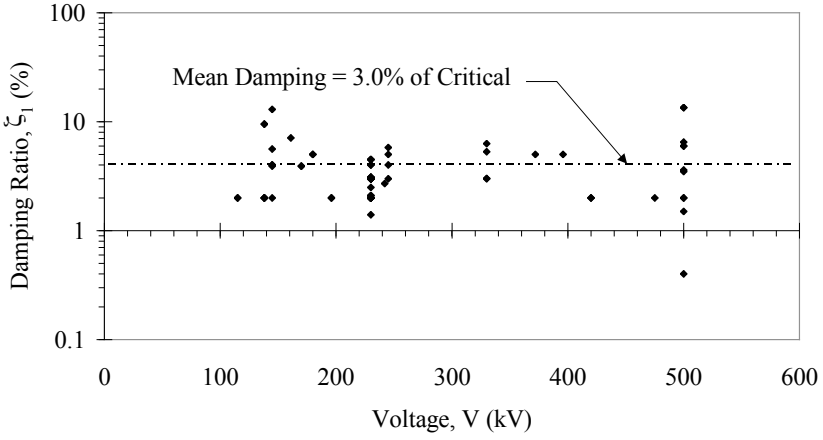

Figure 1.5 Variations of First Modal Damping Ratio with Voltage, All Equipment Categories with Voltage from 115 kV to 500 kV.

Figure 1.6 presents the semi-logarithmic variations of the first modal participation factor with voltage for all equipment categories between 115 kV to 500 kV. Similar to the first modal damping ratio, the first modal participation factor is not correlated with the voltage range. The mean value of the modal correlation factor across the equipment ensemble is 1.3.

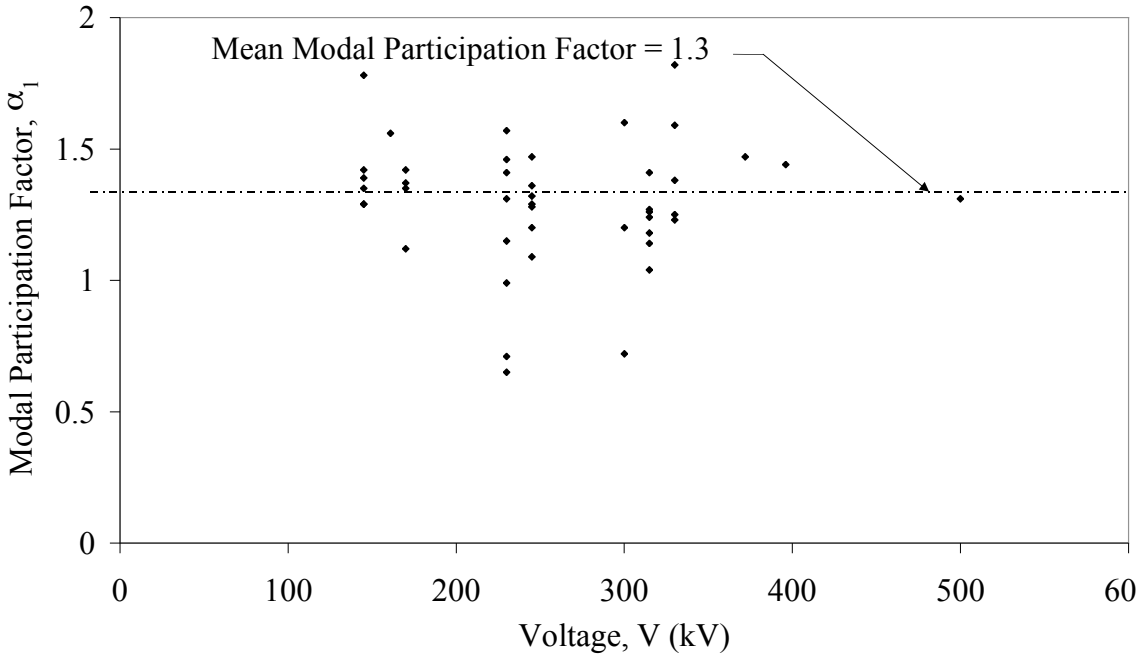

Figure 1.6 Variations of First Modal Participation Factor with Voltage, All Equipment Categories with Voltage from 115 kV to 500 kV.

Note that the correlations obtained in Figs. 1.6 and 1.7 could be stronger if the equipment type were taken separately. However, at the time of writing, the damping and modal participation factor data from the database was insufficient to provide any meaningful correlation per equipment type.

PART 2. EXPERIMENTAL STUDIES

1. QUASI-STATIC BENDING TESTS OF FLEXIBLE CONDUCTORS

This chapter describes the quasi-static bending tests performed on two different full-scale flexible conductors (cables). These tests were performed in the transverse direction of the conductor assemblies under prescribed axial tension and displacement history. The main objectives of the quasi-static tests were to observe the flexural response of flexible conductors and to determine their moment-curvature relationships under various axial tension values.

1.1 Description of Test Specimens

Two different flexible conductor assemblies made of aluminum conductors were supplied by PG&E and were considered for the quasi-static tests. Table 1.1 presents the characteristics of the two conductor specimens.

Table 1.1. Characteristics of Flexible Conductor Specimens.

Designation	Supplier	Construction	Conductor diameter (in)	Strand diameter (in)	Lay angle (degree)	Number of strands
2300 MCM	PG&E	4 aluminum strand layers	1.75	0.194	10	61
MCM 113C	PG&E	4 aluminum strand layers	1.25	0.142	10	61

1.2 Experimental Set-Up for Quasi-Static Tests

The experimental set-up for the quasi-static tests on the flexible conductor assemblies is shown in Fig. 1.1. Four-point transverse cyclic loading tests under constant longitudinal tension were conducted. For this purpose, each flexible conductor specimen was laid out vertically next to a reaction wall. The top of the conductor was hung from a sliding bracket attached to the reaction wall. The connection to this bracket enabled the end of the conductor to freely rotate, and to freely translate in the horizontal direction.

Along a span of 9 ft (L = 9 ft in Fig. 1.1), four simple supports, equally spaced, were installed to create three supported spans on the conductor. The two central supports were

linked to a horizontally loading hydraulic actuator, while the two exterior supports were attached to the reaction wall. The supports were made of pairs of cast iron wheels in order to allow the conductor to translate freely in the vertical direction under combined axial (vertical) tension and transverse (horizontal) loading. Figure 1.2 shows the details of one of these four simple supports.

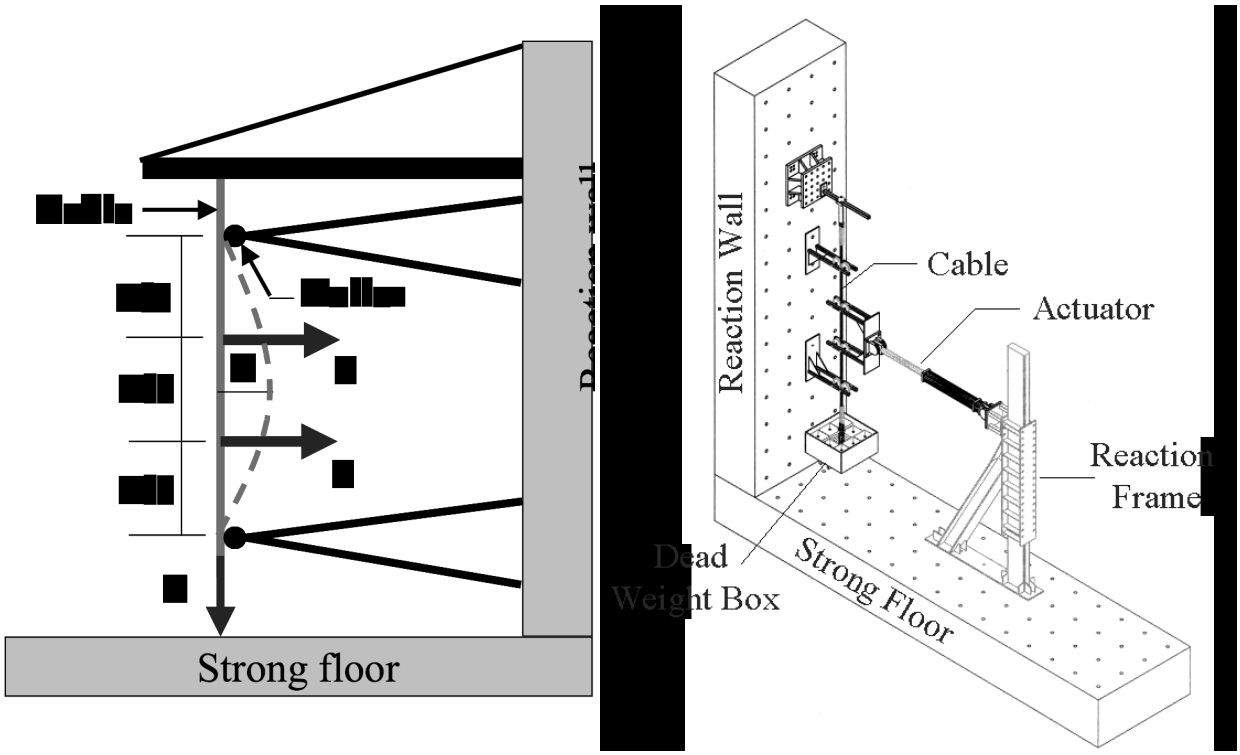

Figure 1.1 Experimental Set-Up for Quasi-Static Tests on Flexible Conductors.

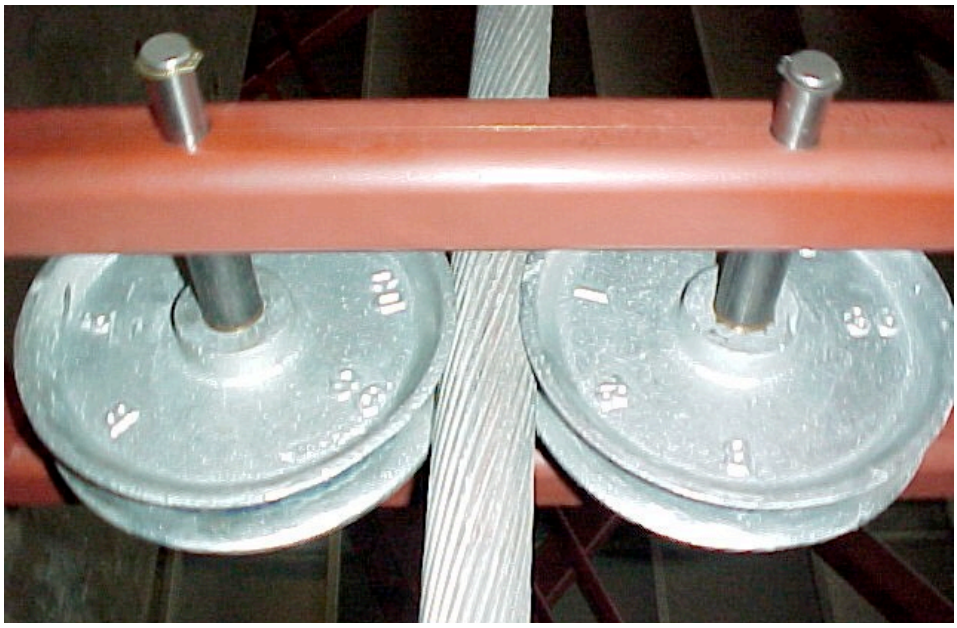

Figure 1.2 Simple Support to Allow Free Vertical Movement of Test Conductor.

At the lower end of the conductor, a dead-weight box was hung to induce a constant axial load in the conductor being tested. The box contained concrete blocks to induce the proper axial tension.

2.3 Instrumentation

Instrumentation required to measure the force-displacement and moment-curvature hysteresis loops in the transverse (horizontal) direction of the flexible conductors was installed. The total lateral force applied to the conductor by the actuator (sum of the force applied by the two central transverse supports) was measured across a load cell that was inserted between the head of the actuator and a steel spreader plate (see Fig 1.1). The bending moment, M, at the center of the conductor can be computed by:

$$M = \frac{FL}{3} - T\Delta \qquad (1.1)$$

where F is the force in each loading support, L is the span of the conductor (9 ft), T is the axial tension in the conductor, and Δ is the lateral deflection at the center of the conductor.

Transverse displacement measurements were taken along 11 different locations along the three supported spans of the conductor by string potentiometers installed between the strong wall and the test conductor, as shown in Fig. 1.3. The exact location of each string potentiometer is included in the CD-ROM accompanying this report.

Curvature was also measured at 18 different locations along the three supported spans of the conductor by inclinometers attached to the surface of the conductor, as shown in Fig. 1.3. The average curvature $\ddot{o}_i$ between two adjacent inclinometers i and i+1 is given by:

$$\ddot{o}_i = \frac{\grave{e}_{i+1} - \grave{e}_i}{d_{i,i+1}} \qquad (1.2)$$

where $\grave{e}_i$ and $\grave{e}_{i+1}$ are the slope measured by inclinometer i and i+1, respectively and $d_{i,i+1}$ is the distance between inclinometers i and i+1.

Each inclinometer was glued to a single surface strand to avoid confining the conductor and slipping between the layers of strands. Figure 1.4 shows a close up of one of the inclinometer installed on one of the conductor specimen.

Finally, the axial load in the conductor was obtained by weighing the dead-weight box filled with concrete and the conductor itself before the test. The axial load at a given section of the conductor was given by the dead weight plus the weight of the conductor below the section considered.

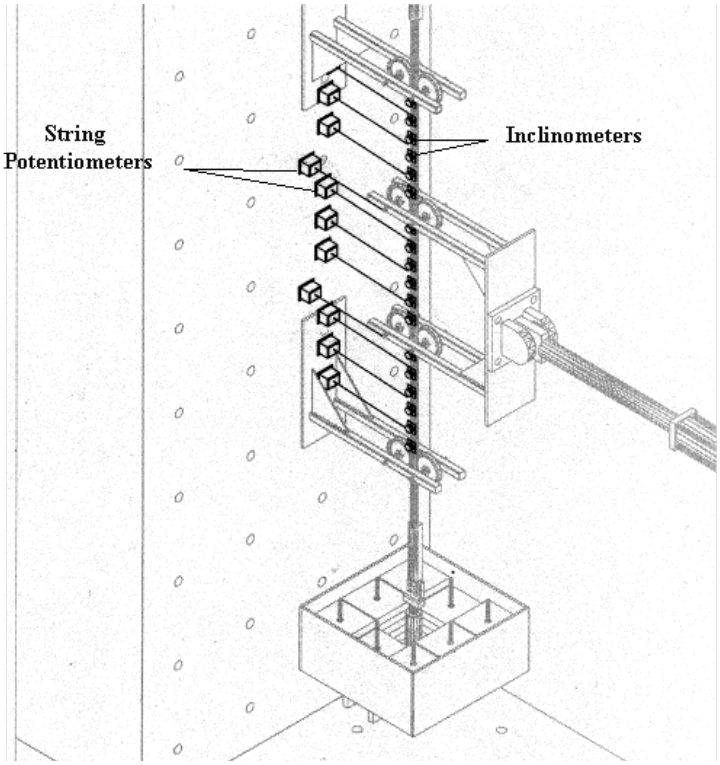

Figure 1.3 Instrumentation for Quasi-Static Tests on Flexible Conductors (Conductors).

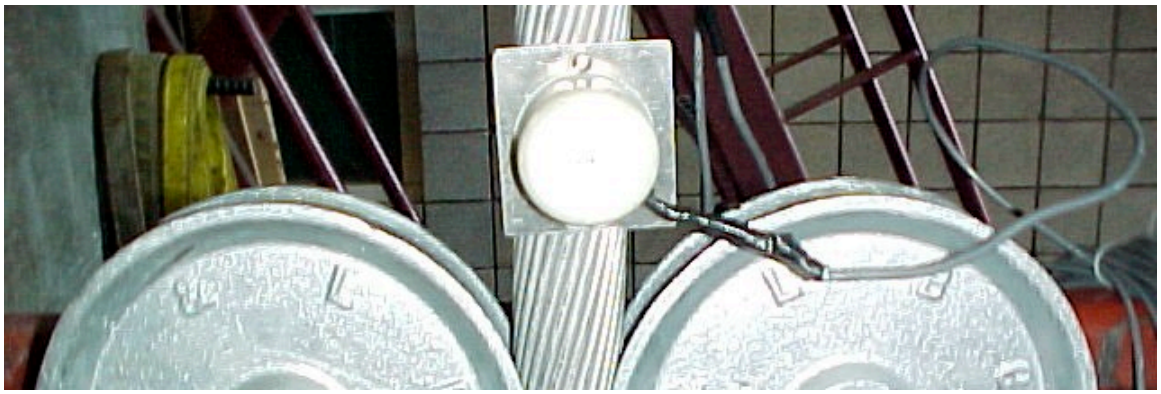

Figure 1.4 Inclinometer Attached to Conductor Surface.

1.4 Test Configurations

The bending tests for each of the two flexible conductor specimens were conducted for seven different axial tensions. Table 1.2 shows the values of axial tension and corresponding axial strain at mid-span of each of the two tested conductors.

Table 1.2. Axial Tension and Axial Strain at Mid-Span of Flexible Conductors.

Tension Level No.	Young's Modulus E (ksi)	Total Mid-Span Tension T (lbs)		Conductor Weight Below Mid-Span (lbs)		Dead Weight (lbs)	Conductor Cross-Sectional Area, A (in^2)		Axial Strain at Mid-Span $å = \frac{T}{EA}\,(iå)$	
		2300 MCM	MCM 1113C	2300 MCM	MCM 1113C		2300 MCM	MCM 1113C	2300 MCM	MCM 1113C
1	10 000	250	200	100	50	150	1.86	0.97	13	21
2		370	320			270			20	33
3		575	525			475			31	54
4		780	730			680			42	75
5		985	945			895			53	97
6		1500	1450			1400			81	150
7		2000	1950			1900			108	201

1.5 Test Protocols

Two types of quasi-static bending tests were conducted on the two flexible conductor specimens: monotonic tests and cyclic tests. For the monotonic tests, the two central supports were pulled at a rate of 0.01 in /sec in one horizontal direction by the hydraulic actuator. The maximum displacement reached at the two loading points was 16 in. for all tests.

The loading protocol used to perform the cyclic tests was inspired by the ATC-24 loading protocol (Applied Technology Council, 1992). This protocol has been developed for the cyclic seismic testing of components of steel structures. As shown in Fig. 1.5, the protocol consists of stepwise increasing displacement, δ, expressed in terms of a displacement ductility factor, μ, defined as:

$$\mu = \frac{\delta}{\delta_y} \tag{1.3}$$

An arbitrary value of 1 in was taken as the yield displacement, δ_y, across each of the specimens.

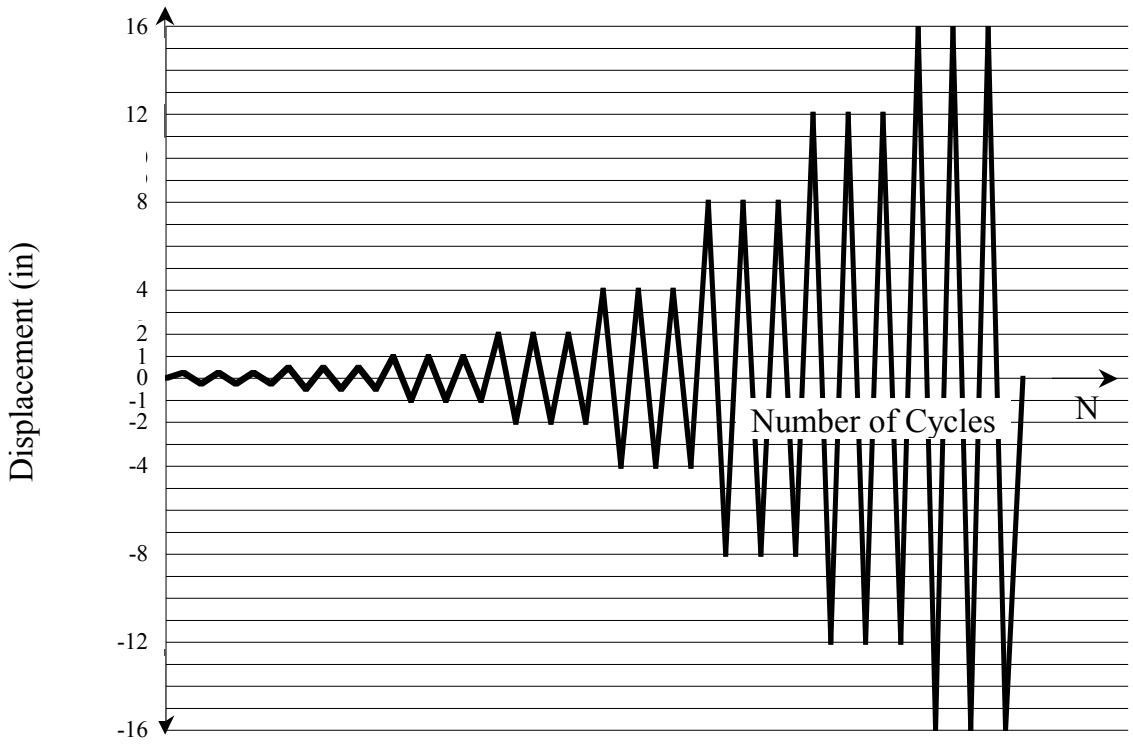

Figure 1.5 Loading Protocol For Cyclic Tests on Flexible Conductors.

1.6 Theoretical Bounds on Flexural Stiffness of Flexible Conductors

The bending response of flexible conductors (cables) is bounded by two theoretical extreme flexural stiffness values. The maximum possible flexural stiffness of a conductor, $EI_{\max}$, occurs at very low curvatures before the strands slip past one another. In this condition, all the strands are able to transfer shear forces over one another and the conductor section acts as a solid cross-section with $EI_{\max}$:

$$EI_{\max} = E\sum_{i=1}^{N_s}\left(\frac{\pi d_{si}^4}{64} + \frac{\pi d_{si}^2}{4} y_{si}^2\right) \approx E\frac{\pi d_c^4}{64} \tag{1.4}$$

where d_{si} is the diameter of the ith strand in the conductor, y_{si} is the distance from the centroid of the ith strand to the centroid of the conductor, d_c is the diameter of the conductor, and N_s is the total number of strands in the conductor.

The minimum possible flexural stiffness of a conductor, $EI_{\min}$, occurs at curvatures for which the friction resistance between the strands has been exhausted. In this condition, all the strands are slipping past each other and are unable able to transfer any shear force. Therefore the flexural stiffness of the conductor section is reduced to the sum of the flexural stiffness of each individual strand:

$$EI_{\min} = E\sum_{i=1}^{N_s}\frac{\pi d_{si}^4}{64} \tag{1.5}$$

Table 1.3 shows the theoretical bounding stiffness values for the two flexible conductors tested under quasi-static tests. It can be seen that the maximum possible flexural stiffness for these cables is approximately 100 times the minimum possible flexural stiffness for both conductors.

Table 1.3. Theoretical Bounding Stiffness for Flexible Conductor Specimens.

Conductor	$EI_{\max}$ (kip-in^2)	$EI_{\min}$ (kip-in^2)
2300 MCM	4600	42
MCM 1113C	1200	12

1.7 Results of Monotonic Tests

Figures 1.6 and 1.7 present the force-displacement plots from the monotonic tests conducted on the two conductor specimens under the seven different axial tension levels (or axial strains) given in Table 1.2. The force was measured from the load cell on the actuator, while the displacement represents the displacement of the actuator. The global behavior of both conductors is linear-elastic with negligible hysteretic response. The global lateral stiffness of the conductors increases with axial tension. Finally, slightly more hysteretic response can be observed for high tension and at large displacement values. It is believed that this apparent energy dissipation is the results of the friction in the support system, rather than an actual damping mechanism in the conductors.

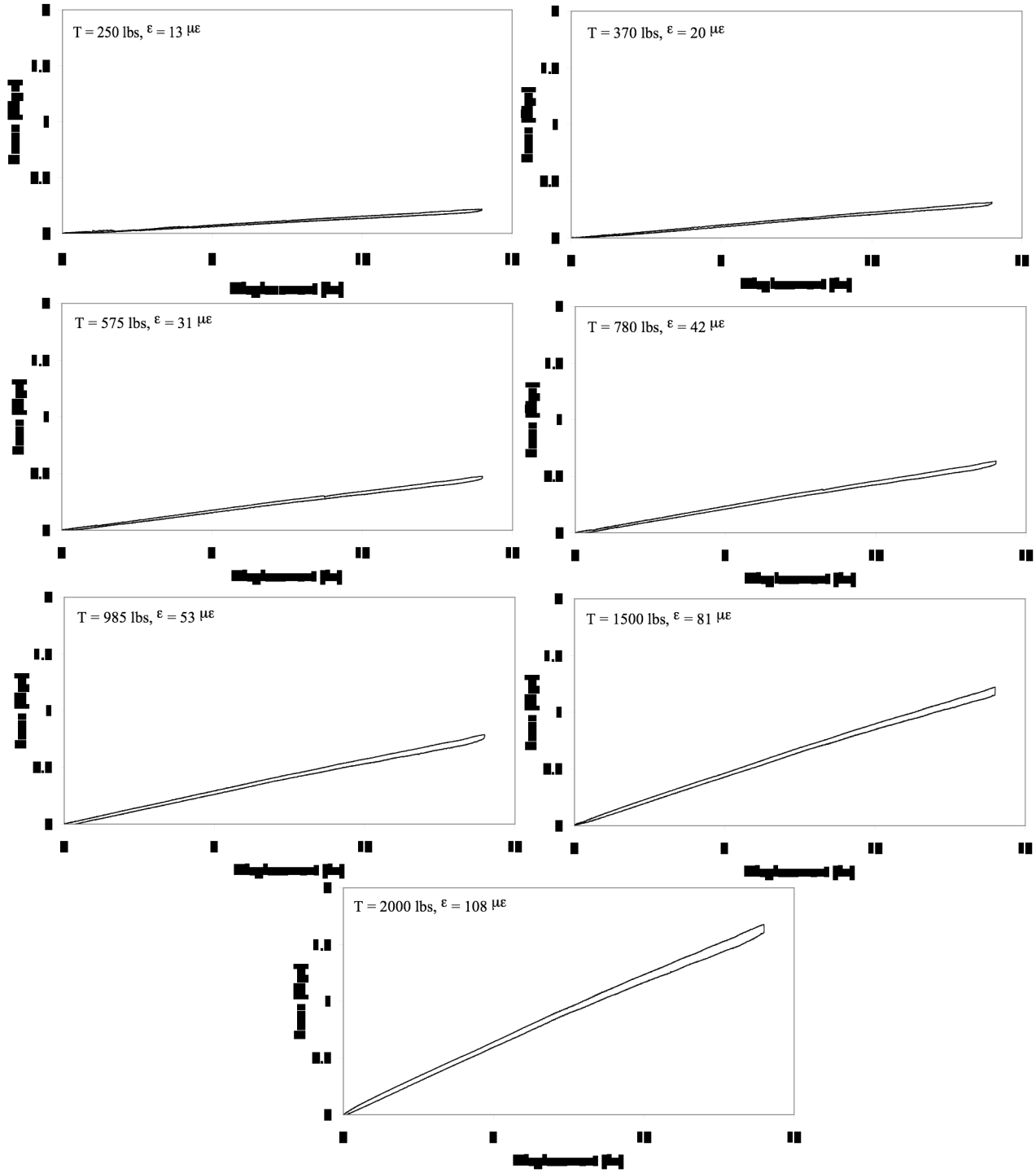

Figure 1.6 Monotonic Force-Displacement Relationships for 2300 MCM Conductor.

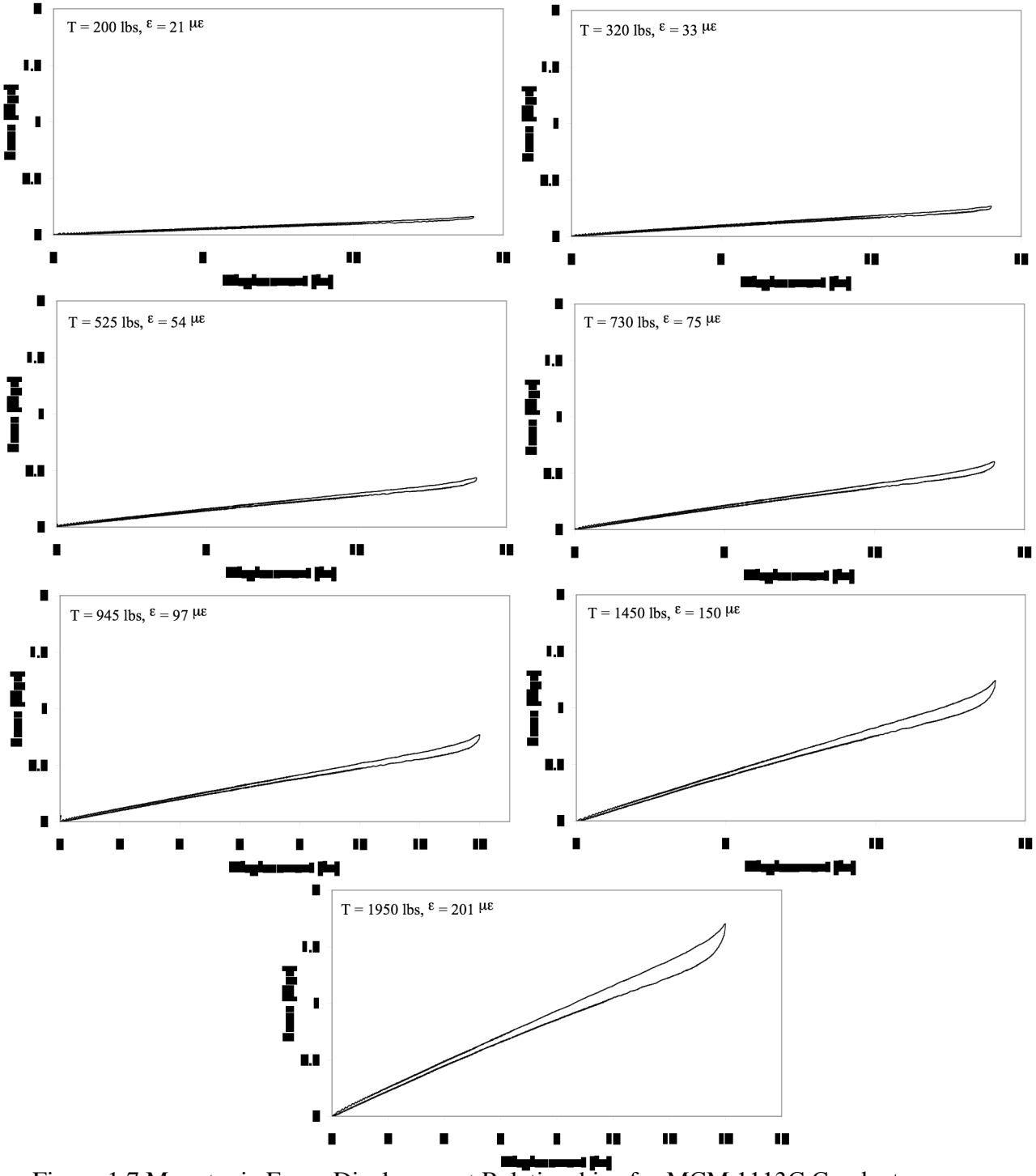

Figure 1.7 Monotonic Force-Displacement Relationships for MCM 1113C Conductor.

Figures 1.8 and 1.9 present the central bending moment – curvature relationships obtained from the monotonic tests conducted on the two conductor specimens under the seven different axial tensions (or axial strains) given in Table 1.2. The bending moments were obtained from equation (1.1), while the central curvatures were calculated from equation (1.2) using the two inclinometers closest to the mid-span of the conductor. Also shown for each conductor are the bounds in flexural stiffness given in Table 1.3. The curves shown in Figs. 1.8 and 1.9 indicate that for most axial strains, the flexural stiffness of both conductors are close to the minimum values given by equation (1.4). This result is particularly evident for the 2300 MCM conductor that exhibited much higher central curvatures than that of the MCM 1113C conductor. Only for very large axial tensions (greater than 1500 lbs), the flexural stiffness of both conductors approaches the maximum stiffness given by equation (1.3). It is believed that these axial tensions are much higher than those observed on real conductors during seismic events.

1.8 Results of Cyclic Tests

Figures 1.10 and 1.11 present the force-displacement plots from the cyclic tests conducted on the two specimens under the seven different levels of axial tension (or axial strain) given in Table 1.2. The results are similar to that of the monotonic tests. Again, the behavior of both conductors is linear-elastic with negligible hysteretic response, and the global lateral stiffness of the conductors increases with axial tension.

Figures 1.12 and 1.13 present the central bending moment – curvature relationships obtained from the cyclic tests conducted on the two conductor specimens under the seven different axial tensions (or axial strains) given in Table 1.2. Because of the very small curvatures and bending moments measured, particularly for the MCM 1113C conductor, the curves shown in Figs. 1.12 and 1.13 are noisy. The trend in the data, however, is identical to that of the monotonic tests. For most axial strains, the flexural stiffness of both conductors is close to the minimum values, and only at large axial tensions (greater than 1500 lbs) that the flexural stiffness of both conductors approaches the maximum stiffness value.

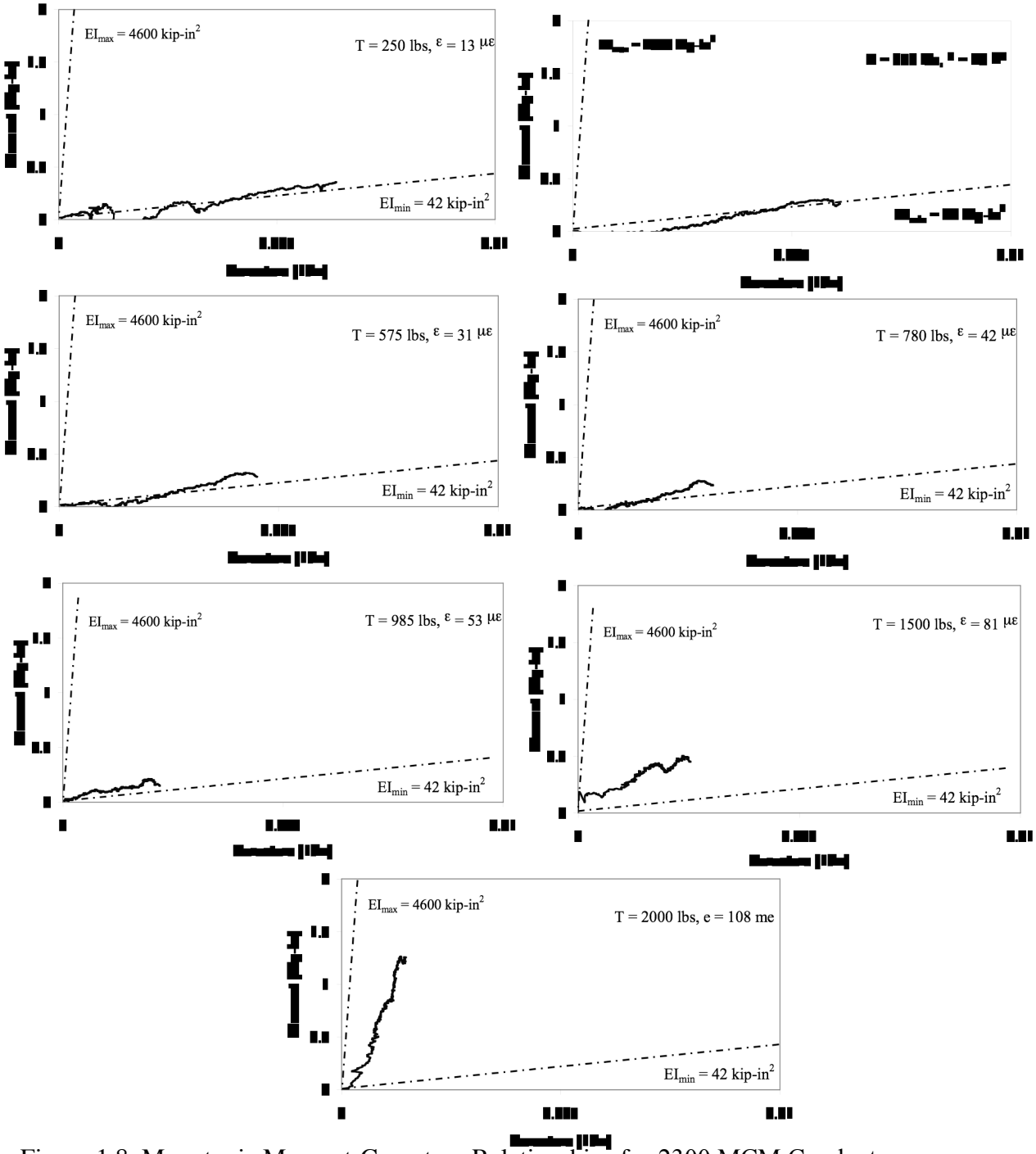

Figure 1.8. Monotonic Moment-Curvature Relationships for 2300 MCM Conductor.

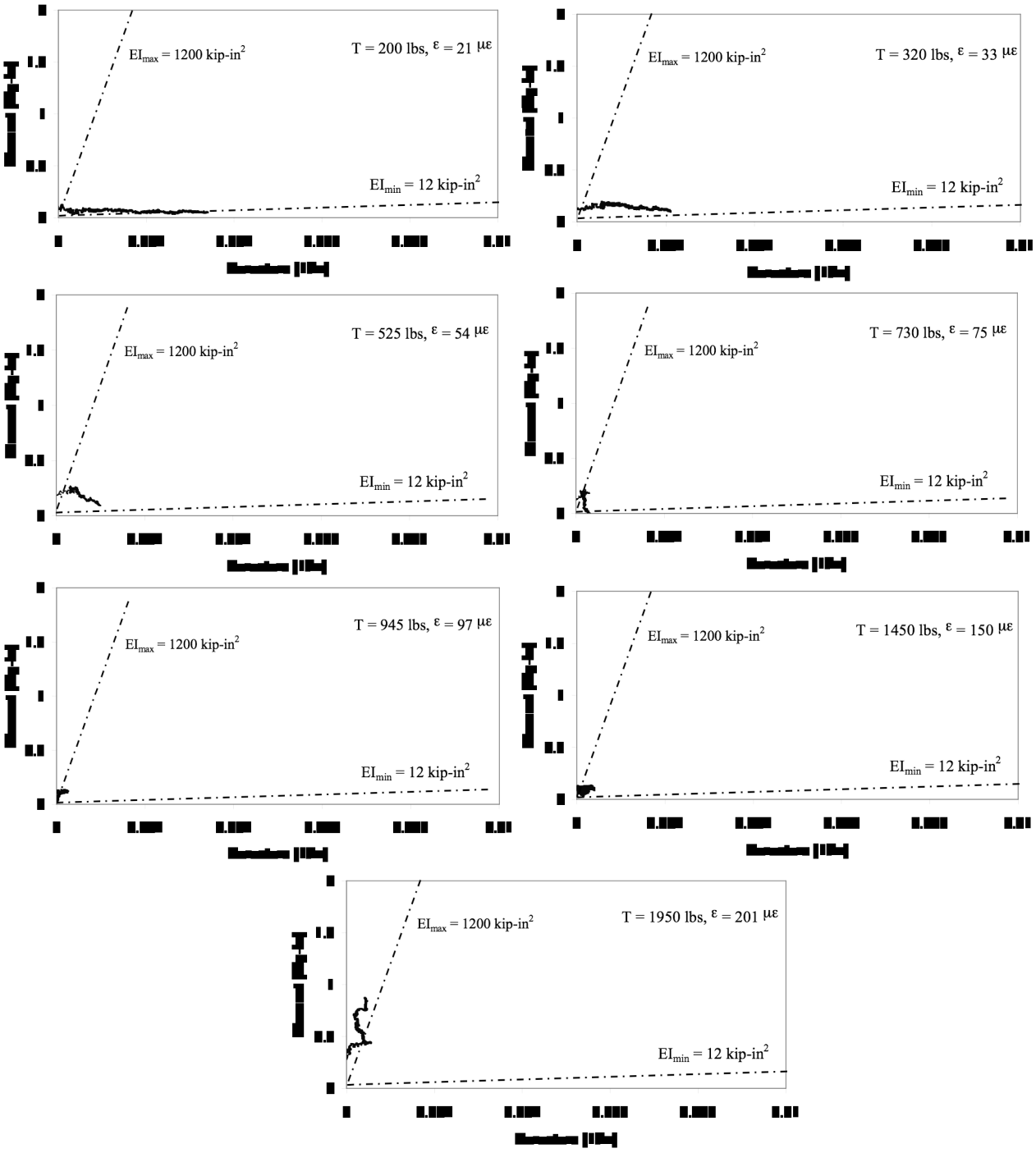

Figure 1.9. Monotonic Moment-Curvature Relationships for MCM 1113C Conductor.

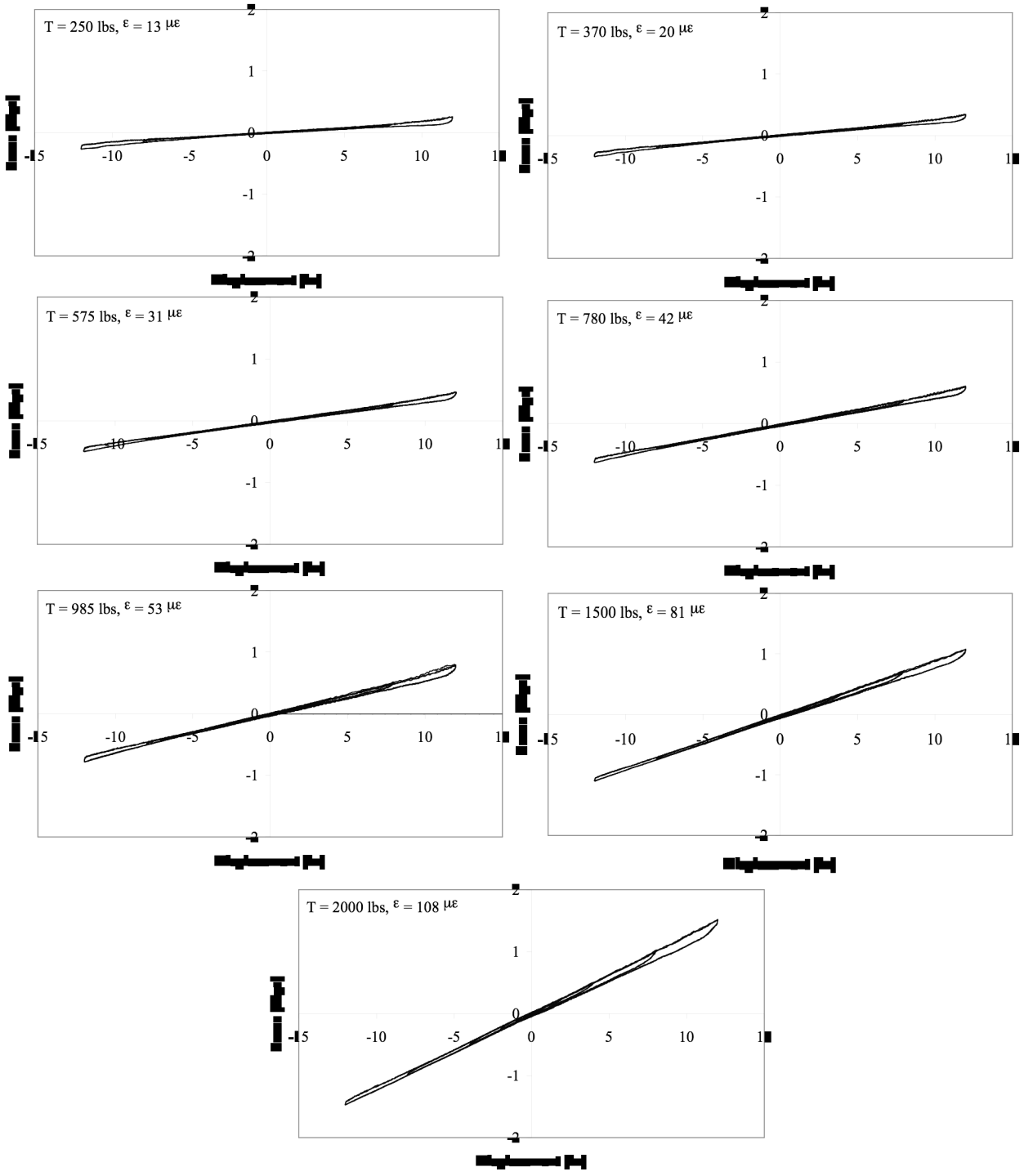

Figure 1.10 Cyclic Force-Displacement Relationships for 2300 MCM Conductor.

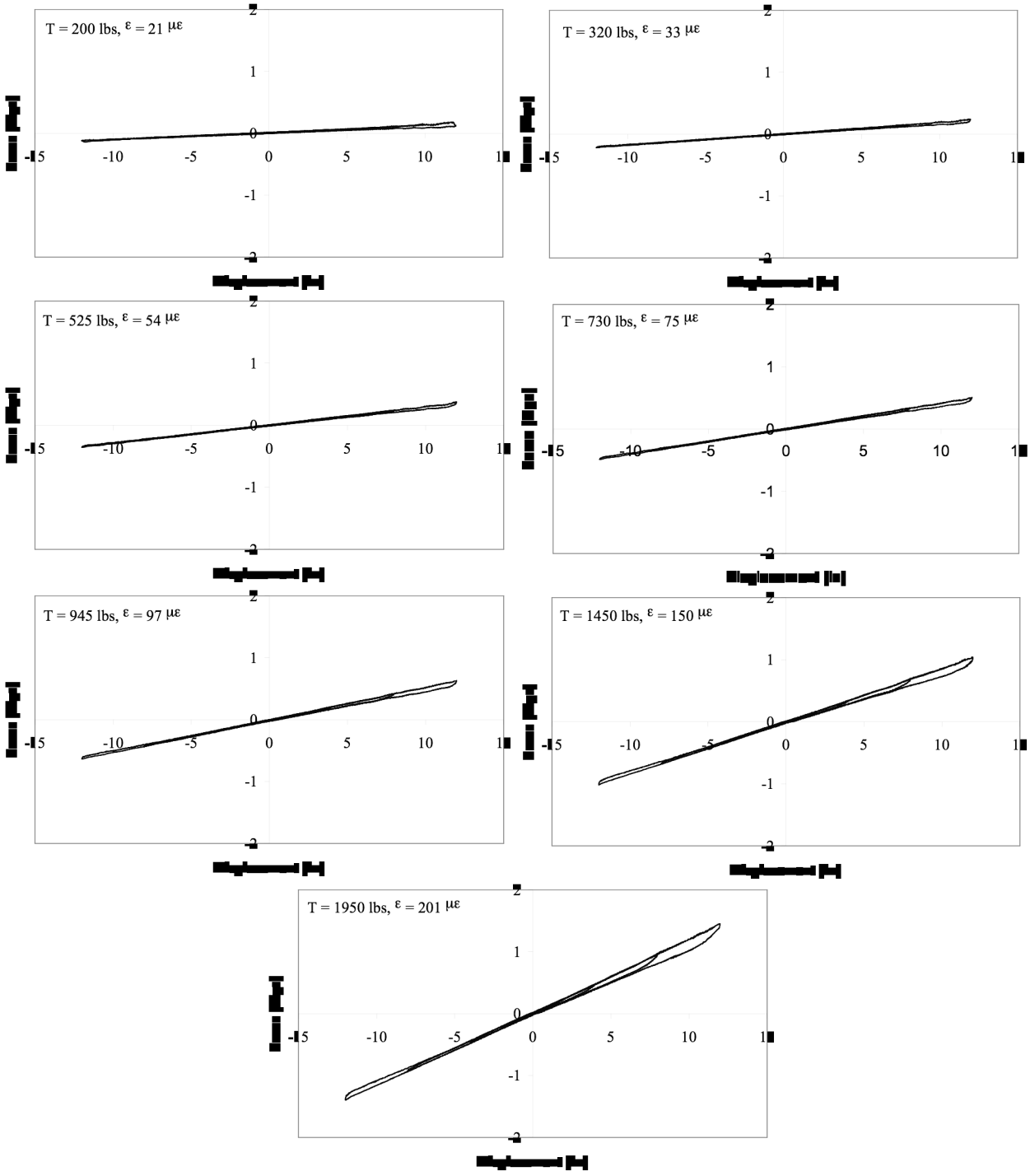

Figure 1.11 Cyclic Force-Displacement Relationships for MCM 1113C Conductor.

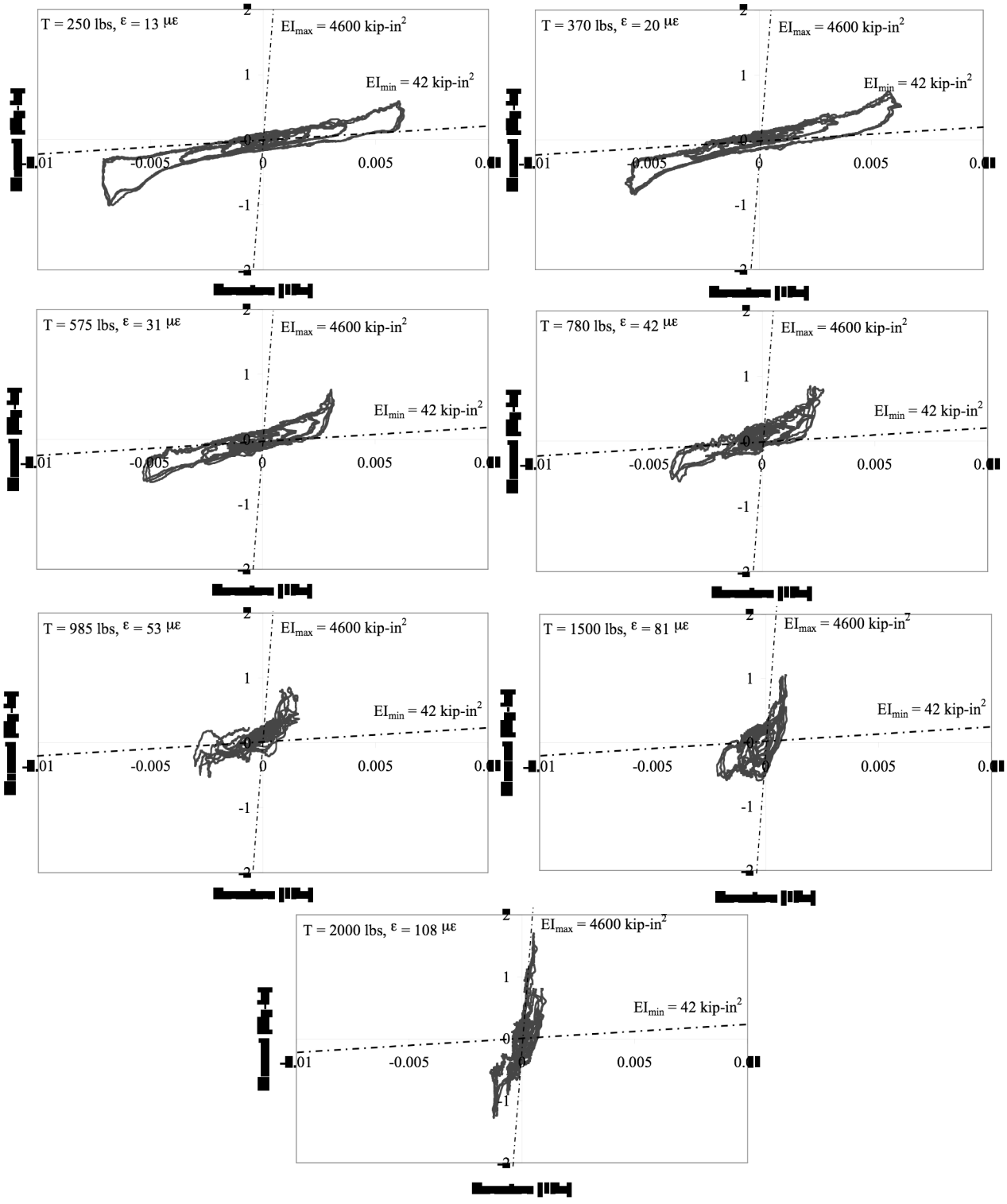

Figure 1.12 Cyclic Moment-Curvature Relationships for 2300 MCM Conductor.

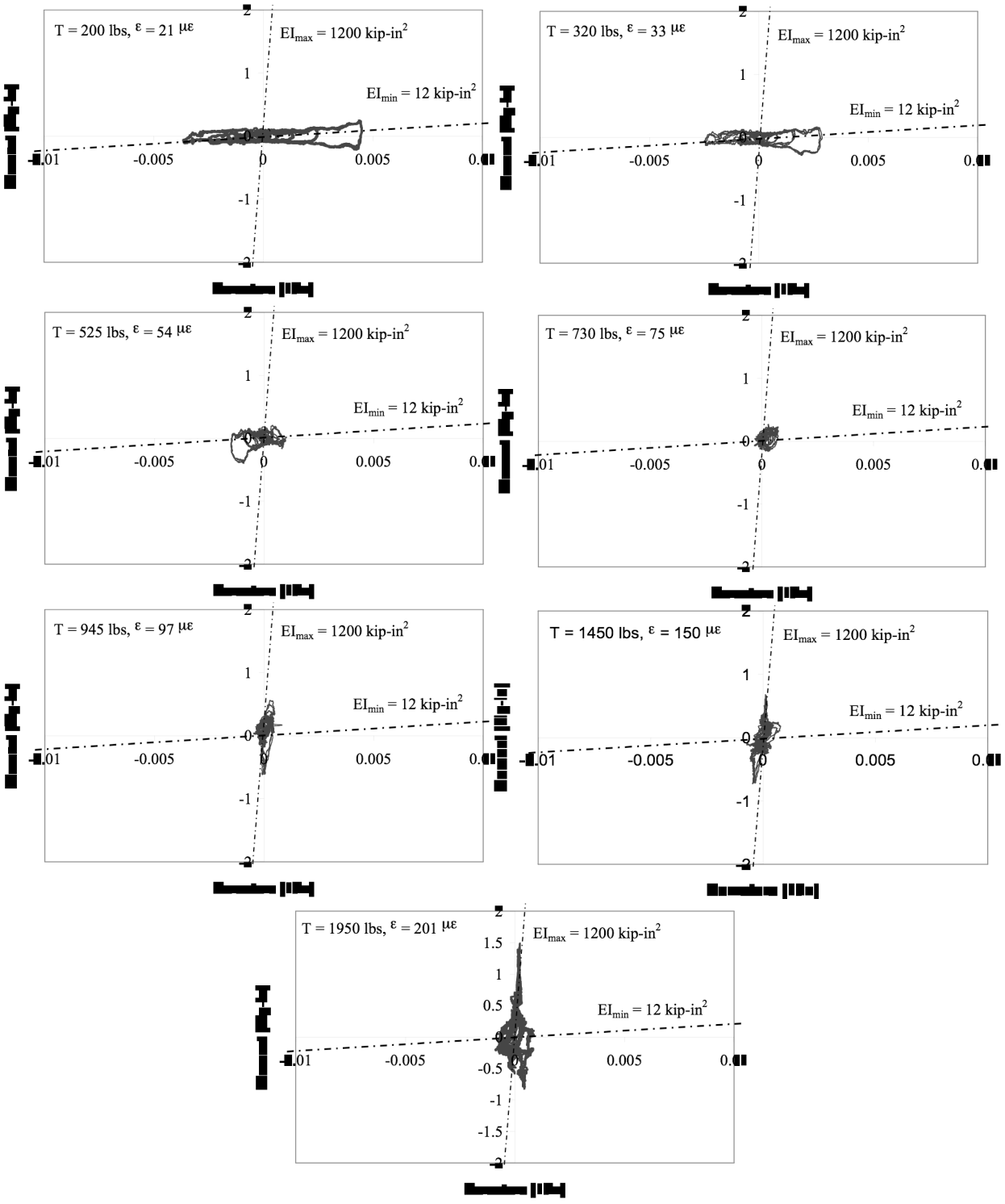

Figure 1.13 Cyclic Moment-Curvature Relationships for MCM 1113C Conductor.

1.9 Computation of Effective Secant Conductor Flexural Stiffness

Another approach to evaluate the flexural properties of a flexible conductor is to determine the equivalent elastic flexural stiffness that reproduces its global deformed shape for given axial tension and displacement amplitude. This effective flexural stiffness is referred herein as the *secant conductor flexural stiffness*.

For this purpose, the conductor is considered as a simply supported Bernoulli-Euler beam loaded by two concentrated forces F and an axial tension T, as shown in Fig. 1.14. In this figure, *x* represents the position along the conductor, v the lateral displacement of the conductor and L the loaded span of the conductor.

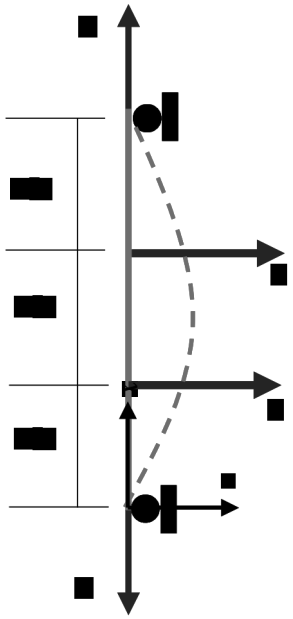

Figure 1.14. Representation of a Flexible Conductor as a Simply Supported Bernoulli-Euler Beam Loaded by Two concentrated Forces and an Axial Tension.

The differential equation governing the lateral displacement of a Bernoulli-Euler beam under axial tension and four-point bending is given by:

$$\begin{aligned} EI\frac{d^2v}{dx^2} - Tv &= -Fx \qquad 0 \le x \le L/3 \\ EI\frac{d^2v}{dx^2} - Tv &= -\frac{FL}{3} \quad L/3 < x \le L/2 \end{aligned} \tag{1.5}$$

where EI is the flexural stiffness. The deflected shape of the connector shown in Fig. 1.14 is symmetric and only one half of the span needs to be solved.

The solution of equation (1.5) is given by:

$$
\begin{aligned}
&v = C_1 \sinh \lambda x + \alpha x \qquad\qquad 0 \le x \le L/3 \\
&v = C_2 \sinh \lambda x + C_3 \cosh \lambda x + \frac{\alpha L}{3} \quad L/3 < x \le L/2 \\
&\lambda = \sqrt{\frac{T}{EI}} \qquad \alpha = \frac{F}{T} \\
&C_1 = \frac{\alpha}{\lambda}\left[\frac{\sinh(\lambda L/2)}{\cosh(\lambda L/2)}\sinh(\lambda L/3) - \cosh(\lambda L/3)\right] \\
&C_2 = \frac{\alpha}{\lambda}\frac{\sinh(\lambda L/2)}{\cosh(\lambda L/2)}\sinh(\lambda L/3) \\
&C_3 = -\frac{\alpha}{\lambda}\sinh(\lambda L/3)
\end{aligned}
\tag{1.6}
$$

For given axial tension and lateral force on the conductor, equation (1.6) was used to determine the secant flexural stiffness EI that matches the deflected shape of the conductor measured by the array of string potentiometers installed along its span. For this purpose, the least square method was used to find the value of EI that minimizes the errors between the deflected shape predicted by equation (1.6) and the measured lateral displacements. Six different displacement amplitudes were considered: 0.25, 0.50, 1.0, 2.0, 4.0 and 8.0 in. Figure 1.15 illustrates this process for the cyclic tests on the 2300 MCM conductor under at an axial tension of 250 lbs.

Tables 1.4 and 1.5 present the secant flexural stiffness values obtained from this least square minimization procedure on the 2300 MCM and MCM 113C conductor, respectively. The results are shown for all tension values and displacement amplitudes. These results are reproduced on three-dimensional plots in Fig. 1.16 that show, for each conductor, the variation of the secant flexural stiffness with axial tension and lateral displacement amplitude. Although the data is scattered (mainly at low displacement amplitudes), two trends can be observed: 1) the secant flexural stiffness increases with increasing axial tension and 2) the secant flexural stiffness decreases with increasing lateral displacement. For most combinations of axial tension and lateral displacement, the secant flexural stiffness is less than 10% of the maximum possible flexural stiffness of each conductor.

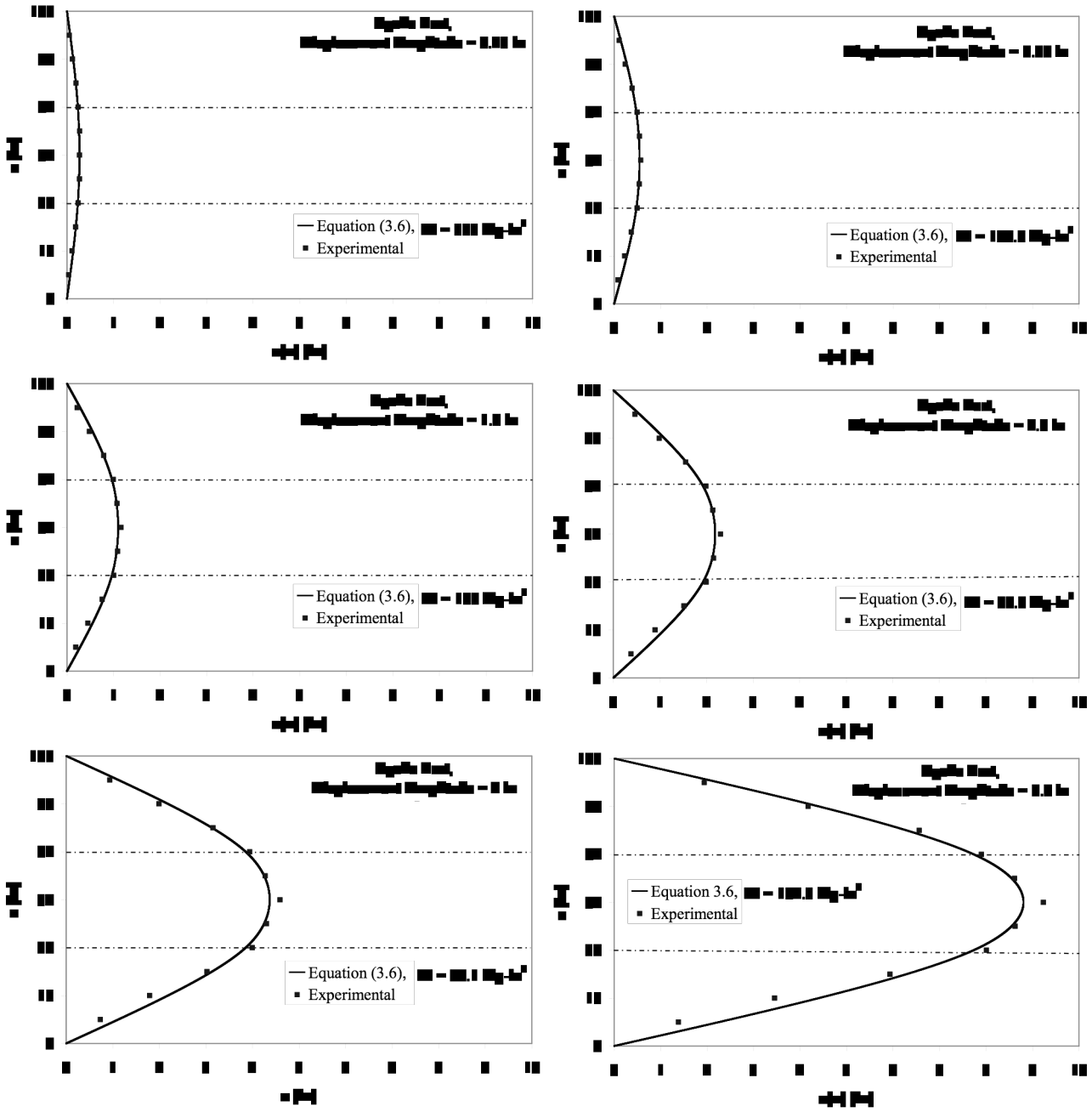

Figure 1.15 Evaluation of Secant Conductor Flexural Stiffness, Cyclic tests, 2300 MCM Conductor, Axial tension of 250 lbs.

Table 1.4 Computed Secant Flexural Stiffness for 2300 MCM Conductor.

Displacement Amplitude (in)	Tension (lbs)	Secant Flexural Stiffness (kip-in^2)
0.25	250	395
	370	104
	575	846
	780	136
	985	1062
	1500	1588
	2000	1020
0.50	250	167
	370	64
	575	494
	780	119
	985	502
	1500	1059
	2000	897
1.0	250	100
	370	78
	575	278
	780	58
	985	310
	1500	619
	2000	457
2.0	250	81
	370	54
	575	163
	780	54
	985	225
	1500	358
	2000	333
4.0	250	70
	370	46
	575	113
	780	50
	985	123
	1500	241
	2000	269
8.0	250	104
	370	94
	575	85
	780	63
	985	110
	1500	121
	2000	196

Table 1.5 Computed Secant Flexural Stiffness for MCM 1113C Conductor.

Displacement Amplitude (in)	Tension (lbs)	Secant Flexural Stiffness ($kip\text{-}in^2$)
0.25	200	1
	320	249
	525	249
	730	173
	945	538
	1450	744
	1950	555
0.50	200	1
	320	121
	525	184
	730	71
	945	341
	1450	622
	1950	530
1.0	200	1
	320	82
	525	84
	730	19
	945	178
	1450	338
	1950	303
2.0	200	1
	320	16
	525	5
	730	3
	945	56
	1450	147
	1950	199
4.0	200	1
	320	3
	525	4
	730	3
	945	25
	1450	91
	1950	157
8.0	200	1
	320	3
	525	2
	730	3
	945	4
	1450	37
	1950	93

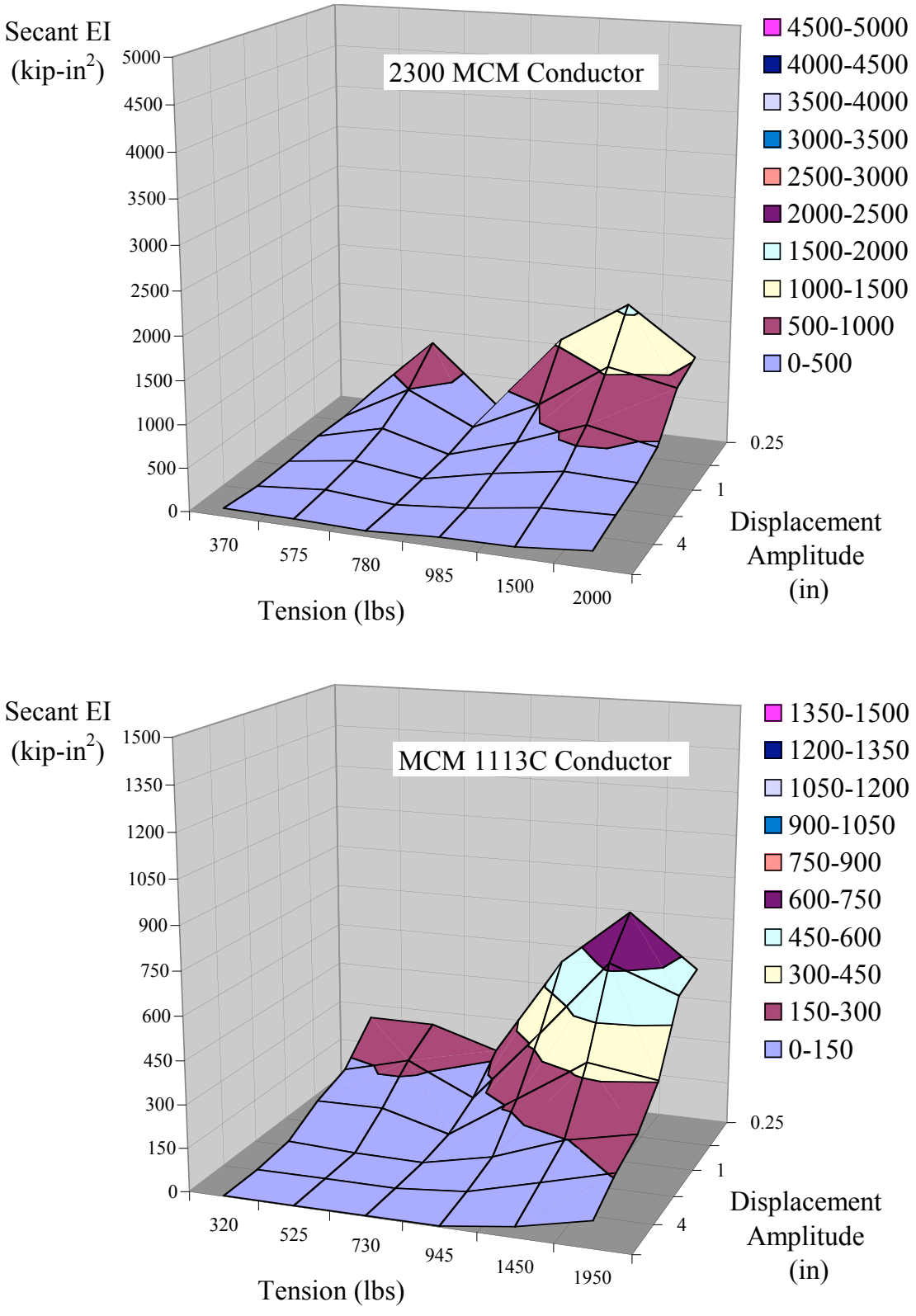

Figure 1.16 Secant Flexural Stiffness for 2300 MCM and MCM 1113C Conductors.

1.10 Discussion

The results obtained from the quasi-static bending tests performed on two different full-scale flexible conductors (cables) indicate that the global force-displacement behavior of both conductors is linear-elastic with negligible hysteretic response. For most combinations of axial tension and lateral conductor displacement, the flexural stiffness exhibited by both conductors is very small, and tends toward the minimum possible flexural stiffness, corresponding to the situation where all the strands are slipping past each other, and are unable able to transfer any shear force. Only for very large axial tension values (more than 1000 lbs or 100 με) the flexural stiffness of the conductors approach the maximum possible flexural stiffness, corresponding to the situation where all the strands are able to transfer longitudinal shear forces over one another, and the conductor section acts as a solid cross-section. It is unlikely that such high axial tension values can be mobilized during the seismic response of interconnected substation electrical equipment.

For the analysis of flexible bus conductors, the IEEE-P1527/D5 Standard (Institute of Electrical and Electronics Engineers, 1998) recommends to use an effective flexural stiffness of conductors EI_{ec} given by:

$$EI_{ec} = (1 + N_l)EI_{\min} \tag{1.7}$$

where N_l is the number of strand layers in the conductor. For both conductors tested, the number of layers is 4. According to equation (1.7), the effective flexural stiffness would be

5 times the minimum possible flexural stiffness. This recommended value corresponds to 210 kip-in^2 for the 2300 MCM conductor and 60 kip-in^2 for the MCM 1113C conductor. The mean value of the secant flexural stiffness computed for the 2300 MCM conductor (see Table 1.4) is 323 kip-in^2, which corresponds to 7.7 times the minimum possible flexural stiffness of the conductor. The corresponding mean value for the MCM 1113C conductor (see Table 1.5) is 149 kip-in^2, which corresponds to 12.4 times the minimum possible flexural stiffness of the conductor. Based on these results, the recommendation of the IEEE-P1527/D5 Standard appears reasonable.

2. SHAKE TABLE TESTS OF PAIRS OF GENERIC SUBSTATION EQUIPMENT CONNECTED WITH FLEXIBLE CONDUCTORS

This chapter describes the shake table tests performed on five pairs of generic substation equipment connected by three different flexible conductor assemblies. Simulated horizontal ground motions were applied in the longitudinal direction of the conductor assemblies by the uniaxial earthquake simulation facility at UC-San Diego. The variables considered in the tests were:

- the dynamic characteristics of the generic equipment
- the types of flexible conductors
- the slackness of the flexible conductors
- the simulated ground motions
- the intensities of the simulated ground motions

2.1 Description of UC-San Diego Uniaxial Earthquake Simulation Facility

The uniaxial earthquake simulation system at UC-San Diego features a 4.8-ton shake table made of an all-welded steel construction, as shown in Figure 2.1. The shake table has plan dimensions of 10 ft x 16 ft with a specimen payload capacity of 40 tons. A 90-kips fatigue-rated actuator drives the system. The bearing system consists of eight 5-in Garlock DU cylinders sliding on two stationary shafts. The usable peak-to-peak stroke is 12 in. The flow rate of the hydraulic system allows a peak sinusoidal velocity of 40 in/s. The actuator can induce peak accelerations of 9.0 g for the bare table and 1.0 g for the fully loaded table. The workable frequency range of the simulator spans from 0 to 50 Hz.

The control system of the shake table includes an advanced, second generation, digital controller incorporating a Three-Variable-Control (TVC), together with Adaptive Inverse Control (AIC), On-Line Iteration (OLI) techniques and Resonance Canceling Notch Filters. This advanced control system allows the reproduction of earthquake ground motions with high fidelity (Filiatrault et al., 1996, 2000).

Figure 2.1 Shake Table of the UC-San Diego Uniaxial Earthquake Simulation System.

2.2 Description of Generic Substation Equipment

Five different pairs of generic substation equipment were considered for the shake table tests. Each pair of generic equipment was designed to be representative of the range of dynamic properties of actual interconnected substation electrical equipment. Table 2.1 presents the target dynamic characteristics of the five pairs of generic equipment.

Table 2.1 Target Dynamic Characteristics of Pairs of Generic Equipment.

Pair	Equipment A			Equipment B		
	Equipment No.	Seismic Weight (lbs)	Natural Frequency (Hz)	Equipment No.	Seismic Weight (lbs)	Natural Frequency (Hz)
1	1	1000	1.5	3	250	5
2	1	1000	1.5	4	350	7.5
3	2	200	1.5	3	250	5.0
4	2	200	1.5	4	350	7.5
5	1	1000	1.5	5	350	12.0

From Table 2.1, five different generic equipment specimens are required to satisfy the test schedule. For each specimen, the seismic weight and the natural frequency are fixed. Therefore, the design variables are the lateral stiffness of each specimen and the appropriate strength to assure a linear-elastic dynamic response. For simplicity, steel cantilevered columns anchored to the shake table surface represented the equipment items. Figure 2.2 presents a photograph of the test set-up for the shake table tests. In order to mobilize sufficient strength for a given lateral stiffness, the height of all cantilevers was fixed at 14 ft. Table 2.2 presents the tubular steel sections used to fabricate each column. Appendix B presents the shop drawings used to fabricate the specimens. In order to adjust the slackness of the conductor, the columns were mounted on a rigid cantilever steel base that was bolted onto the shake table surface.

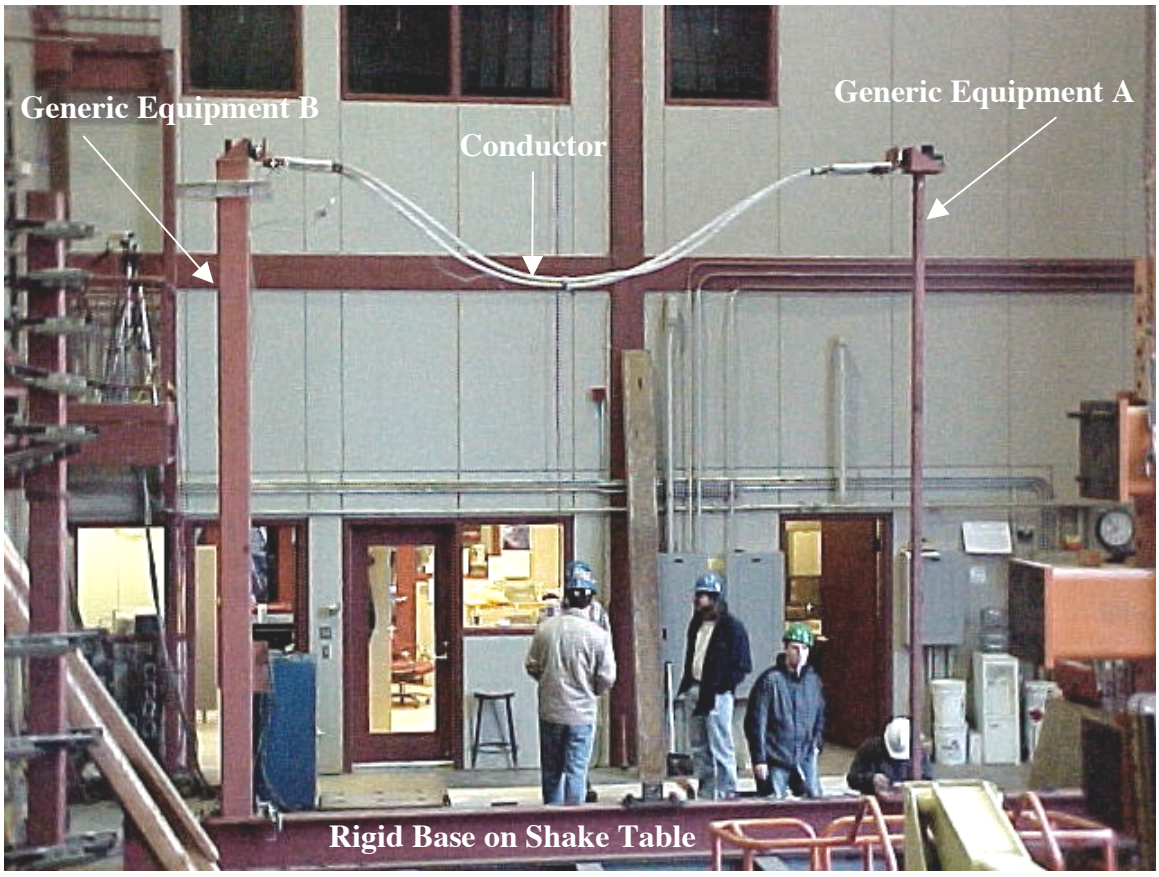

Figure 2.2 Test Set-Up for Shake Table Tests.

Table 2.2 Tubular Steel Sections Used for Generic Equipment Specimens.

Equipment	Target Seismic Weight (lbs)	Target Natural Frequency (Hz)	Tubular Section
1	1000	1.5	7x5x3/16 in
2	200	1.5	3-1/2x2-1/2x1/4 in
3	250	5.0	8x6x3/16 in
4	350	7.5	12x8x5/16 in
5	350	12.0	12x8x5/16 in

Note that Equipment 5 is the same as Equipment 4 but is equipped with a lateral bracing member (2 angles 3x3x3/8 back-to-back) to increase its target natural frequency to approximately 12 Hz. Figure 2.3 presents a photograph of Equipment 5.

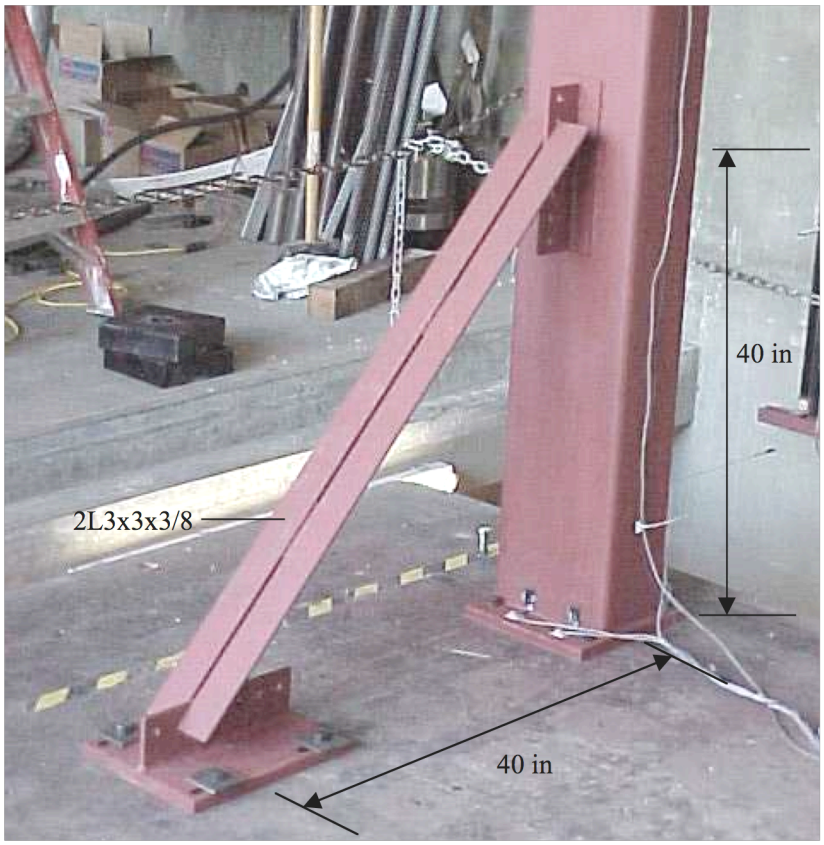

Figure 2.3. Equipment 5.

In order to adjust the natural frequency of each equipment specimen, supplemental steel weights were added at the top of the columns, as illustrated in Fig. 2.4. Table 2.3 indicates the final lumped weight added at the top of each equipment specimen along with the total weight of each specimen.

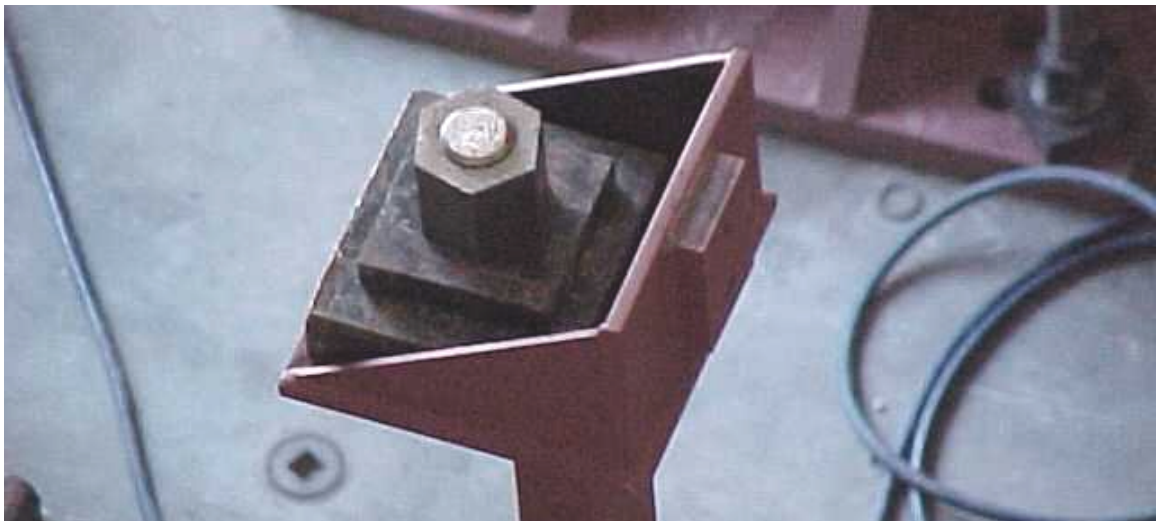

Figure 2.4 Supplemental Steel Weights at Top of Generic Equipment Specimen.

Table 2.3 Values of Lumped Weights at Top of Generic Equipment Specimens.

Equipment	Target Seismic Weight (lbs)	Target Natural Frequency (Hz)	Lumped Top Weight (lbs)	Total Weight (lbs)
1	1000	2	854	1058
2	200	2	147	271
3	250	5	140	380
4	350	7.5	91	656
5	350	12.0	91	656

2.3 Instrumentation

The instrumentation used during the shake table tests of the generic interconnected equipment included the following measurements:

- Absolute displacement, velocity and acceleration of the shake table
- Absolute displacement, velocity and acceleration at the top of each equipment
- Horizontal force at both ends of the conductor

- Longitudinal, transverse and vertical acceleration at mid-span of the conductor

The velocity measurements were obtained directly with special string potentiometers calibrated to velocity.

2.4 Earthquake Ground Motions and Shake Table Fidelity

Two recorded components of near-field earthquake ground motions were used for the seismic tests on the shake table: Tabas (1978 Iran earthquake) and Newhall (1994 Northridge, California, earthquake). These two records are representative of earthquakes known to have a high potential for damaging structures and equipment. Figure 2.5 presents the acceleration time-histories for both full-scale records (full scale herein is referred as 100% span).

The Tabas record was modified using a non-stationary response-spectrum matching technique developed by Abrahamson (1997) to match the IEEE 693 target response spectrum for testing, and it was further high-pass filtered using a cut-off frequency of 1.5 Hz so as not to exceed the displacement limit of 6 in of the shake table.

Preliminary nonlinear dynamic time-history analyses were performed to estimate the response of the interconnected equipment. Based on the results of these preliminary analyses, different intensities were retained for each ground motion record. Table 2.4 presents these intensities for the two ground motions considered. Note that certain tests were not conducted at high intensity levels in order to prevent yielding of the generic equipment items.

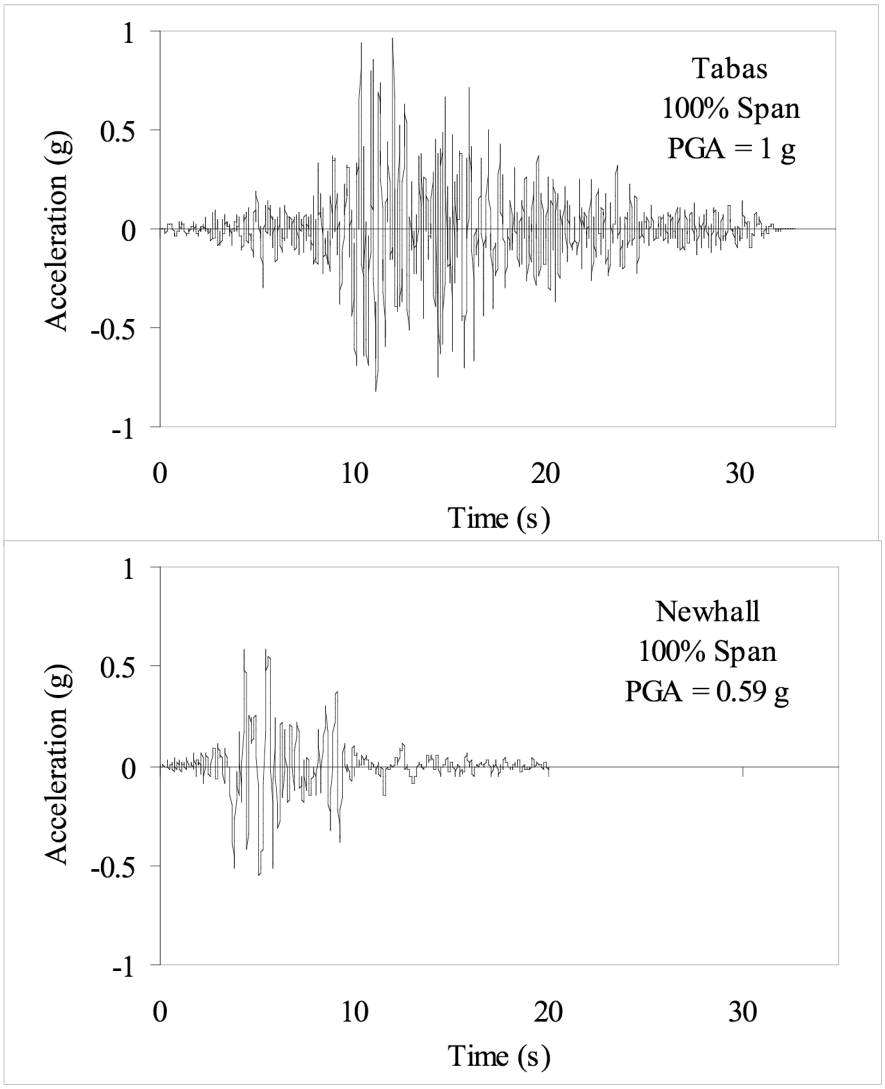

Figure 2.5 Acceleration Time-Histories of Earthquake Ground Motions.

Table 2.4 Intensities of Earthquake Ground Motions Retained for the Shake Table Tests

Record	Intensity 1 (% Span)	Intensity 2 (% Span)
Tabas	25	50
Newhall	30	100

The performance of the shake table was optimized for each record and intensity using the On-Line Iteration (OLI) technique of the electronic controller. Figure 2.6 compares the

absolute acceleration response spectra, at 5% damping, of the accelerograms of Fig. 2.5 scaled at the different intensities listed in Table 2.4 (desired signals) with the response spectra of the acceleration time-histories recorded on the shake table (feedback signals). The feedback signals shown represent the mean values of three different tests on the shake table.

As discussed earlier, the target natural frequencies of the generic equipment varied between 1.5 and 12 Hz. The mean differences (in %) between the desired and the feedback spectral values in the 1.5-12 Hz frequency range are also indicated in Fig. 2.6. The maximum difference for all records is less than 6%. Based on this result, the performance of the shake table was considered adequate. For comparison purposes, each graph in Fig. 2.6 shows also the IEEE 693 required response spectrum (at 2% damping) for high performance level amplified by a factor of two to account for the amplification of earthquake motion at the base of the generic equipment.

2.5 Shake Table Test Program

Three different types of shake table tests were conducted on the pairs of generic equipment models interconnected by flexible conductor assemblies:

1) Frequency Evaluation Tests
2) Damping Evaluation Tests
3) Seismic Tests

These tests are briefly described below.

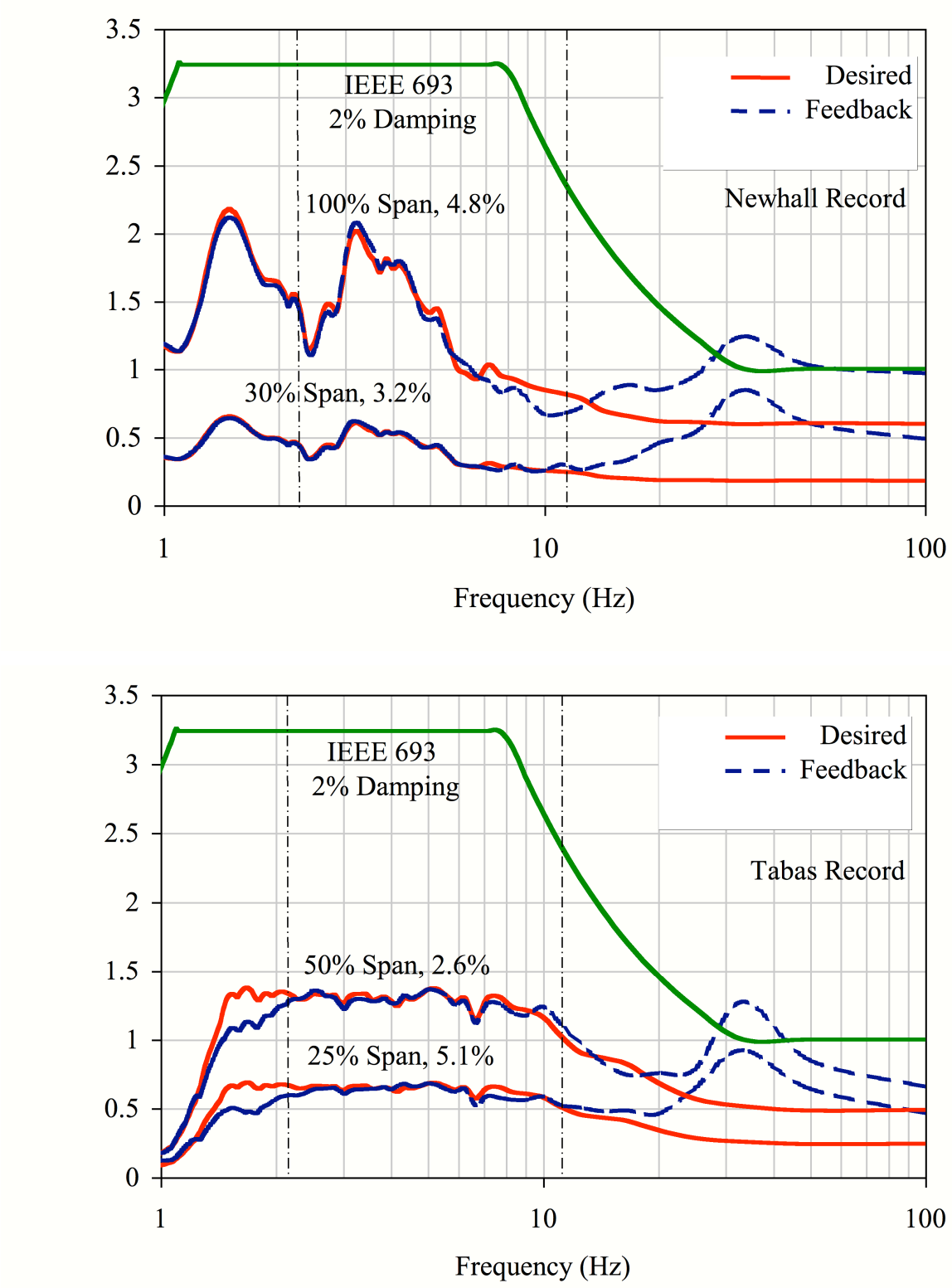

Figure 2.6 Absolute Acceleration Response Spectra, 5% Damping, Bare Shake Table.

2.5.1 Frequency Evaluation Tests

The purpose of the frequency evaluation tests was to identify the natural frequencies and mode shapes of the various pairs of interconnected generic equipment. For this purpose, a low-amplitude 0-40 Hz, clipped-band, and flat white noise excited each configuration. A dedicated ambient vibration analysis software (Experimental Dynamic Investigations, 1993) was used to determine the natural frequencies from power spectral density plots of the absolute acceleration records at the top of each equipment. The natural frequencies were obtained from the amplitudes of the spectral peaks. For all frequency evaluation tests, the following test protocol was followed:

- Nyquist frequency = 40 Hz
- Sampling rate = 80 Hz
- Number of points per sampling windows = 2048
- Duration of each sampling window = 25.6 s
- Frequency resolution = 0.0391 Hz
- Number of sampling windows = 8
- Total duration = 204.8 s

2.5.2 Damping Evaluation Tests

The purpose of the damping evaluation tests was to estimate the first equivalent modal viscous damping of each equipment configuration. In these tests, each pair of generic equipment was excited by a low-amplitude base sinusoidal input at its previously identified fundamental frequency. When a steady-state response was obtained, the input was suddenly stopped and the absolute accelerations at the top of the equipment were recorded. The first modal damping ratio of the structural configuration was then established by the logarithmic decrement method (Clough and Penzien, 1993).

2.5.3 Seismic Tests

In the seismic tests, the ground motions defined in section 2.4 excited the pairs of interconnected equipment. All seismic test data were acquired at a sampling rate of 200 Hz and low-pass filtered at 30 Hz.

2.6 Flexible Conductor Specimens

Three different flexible conductor assemblies were tested with the five pairs of interconnected equipment defined in Table 2.1. These flexible conductor assemblies were:

1) A pair of MCM 1113C bundle conductors, each conductor having the properties described in Section 3.1.
2) A single 2300 MCM conductor having the properties described in Section 3.1.
3) A single Lupine connector.

The first two types of flexible conductors were tested previously under quasi-static loading, as described in Chapter 3. The third flexible (Lupine) conductor was provided by San Diego Gas and Electric (SDG&E) only for the shake table tests and was not tested under quasi-static loading. Table 2.5 lists the characteristics of the Lupine conductor. All conductors were 15 ft long.

Table 2.5 Characteristics of Lupine Flexible Conductor.

Construction	Conductor diameter (in)	Strand diameter (in)	Lay angle (degree)	Number of strands
All aluminum	1.823	0.1657	10	91

Three different slackness values were considered for interconnecting the generic equipment with the flexible conductors. The slackness *s* is defined as:

$$s = \frac{l_c - l_{ch}}{l_{ch}} \tag{2.1}$$

where l_c are the conductor length and l_{ch} the chord length, which for a pair of equipment of similar height is the horizontal distance between the ends of the conductor.

Slackness values of 2, 5 and 10% were considered in the shake table tests, as shown in Fig. 2.7. At 5 and 10% slackness values, the individual fundamental frequencies of connected equipment were not affected significantly by the connections (the available slack not being all used up during the tests). At 2% slackness, significant nonlinear interaction occurred between the equipment, even at low amplitude, which drastically changed their dynamic characteristics.

Slackness = 10% Slackness = 5% Slackness = 2%

Figure 2.7 Equipment Pair 4 Connected by 1113C conductor.

2.7 Test Sequence

Table 2.6 presents the test sequence that was adopted for the shake table tests. Included are the frequency and damping evaluation tests, as well as the seismic tests under the various earthquake ground motion records. Note that some test numbers are missing from Table 2.6. These are tests that were originally scheduled but later cancelled in order to maintain the integrity of the equipment configurations until the end of the test sequence.

Table 2.6 Shake Table Test Sequence

Test FB-#	Pair No.	Conductor	Slackness	Test Description	Input Signal	Span (%)
1	4	None	None	Frequencies of Uncoupled Equipment	White Noise	---
2	4			Damping - A	Sinusoidal	---
3	4			Damping - B	Sinusoidal	---
4	4	1113 MCM bundle	10%	Frequencies of Coupled Equipment	White Noise	---
5	4			Damping - A & B	Sinusoidal	---
6	4			Seismic	Newhall	30
7	4			Seismic	Newhall	100
8	4			Seismic	Tabas	25
9	4			Seismic	Tabas	50
10	4	None	None	Seismic	Newhall	30
11	4			Seismic,	Newhall	100
12	4			Seismic	Tabas	25
13	4			Seismic	Tabas	50
14	3			Frequencies of Uncoupled Equipment	White Noise	---
15	3			Damping - B	Sinusoidal	---
16	3	1113 MCM bundle	10%	Frequencies of Coupled Equipment	White Noise	---
17	3			Damping – A & B	Sinusoidal	---
18	3			Seismic	Newhall	30
19	3			Seismic	Newhall	100
20	3			Seismic	Tabas	25
21	3			Seismic	Tabas	50
22	3	None	None	Seismic	Newhall	30
23	3			Seismic	Newhall	100
24	3			Seismic	Tabas	25
25	3			Seismic	Tabas	50
26	1			Frequencies	White Noise	---
27	1	None	None	Damping - A	Sinusoidal	---
28	1			Damping - B	Sinusoidal	100
29	1	1113 MCM bundle		Frequencies of Coupled Equipment	White Noise	---
30	1			Damping – A & B	Sinusoidal	---
31	1			Seismic	Newhall	30
32	1			Seismic	Tabas	25
33	2	1113 MCM bundle	10%	Frequencies of Coupled Equipment	White Noise	---
34	2			Damping – A & B	Sinusoidal	---
35	2			Seismic	Newhall	30
36	2			Seismic	Tabas	25
40	2	None	None	Seismic	Newhall	30
41	2			Seismic	Tabas	25
44	5			Frequencies of Uncoupled Equipment	White Noise	---
46	5			Damping - B	Sinusoidal	---
47	5		10%	Frequencies of Coupled Equipment	White Noise	---

48	5	1113 MCM bundle		Damping - A & B	Sinusoidal	---
Test FB-#	Pair No.	Conductor	Slackness	Test Description	Input Signal	Span (%)
49	5	1113 MCM bundle	10%	Seismic	Newhall	30
51	5			Seismic	Tabas	25
52	5			Seismic	Tabas	50
53	5	None	None	Seismic	Newhall	30
55	5		10%	Seismic	Tabas	25
56	5			Seismic	Tabas	50
57	2	2300 MCM single	10%	Frequencies of Coupled Equipment	White Noise	---
58	2			Damping – A & B	Sinusoidal	---
59	2			Seismic	Newhall	30
60	2			Seismic	Tabas	25
61	2			Seismic	Tabas	50
64	5	2300 MCM single	10%	Frequencies of Coupled Equipment	White Noise	---
65	5			Damping - A & B	Sinusoidal	---
66	5			Seismic	Newhall	30
68	5			Seismic	Tabas	25
69	5			Seismic	Tabas	50
70	2	2300 MCM single	5%	Frequencies of Coupled Equipment	White Noise	---
71	2			Damping – A & B	Sinusoidal	---
72	2			Seismic	Newhall	30
73	2			Seismic	Tabas	25
74	2			Seismic	Tabas	50
77	5			Frequencies of Coupled Equipment	White Noise	---
78	5			Damping - A & B	Sinusoidal	---
79	5			Seismic	Newhall	30
81	5			Seismic	Tabas	25
82	5			Seismic	Tabas	50
83	2	1113 MCM bundle	5%	Frequencies of Coupled Equipment	White Noise	---
84	2			Damping – A & B	Sinusoidal	---
85	2			Seismic	Newhall	30
86	2			Seismic	Tabas	25
87	2			Seismic	Tabas	50
90	5			Frequencies of Coupled Equipment	White Noise	---
91	5			Damping - A & B	Sinusoidal	---
92	5			Seismic	Newhall	30
94	5			Seismic	Tabas	25
95	5			Seismic	Tabas	50
96	2	1113 MCM bundle	2%	Frequencies of Coupled Equipment	White Noise	---
97	2			Damping – A & B	Sinusoidal	---
98	2			Seismic	Newhall	30
99	2			Seismic	Tabas	25
100	2			Seismic	Tabas	50
101	2			Seismic	Newhall	100
103	5			Frequencies of Coupled Equipment	White Noise	---
104	5			Damping - A & B	Sinusoidal	---

Test FB-#	Pair No.	Conductor	Slackness	Test Description	Input Signal	Span (%)
105	5	1113 MCM bundle	2%	Seismic	Newhall	30
106	5			Seismic	Newhall	100
107	5			Seismic	Tabas	25
108	5			Seismic	Tabas	50
109	2	2300 MCM single		Frequencies of Coupled Equipment	White Noise	---
110	2			Damping – A & B	Sinusoidal	---
111	2			Seismic	Newhall	30
112	2			Seismic	Tabas	25
113	2			Seismic	Tabas	50
116	5			Frequencies of Coupled Equipment	White Noise	---
117	5			Damping – A & B	Sinusoidal	---
118	5			Seismic	Newhall	30
119	5			Seismic	Newhall	100
120	5			Seismic	Tabas	25
121	5			Seismic	Tabas	50
122	2	Lupine single		Frequencies of Coupled Equipment	White Noise	---
123	2			Damping – A & B	Sinusoidal	---
124	2			Seismic	Newhall	30
125	2			Seismic	Tabas	25
126	2			Seismic	Tabas	50
127	2			Seismic	Newhall	100
129	5			Frequencies of Coupled Equipment	White Noise	---
130	5			Damping - A & B	Sinusoidal	---
131	5			Seismic	Newhall	30
132	5			Seismic	Newhall	100
133	5	Lupine single	2%	Seismic	Tabas	25
134	5			Seismic	Tabas	50
135	2		5%	Frequencies of Coupled Equipment	White Noise	---
136	2			Damping – A & B	Sinusoidal	---
137	2			Seismic	Newhall	30
138	2			Seismic	Tabas	25
139	2			Seismic	Tabas	50
140	5			Frequencies of Coupled Equipment	White Noise	---
141	5			Damping - A & B	Sinusoidal	---
144	5			Seismic	Newhall	30
146	5			Seismic	Tabas	25
147	5			Seismic	Tabas	50
148	2		10%	Frequencies of Coupled Equipment	White Noise	---
149	2			Damping – A & B	Sinusoidal	---
150	2			Seismic	Newhall	30
151	2			Seismic	Tabas	25
152	2			Seismic	Tabas	50
155	5			Frequencies of Coupled Equipment	White Noise	---
156	5			Damping - A & B	Sinusoidal	---
Test FB-#	Pair No.	Conductor	Slackness	Test Description	Input Signal	Span (%)

157	5	Lupine Single	10%	Seismic	Newhall	30
159	5			Seismic	Tabas	25
160	5			Seismic	Tabas	50

2.8 Results of Frequency Evaluation Tests

The detailed results of all frequency evaluation tests conducted on all generic equipment combinations are presented in Appendix C. Included are power spectral density, phase, and coherence plots obtained from the absolute acceleration records at the top of each equipment item.

Table 2.7 summarizes the results of the frequency evaluation tests on the stand-alone (unconnected) generic equipment specimens. The fundamental frequencies of all equipment items agree reasonably well with the target frequencies shown in Table 2.1.

Table 2.7 Measured Fundamental Natural Frequencies of Generic Equipment Specimens

Equipment	Natural Frequency (± 0.04 Hz)
	Mode 1
1	1.60
2	1.56
3	5.00
4	7.38
5	11.33

Tables 2.8 to 2.10 summarize the results of the frequency and damping evaluation tests on the five pairs of generic equipment specimens interconnected by the three different flexible conductor assemblies.

Because of the slackness introduced in the conductor assemblies (mainly for the tests at 5% and 10% slackness), very little dynamic interaction was observed between the two interconnected equipment items at low amplitudes of vibrations. For all tests, a distinct fundamental frequency was identified for each equipment item.

For all tests at 5 and 10% slackness, the fundamental frequencies of the equipment items are not affected significantly by the presence of the conductor assemblies. In fact, the coupled fundamental frequency of each equipment item is reduced slightly when a conductor assembly is introduced. This reduction in fundamental frequency can be attributed to the added mass of the conductors on both interconnected equipment. This result can be seen by the coupled/uncoupled frequency ratios that are less or equal than unity for 5 and 10% slackness in Tables 2.8 to 2.10. This reduction in fundamental frequency is more pronounced for the more rigid interconnected equipment item (Equipment B). This reduction in fundamental frequency is also more pronounced for the equipment connected by the Lupine conductor, which represents the heaviest of the three conductor assemblies used in the test.

The change in fundamental frequencies is not as consistent for the tests at 2% slackness. For these tests, the behavior of the interconnected equipment was nonlinear and depended heavily on the excitation amplitude of the random white noise input signal. For low amplitudes, the behavior was uncoupled and similar to the 5 and 10% slackness tests. When the amplitudes increased, the slackness in the conductor was taken up and the conductor became very tight and transmitted axial vibrations between the interconnected equipment. This nonlinear amplitude dependency phenomenon can be seen by the several power spectral peaks shown for the tests at 2% slackness in Appendix C.

Table 2.8 Results of Frequency Evaluation Tests on Equipment Interconnected by a pair of MCM 1113C conductors

Slackness	Pair	Fundamental Frequency (± 0.04 Hz)			
		Equipment A	Coupled/Uncoupled Frequency Ratio	Equipment B	Coupled/Uncoupled Frequency Ratio
10%	1	1.60	1.00	4.61	0.92
	2	1.60	1.00	6.88	0.93
	3	1.45	0.93	4.57	0.91
	4	1.45	0.93	6.84	0.93
	5	1.56	0.98	10.43	0.92
5%	2	1.56	0.98	6.48	0.88
2%	2	2.03	1.27	4.38	0.59
	5	1.68	1.05	7.46	0.72

Table 2.9 Results of Frequency Evaluation Tests on Equipment Interconnected by a single 2300 MCM bundled conductor

Slackness	Pair	Fundamental Frequency (± 0.04 Hz)			
		Equipment A	Coupled/Uncoupled Frequency Ratio	Equipment B	Coupled/Uncoupled Frequency Ratio
10%	2	1.60	1.00	7.19	0.97
	5	1.60	1.00	10.98	0.97
5%	2	1.60	1.00	7.11	0.96
	5	1.56	0.98	10.94	0.97
2%	2	1.56	0.98	6.09	0.83
	5	1.64	1.03	9.10	0.80

Table 2.10 Results of Frequency Evaluation Tests on Equipment Interconnected by a single Lupine conductor

Slackness	Pair	Fundamental Frequency (± 0.04 Hz)			
		Equipment A	Coupled/Uncoupled Frequency Ratio	Equipment B	Coupled/Uncoupled Frequency Ratio
10%	2	1.60	1.00	5.70	0.77
	5	1.60	1.00	10.98	0.96
5%	2	1.60	1.00	5.51	0.75
	5	1.60	1.00	10.70	0.94
2%	2	1.60	1.00	5.70	0.77
	5	1.60	1.00	9.06	0.80

2.9 Results of Damping Evaluation Tests

The detailed results of all damping evaluation tests are presented in Appendix D. For each damping evaluation test, the logarithmic decrement method was applied to a succession of pairs of adjacent response cycles in order to obtain the variation of equivalent damping ratio with displacement amplitude. For this purpose, the displacement amplitude was defined as the mean amplitude of two adjacent response cycles.

Figure 2.8 presents the resulting variations of damping ratio with displacement amplitude for the five equipment items considered. For each equipment item, the results are presented for the uncoupled configuration and for all the coupled configurations tested. The presence of the conductor assemblies increases significantly the damping ratios of both interconnected equipment for all tests but one. The higher damping values were obtained for 2% slackness in the conductors. Note, however, that for this slackness value, the vibrational response of both interconnected equipment is nonlinear and a function of the amplitude of the response. Therefore, these apparent damping ratios at 2% slackness may not be representative of the actual free vibration responses of interconnected equipment items.

Another interesting result shown in Fig. 4.8 is the reduction of the damping ratio with displacement amplitude. This phenomenon occurs for about 50% of the tests and is contrary to the results observed for most structures where damping increases with displacement amplitude. Further studies are required to understand this phenomenon.

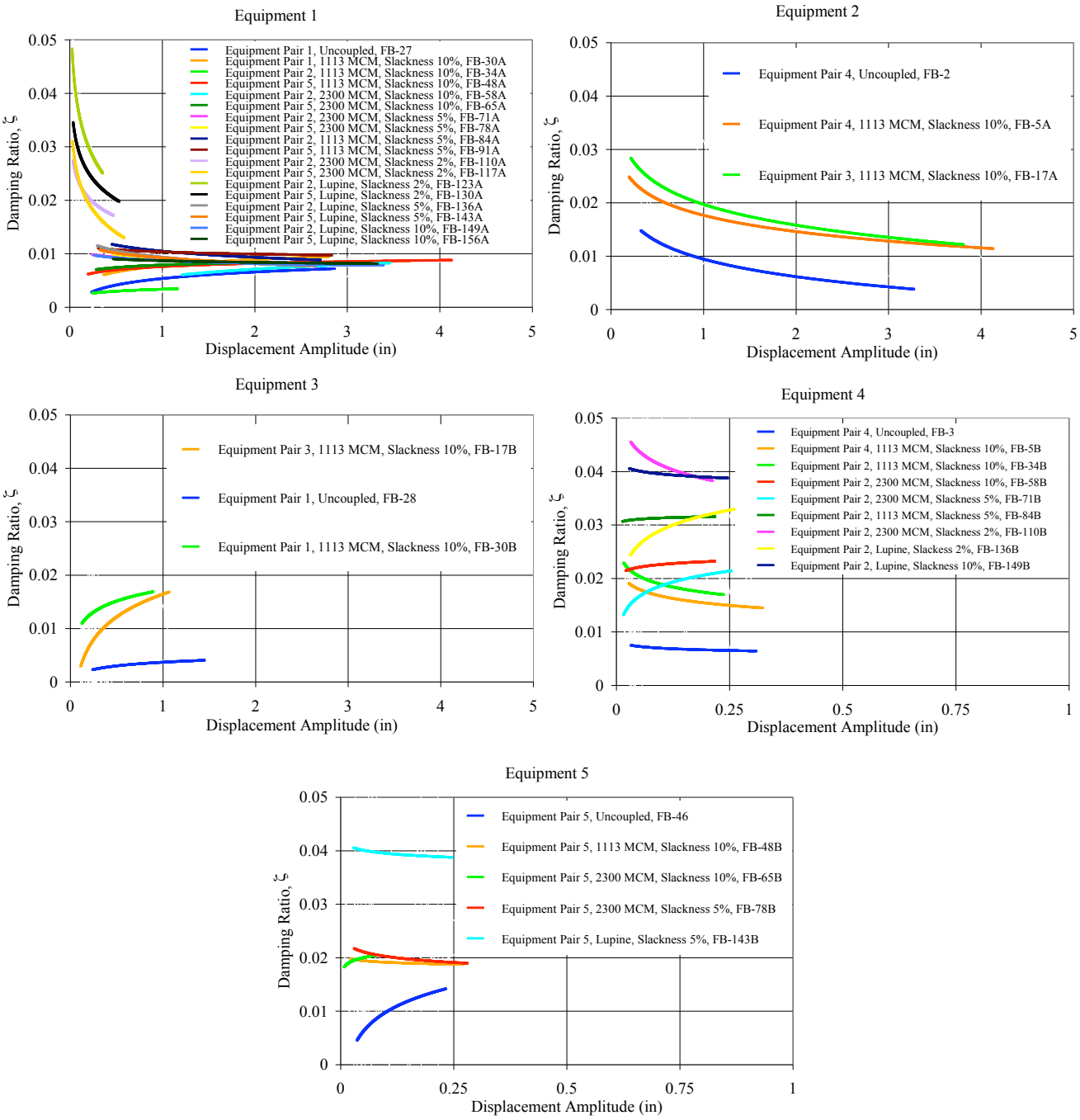

Figure 2.8 Variations of Equivalent Viscous Damping Ratio with Displacement Amplitude.

2.10 Results of Seismic Tests

The results of all seismic tests conducted on the five pairs of generic equipment specimens interconnected by the three different flexible conductor assemblies are presented in Appendix E. Included for each seismic test are time-history plots of:

- Absolute acceleration of the shake table
- Relative horizontal displacement at the top of Equipment A
- Relative horizontal displacement at the top of Equipment B
- Absolute horizontal acceleration at the top of Equipment A
- Absolute horizontal acceleration at the top of Equipment B
- Relative displacement between Equipment A and Equipment B
- Longitudinal absolute acceleration at mid-span of the conductor
- Transverse absolute acceleration at mid-span of the conductor
- Vertical absolute acceleration at mid-span of the conductor
- Horizontal force at the end of the conductor connected to Equipment A
- Horizontal force at the end of the conductor connected to Equipment B
- Force-displacement hysteresis loops at the connection of Equipment A
- Force-displacement hysteresis loops at the connection of Equipment B

For the seismic tests involving the stand-alone (uncoupled) equipment, it was observed that some horizontal forces were measured by the load-cells at the top of each equipment item. These forces were developed because of the inertia effect of the load cells themselves and of the connecting elements. The seismic tests involving interconnected equipment were corrected for this inertia effect by first computing an equivalent load cell mass m_{lc} as:

$$m_{lc} = \frac{F_u}{a_u} \tag{2.2}$$

where F_u is the force measured by the load cell at the top of an equipment during an uncoupled seismic test and a_u is the horizontal acceleration measured at the top of an equipment during an uncoupled seismic test.

The net horizontal force F_{nh} developed during a coupled seismic test was then computed by:

$$F_{nh} = F_c - m_{lc}\, a_c \tag{2.3}$$

where F_c is the force measured by the load cell at the top of an equipment during a coupled seismic test and a_c is the horizontal acceleration measured at the top of the equipment under consideration. This net horizontal force is reported in Appendix E for each equipment item under consideration.

No damage to any of the three flexible conductors was observed during all the seismic tests conducted. Two different types of dynamic response were observed during the seismic tests. The first type involves low interaction between the interconnected equipment due to a large slack (5 and 10%) and/or under low intensity ground motions. This low interaction response is illustrated in Fig. 2.9 that shows the various measured time-histories for the seismic test FB-21 involving Equipment Pair 3 connected by a pair of MCM 1113C conductors at 10% slackness and excited by the Tabas record at 50% of its amplitude. For this test, very little interaction between the equipment items took place. This can be seen by the completely different frequency contents between the relative displacement and absolute acceleration response of each equipment item. It is also interesting to note that the absolute vertical acceleration at mid-span of the connector is in phase with the absolute horizontal acceleration at the top of the flexible equipment A. This result indicates that the large horizontal movement of the flexible equipment A is transferred almost entirely into a vertical motion of the conductor with little transmission to the rigid equipment B.

The second type of dynamic response involves high interaction between the interconnected equipment due to a small slack (2%) and/or under high intensity ground motions. This high interaction response is illustrated in Fig. 2.10 that shows the various measured time-histories for the seismic test FB-19 involving the same configuration as that of Fig. 2.9 but excited this time by the Newhall record at 100% span. Because of the higher intensity ground motion, significant interaction occurred between the two interconnected equipment items. This in particular can be seen by observing the large vertical acceleration pulses (above 10 g) observed at mid-span of the conductor. These pulses induce peak horizontal forces simultaneously at both ends of the conductor.

Another interesting effect noted during the seismic tests is the transmission of horizontal forces at both ends of the conductor as a function of its slackness. Figure 2.11 illustrates this observation by showing the net horizontal force time-histories measured at the top of each equipment items for Tests FB-41, FB-36 and FB-91 involving Equipment Pair 2 connected by a pair of MCM 1113C conductors and excited by the Tabas record at 25% of its amplitude. The results are presented for the uncoupled equipment and for the coupled equipment at 10 and 2% slackness, respectively. When the two equipment items are uncoupled, the force at the top of each equipment item is obviously independent, involving very different frequency contents with peak values occurring at different times. When the conductor is introduced at a slackness of 10%, the force time-histories are still very different because of the lack of strong interaction, but some similar modulations begin to appear with peak values occurring at similar times. When the slackness is reduced to 2%, the two force time-histories have similar frequency contents and modulation. The peaks occur at similar times. Note also that much larger forces occur in tension than in compression since the acts as a tension-only longitudinal spring, since it is much tighter.

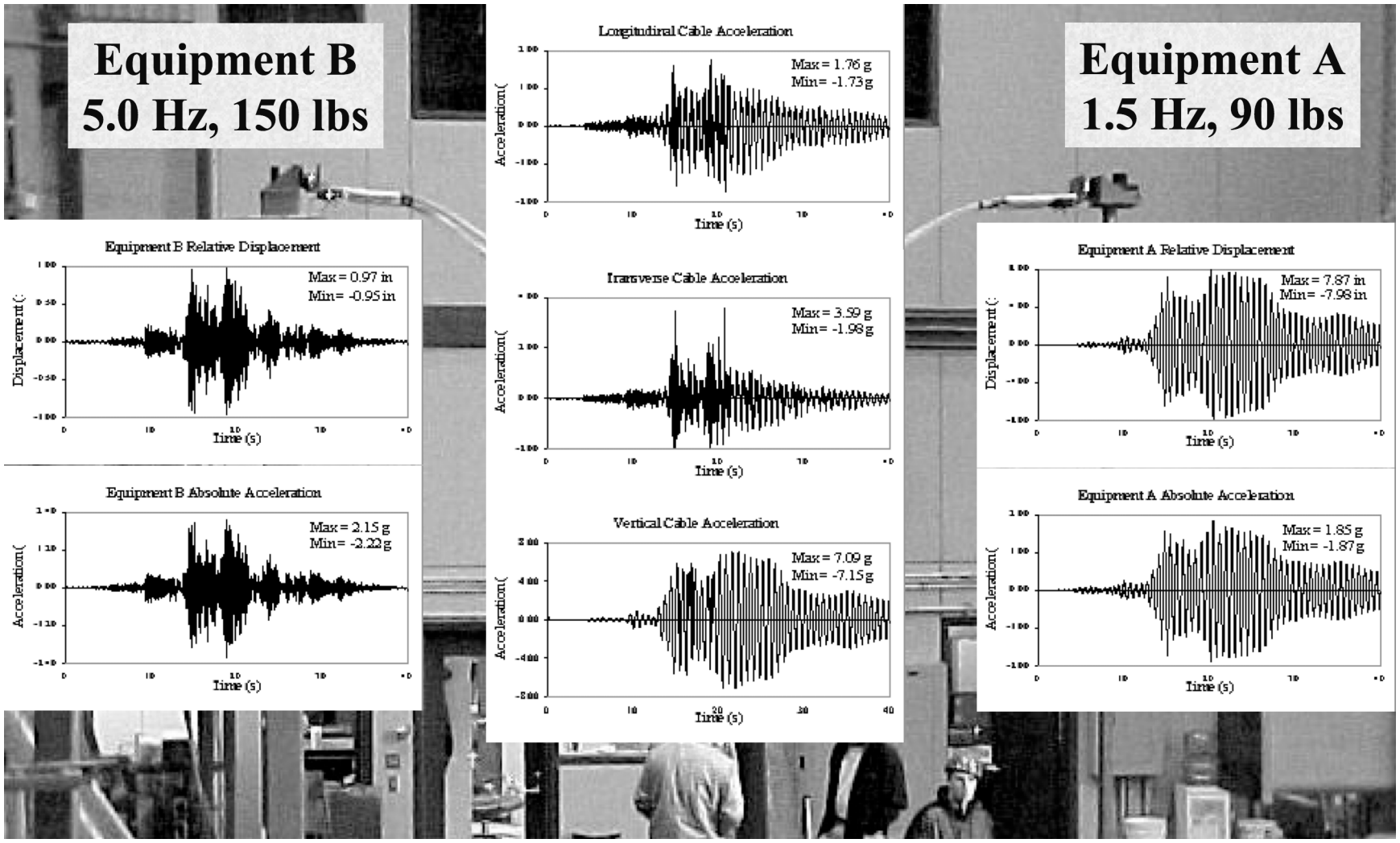

Figure 2.9 Measured Time-Histories for Seismic Test FB-21, Equipment Pair 3, Pair of MCM 1113C Conductors, 10% Slackness, Tabas Record, 50% Span.

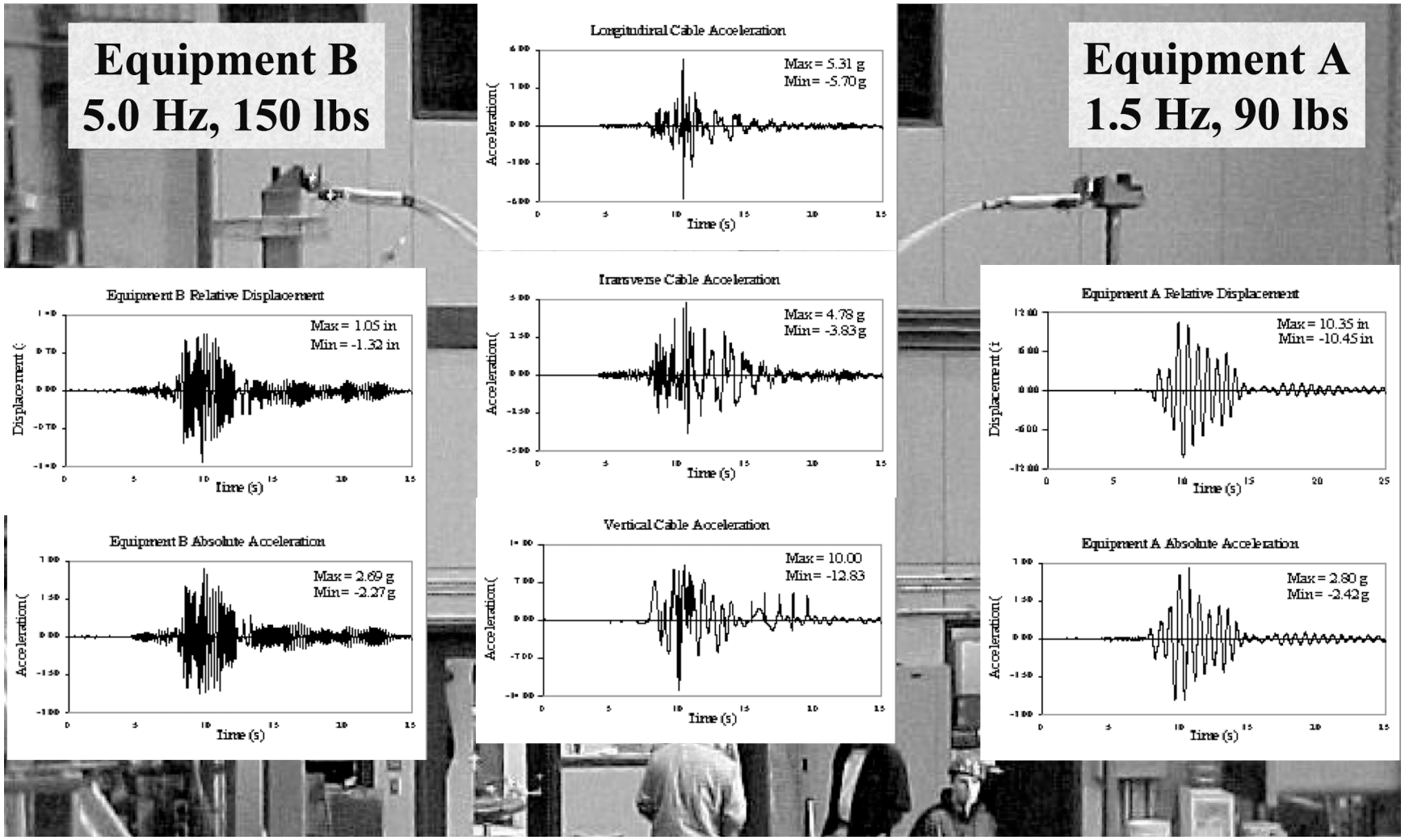

Figure 2.10 Measured Time-Histories for Seismic Test FB-19, Equipment Pair 3, Pair of MCM 1113C Conductors, 10% Slackness, Newhall Record, 10% Span.

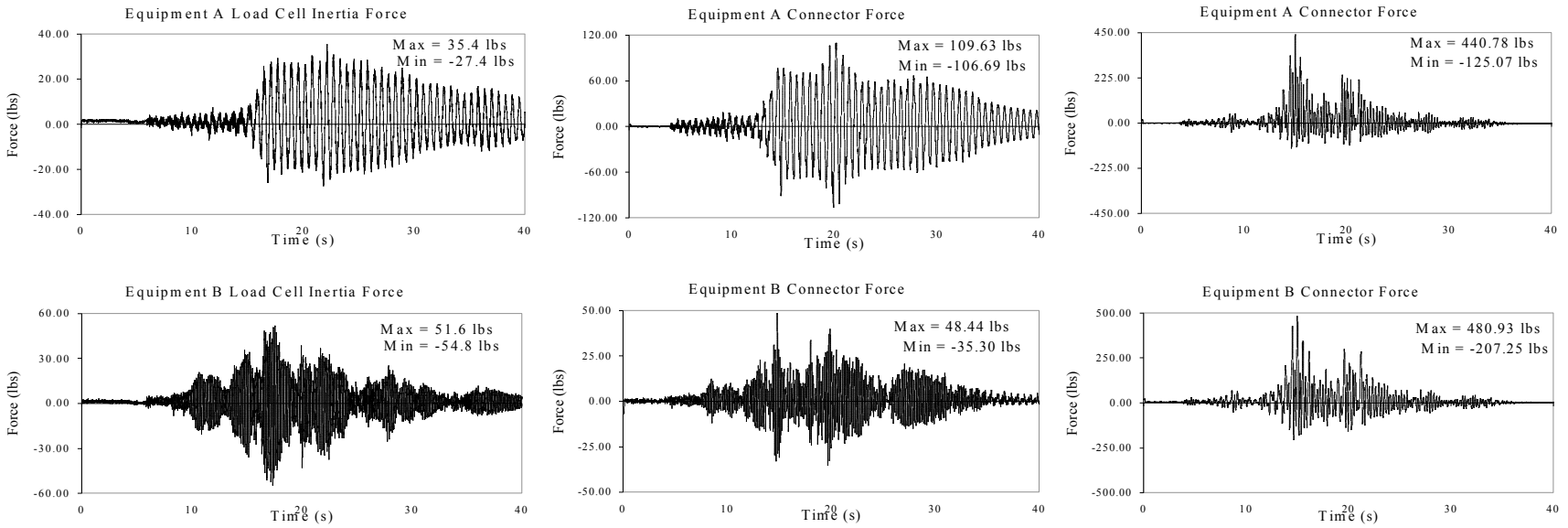

Figure 2.11 Net Horizontal Force Time-Histories at top of equipment items for Tests FB-41, FB-36 and FB-91, Equipment Pair 2, Pair of MCM 1113C Conductors, Tabas Record, 25% Span (Note: Different Vertical Scales).

The maximum experimental values recorded for all seismic tests are summarized in Tables 2.11 to 2.13 for 10, 5 and 2% slackness, respectively. Included in these tables for each seismic test are: the maximum relative displacement and maximum absolute acceleration at the top of both equipment specimens. The results for the stand-alone (uncoupled) tests are also included in each table. Note that, although no yielding occurred in the equipment specimens, the behavior of the uncoupled equipment specimens is not perfectly linear (e.g. the maximum displacement and acceleration values more than doubled when the ground motion intensity is increased by a factor of two). This non-linearity is particularly important for the flexible equipment A (1 and 2), and is believed to be the results of the rocking of the base and of the variation of effective damping with displacement amplitude.

The effect of the various flexible conductors on the dynamic response of the generic equipment specimens can be evaluated by defining a Displacement Amplification Factor (DAF) and an Acceleration Amplification Factor (AAF) as (Der Kiereghian et al., 1999; Filiatrault et al., 1999; Filiatrault and Kremmidas, 2000):

$$\text{DAF} = \frac{\text{Maximum Relative Displacement of Interconnected Equipment}}{\text{Maximum Relative Displacement of Stand Alone Equipment}} \tag{2.4}$$

$$\text{AAF} = \frac{\text{Maximum Absolute Acceleration of Interconnected Equipment}}{\text{Maximum Absolute Acceleration of Stand Alone Equipment}} \tag{2.5}$$

The DAF and AAF values computed at the top of Equipment A and Equipment B during the seismic tests are presented in Figs 2.12 to 2.17. The results are presented for Equipment Pairs 2 and 5 and for each ground motion, intensity level, conductor type, and slackness.

Table 2.11 Maximum Experimental Values from Seismic Tests, 10% slackness.

Pair	Ground Motion-Span (%)	Peak Relative Displacement Equipment A (in)				Peak Relative Displacement Equipment B (in)				Peak Absolute Acceleration Equipment A (g)				Peak Absolute Acceleration Equipment B (g)			
		1113C	2300 MCM	Lupine	Stand Alone	1113C	2300 MCM	Lupine	Stand Alone	1113C	2300 MCM	Lupine	Stand Alone	1113C	2300 MCM	Lupine	Stand Alone
1	Newhall-30	2.91	---	---	2.87	0.44	---	---	0.35	0.87	---	---	0.98	0.89	---	---	0.98
	Tabas-25	3.93	---	---	3.53	0.56	---	---	0.86	1.16	---	---	1.89	1.20	---	---	2.29
2	Newhall-30	3.04	2.98	2.91	2.87	0.11	0.10	0.20	0.13	0.88	0.89	0.89	0.98	0.54	0.45	0.65	0.56
	Tabas-25	4.21	4.00	3.91	3.53	0.26	0.26	0.37	0.35	1.26	1.22	1.19	1.89	1.30	1.34	1.43	1.98
	Tabas-50	---	7.71	7.52	7.37	---	0.51	0.62	0.61	---	2.26	2.18	3.67	---	2.77	2.64	3.21
3	Newhall-30	3.97	---	---	3.67	0.50	---	---	0.35	0.94	---	---	1.11	1.01	---	---	0.98
	Newhall-100	10.45	---	---	10.88	1.32	---	---	1.11	2.80	---	---	3.36	2.69	---	---	2.74
	Tabas-25	3.75	---	---	5.51	0.56	---	---	0.86	0.92	---	---	1.66	1.24	---	---	2.29
	Tabas-50	7.98	---	---	11.23	0.97	---	---	1.57	1.87	---	---	3.01	2.22	---	---	4.05
4	Newhall-30	3.91	---	---	3.67	0.15	---	---	0.13	0.95	---	---	1.11	0.52	---	---	0.56
	Newhall-100	11.65	---	---	10.88	0.49	---	---	0.49	2.80	---	---	3.36	2.31	---	---	2.45
	Tabas-25	3.72	---	---	5.51	0.29	---	---	0.35	0.89	---	---	1.66	1.45	---	---	1.98
	Tabas-50	7.48	---	---	11.23	0.58	---	---	0.61	1.74	---	---	3.01	2.92	---	---	3.21
5	Newhall-30	3.01	2.94	2.81	2.87	0.06	0.07	0.06	0.07	0.89	0.88	0.88	0.98	0.42	0.60	0.64	0.74
	Tabas-25	4.21	3.91	3.51	3.53	0.06	0.09	0.08	0.12	1.25	1.48	1.12	1.89	0.83	1.11	0.99	1.57
	Tabas-50	7.73	7.66	7.48	7.37	0.12	0.15	0.15	0.17	2.25	2.21	2.13	3.67	1.47	2.01	1.88	2.30

Table 2.12 Maximum Experimental Values from Seismic Tests, 5% slackness.

Pair	Ground Motion-Span (%)	Peak Relative Displacement Equipment A (in)				Peak Relative Displacement Equipment B (in)				Peak Absolute Acceleration Equipment A (g)				Peak Absolute Acceleration Equipment B (g)			
		1113C	2300 MCM	Lupine	Stand Alone	1113C	2300 MCM	Lupine	Stand Alone	1113C	2300 MCM	Lupine	Stand Alone	1113C	2300 MCM	Lupine	Stand Alone
2	Newhall-30	3.32	2.94	2.82	2.87	0.11	0.12	0.24	0.13	0.90	0.87	0.85	0.98	0.41	0.53	0.63	0.56
	Tabas-25	3.67	4.03	3.76	3.53	0.20	0.21	0.36	0.35	1.08	1.21	1.12	1.89	0.94	1.15	1.16	1.98
	Tabas-50	6.86	7.38	5.97	7.37	0.37	0.47	0.73	0.67	2.05	2.62	2.05	3.67	1.69	2.35	1.97	3.21
5	Newhall-30	3.27	3.18	2.92	2.87	0.07	0.07	0.07	0.07	0.94	0.92	0.86	0.98	0.37	0.64	0.52	0.74
	Tabas-25	3.57	4.19	3.88	3.53	0.08	0.07	0.08	0.12	1.01	1.23	1.18	1.89	0.70	0.88	0.89	1.57
	Tabas-50	6.83	7.35	6.06	7.37	0.18	0.14	0.45	0.17	2.07	2.14	1.95	3.67	2.27	1.91	1.97	2.30

Table 2.13 Maximum Experimental Values from Seismic Tests, 2% slackness.

Pair	Ground Motion-Span (%)	Peak Relative Displacement Equipment A (in)				Peak Relative Displacement Equipment B (in)				Peak Absolute Acceleration Equipment A (g)				Peak Absolute Acceleration Equipment B (g)			
		1113C	2300 MCM	Lupine	Stand Alone	1113C	2300 MCM	Lupine	Stand Alone	1113C	2300 MCM	Lupine	Stand Alone	1113C	2300 MCM	Lupine	Stand Alone
2	Newhall-30	1.01	2.46	2.42	2.87	0.33	0.16	0.32	0.13	0.72	0.92	0.88	0.98	0.77	0.61	1.13	0.56
	Newhall-100	3.69	---	6.71	---	0.66	---	0.98	---	2.38	---	3.44	---	2.72	---	5.69	---
	Tabas-25	1.62	3.03	2.59	3.53	0.45	0.26	0.40	0.35	0.95	1.32	1.01	1.89	1.27	1.38	1.29	1.98
	Tabas-50	3.62	6.45	5.51	7.37	0.58	1.85	1.59	0.67	2.14	3.06	2.96	3.67	3.32	5.09	4.84	3.21
5	Newhall-30	1.34	2.83	2.47	2.87	0.27	0.09	0.15	0.07	0.98	0.97	0.84	0.98	1.45	0.60	0.92	0.74
	Newhall-100	3.63	6.64	6.16	---	0.26	1.91	1.84	---	2.89	3.87	3.93	---	3.59	4.74	4.93	---
	Tabas-25	1.93	2.98	2.67	3.53	0.35	0.08	0.22	0.12	1.37	1.23	0.93	1.89	2.14	1.01	1.41	1.57
	Tabas-50	3.78	6.22	5.20	7.37	0.90	0.61	1.10	0.17	3.39	3.77	2.82	3.67	3.80	5.17	4.41	2.30

Equipment Pair 2

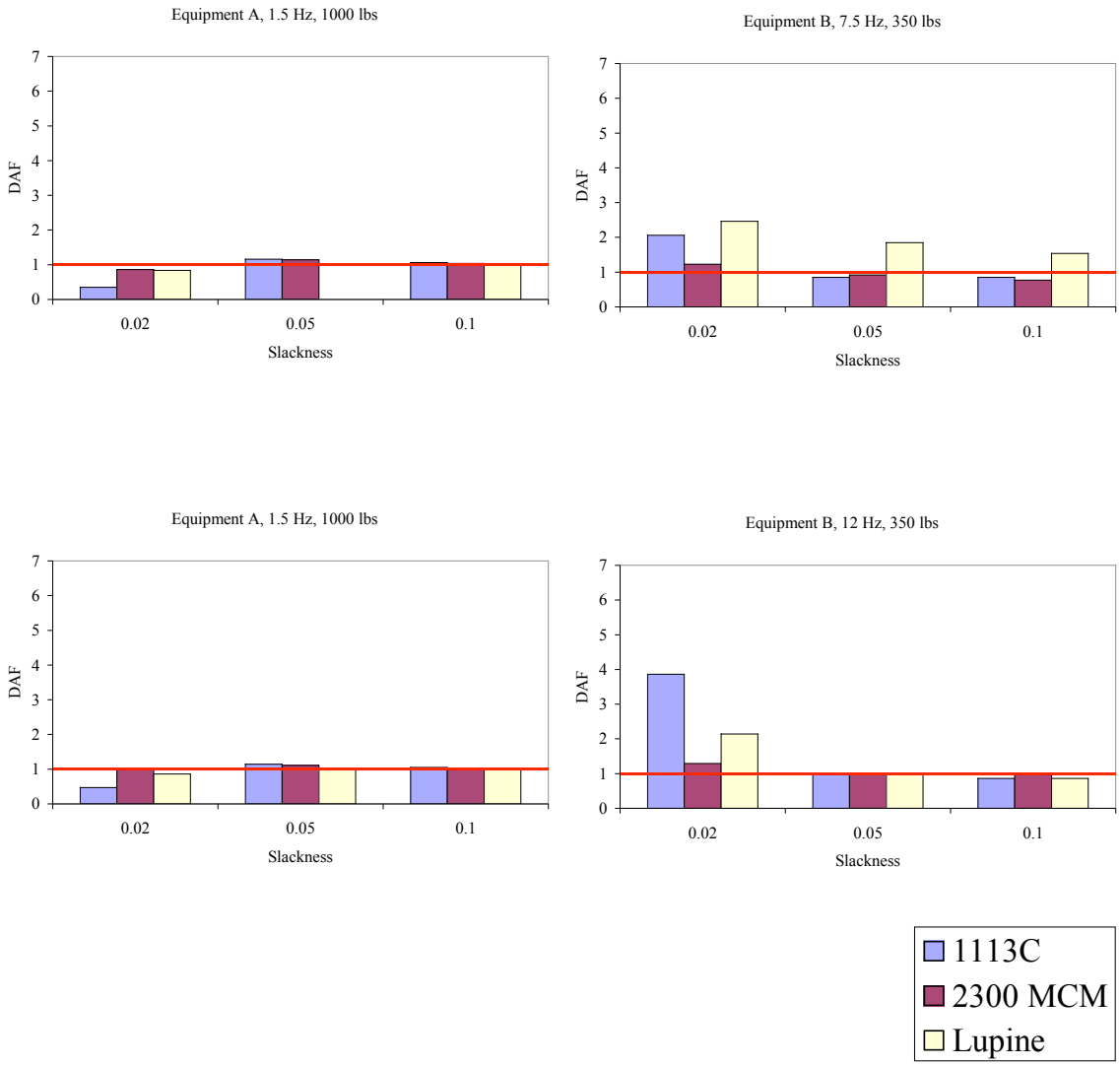

Equipment Pair 5

Figure 2.12 Displacement Amplification Factor (DAF)

Newhall Ground Motion, 30% Span.

Equipment Pair 2

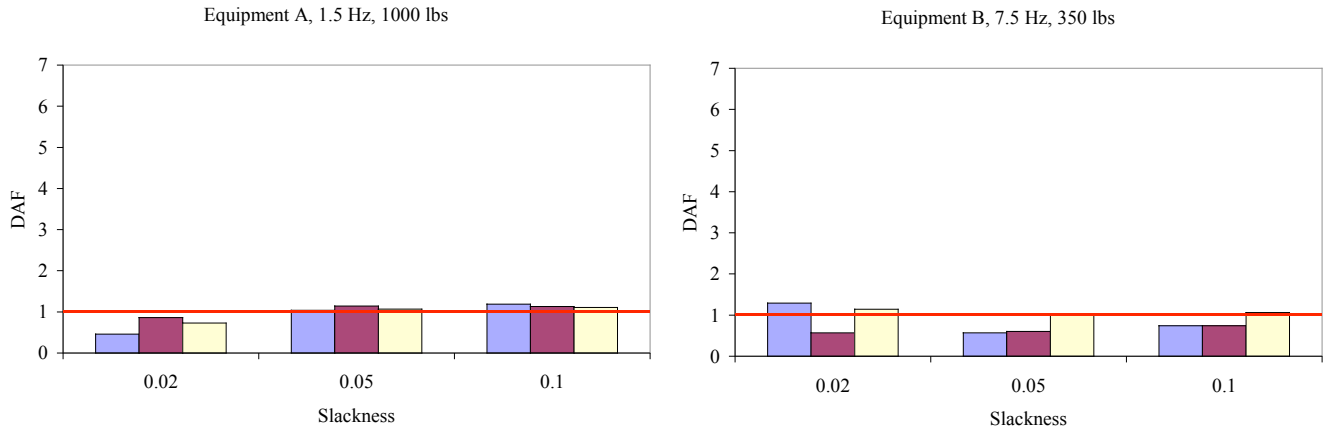

Equipment Pair 5

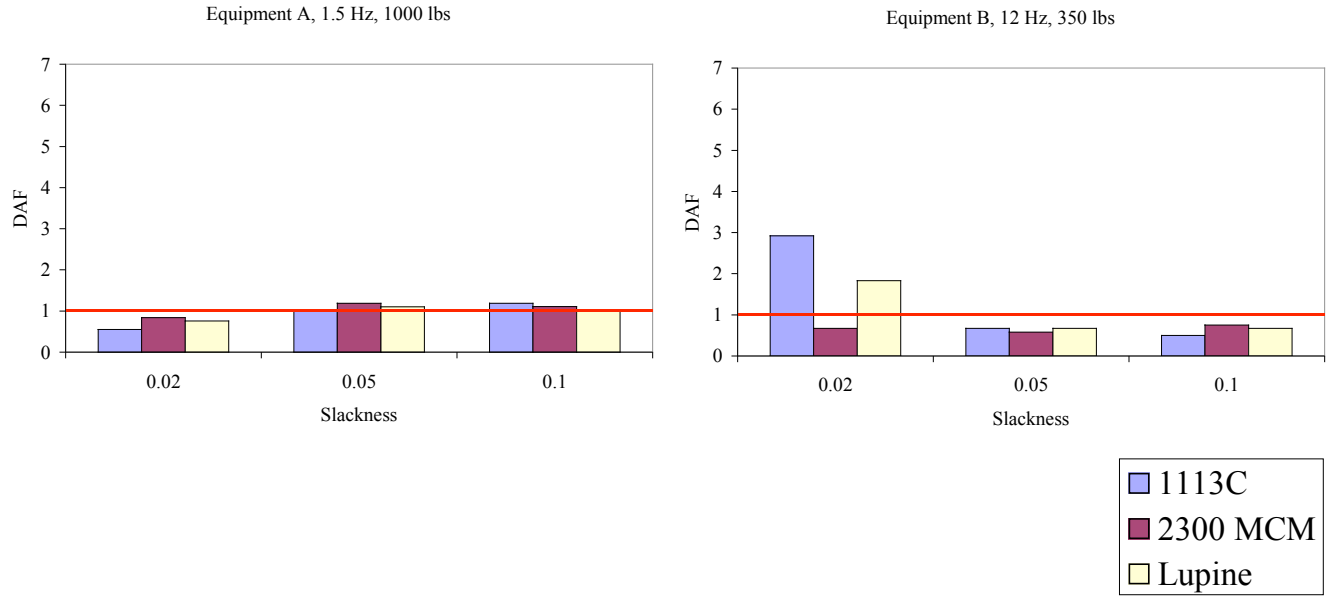

Figure 2.13 Displacement Amplification Factor (DAF)

Tabas Ground Motion, 25% Span.

Equipment Pair 2

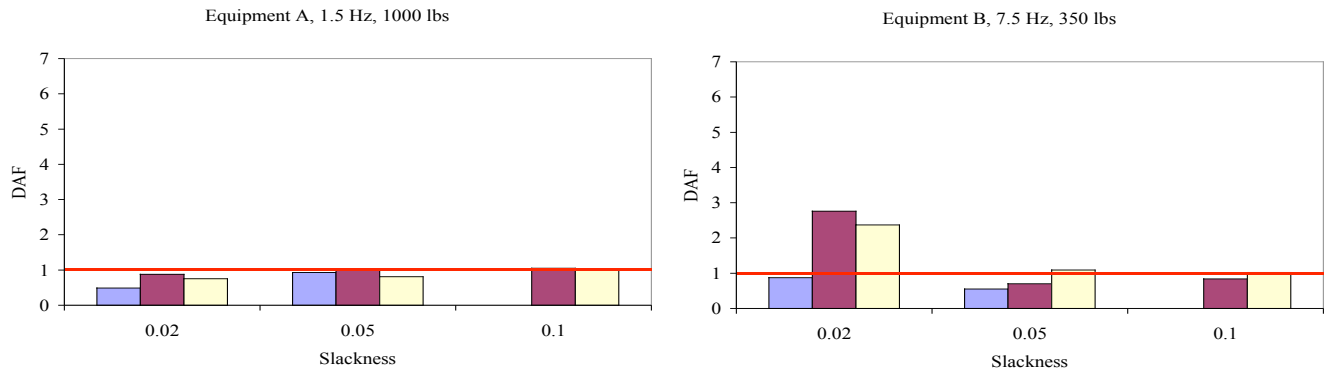

Equipment Pair 5

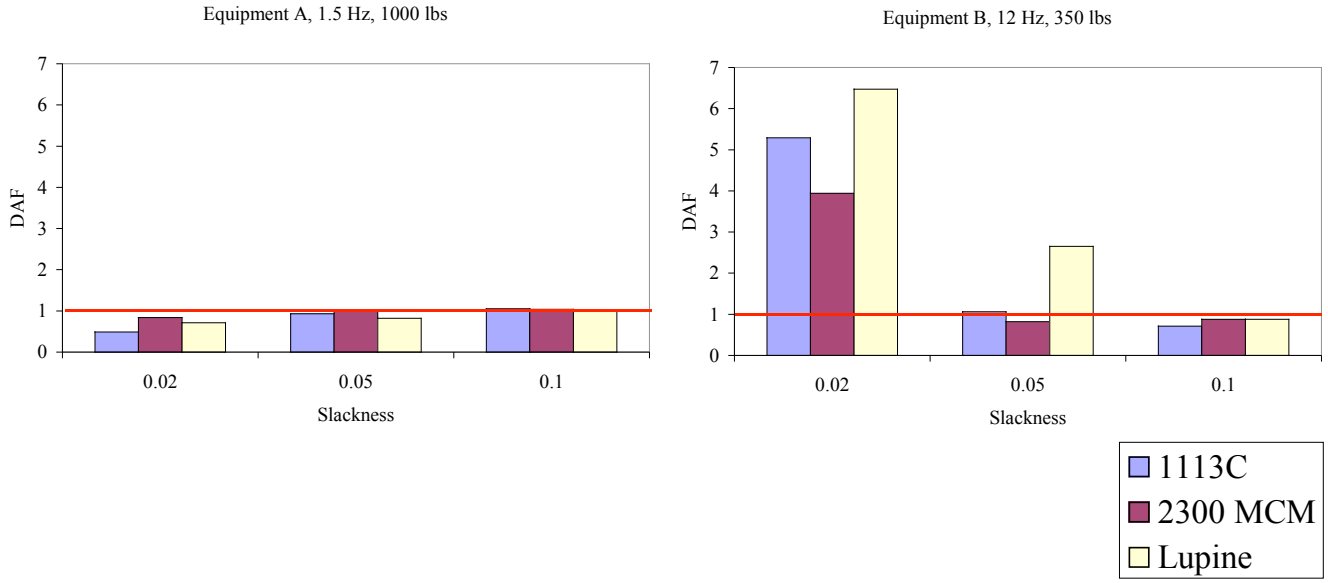

Figure 2.14 Displacement Amplification Factor (DAF)

Tabas Ground Motion, 50% Span.

Equipment Pair 2

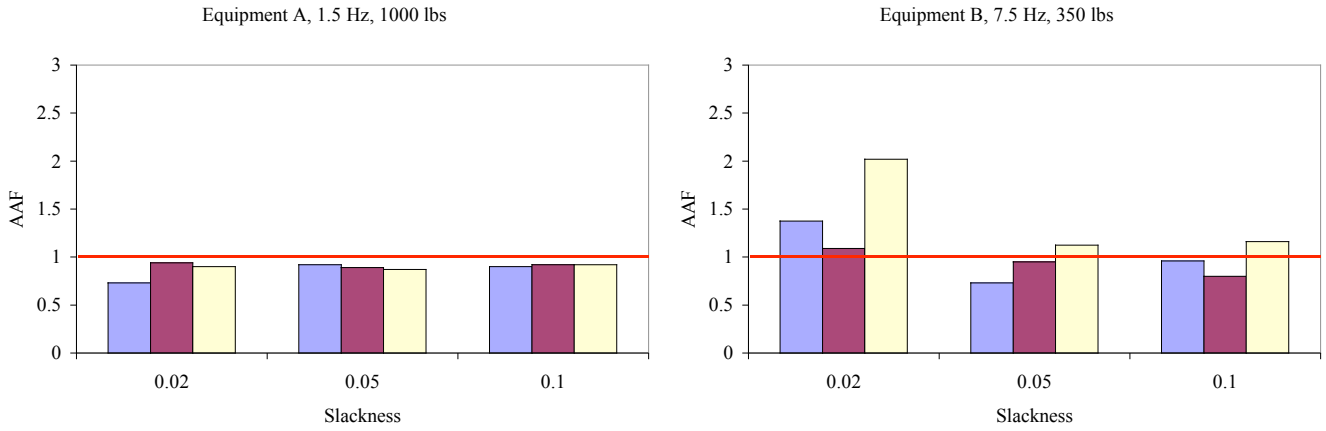

Equipment Pair 5

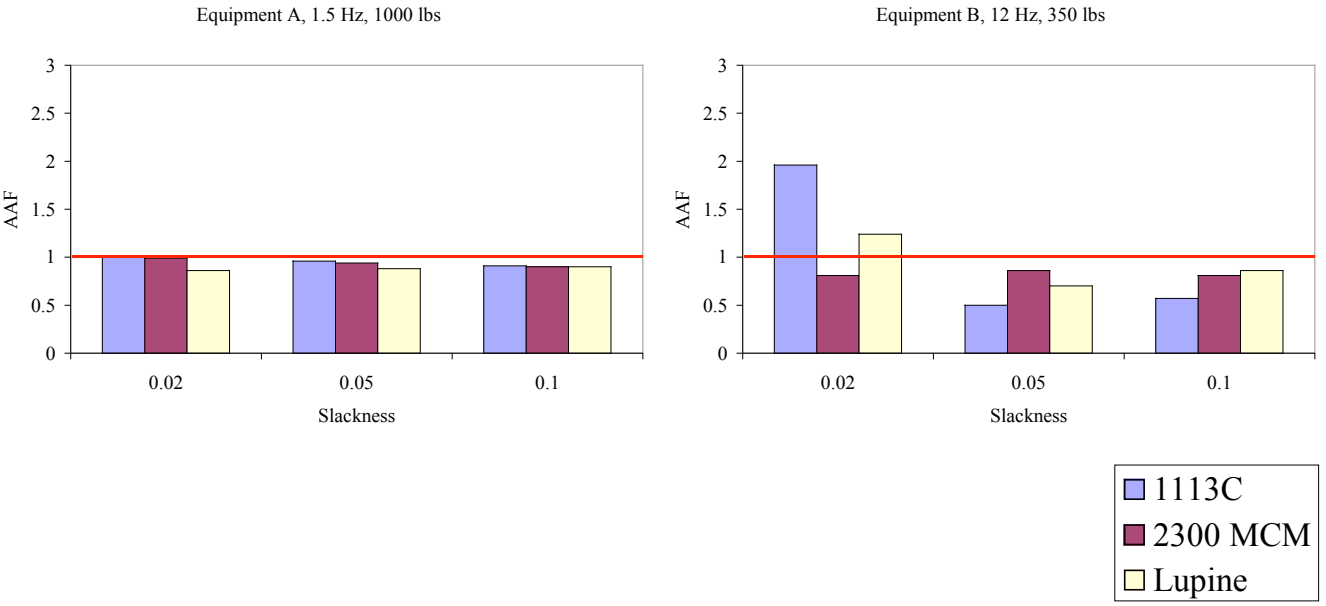

Figure 2.15 Acceleration Amplification Factor (AAF)

Newhall Ground Motion, 30% Span.

Equipment Pair 2

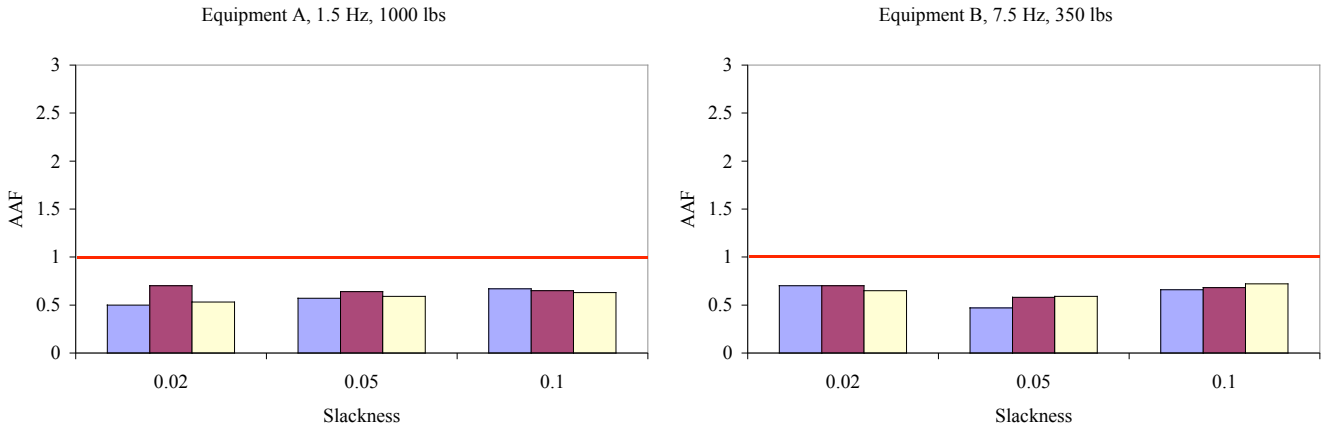

Equipment Pair 5

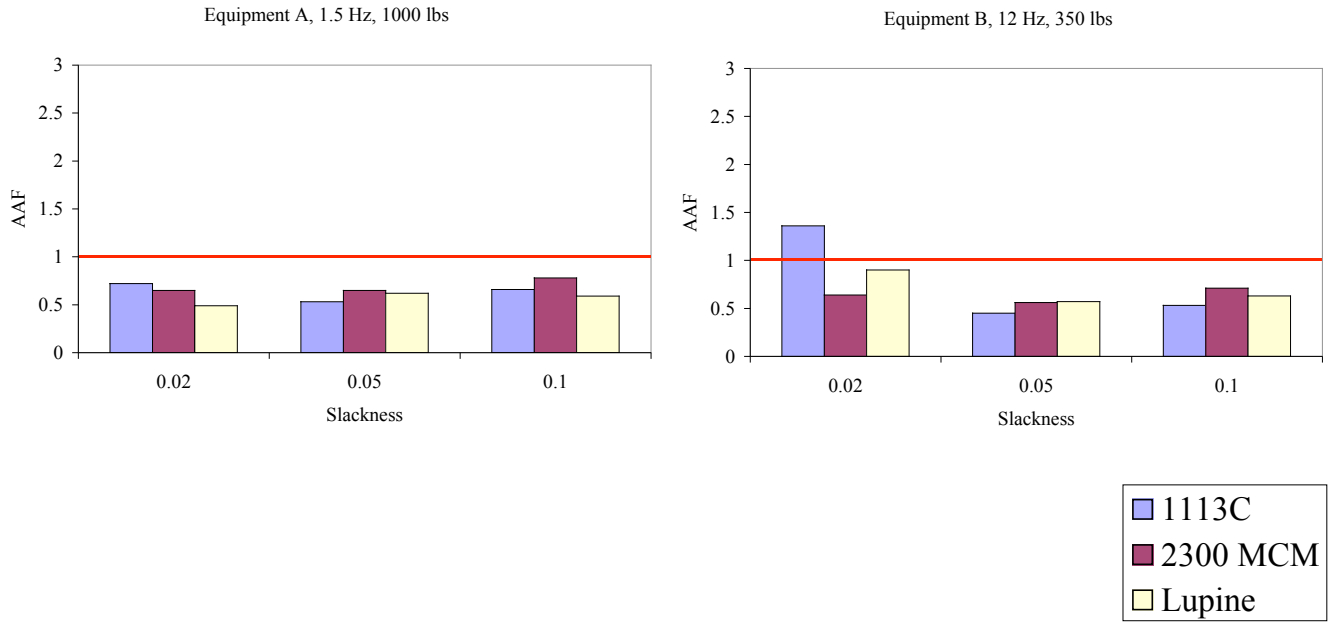

Figure 2.16 Acceleration Amplification Factor (AAF)

Tabas Ground Motion, 25% Span.

Equipment Pair 2

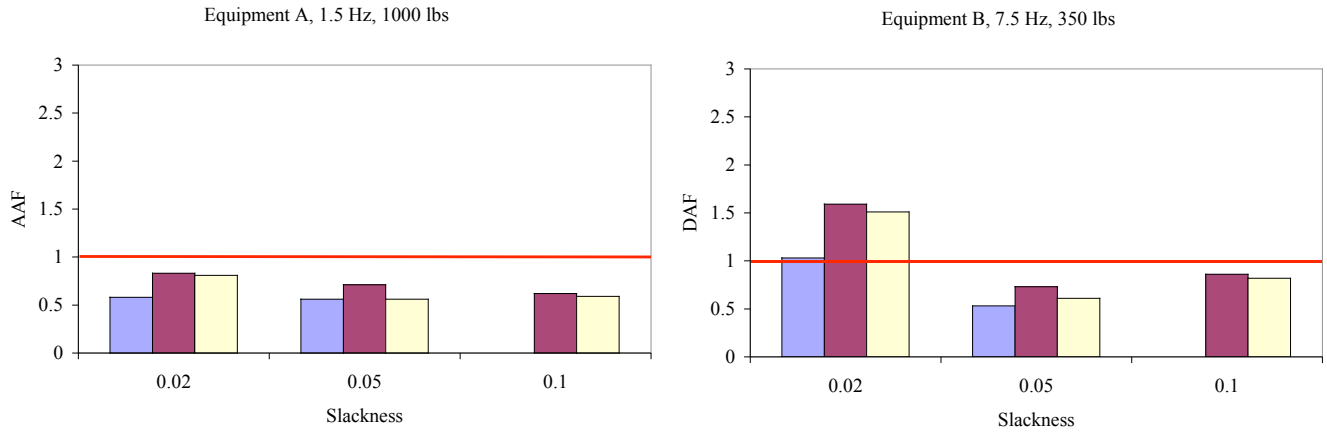

Equipment Pair 5

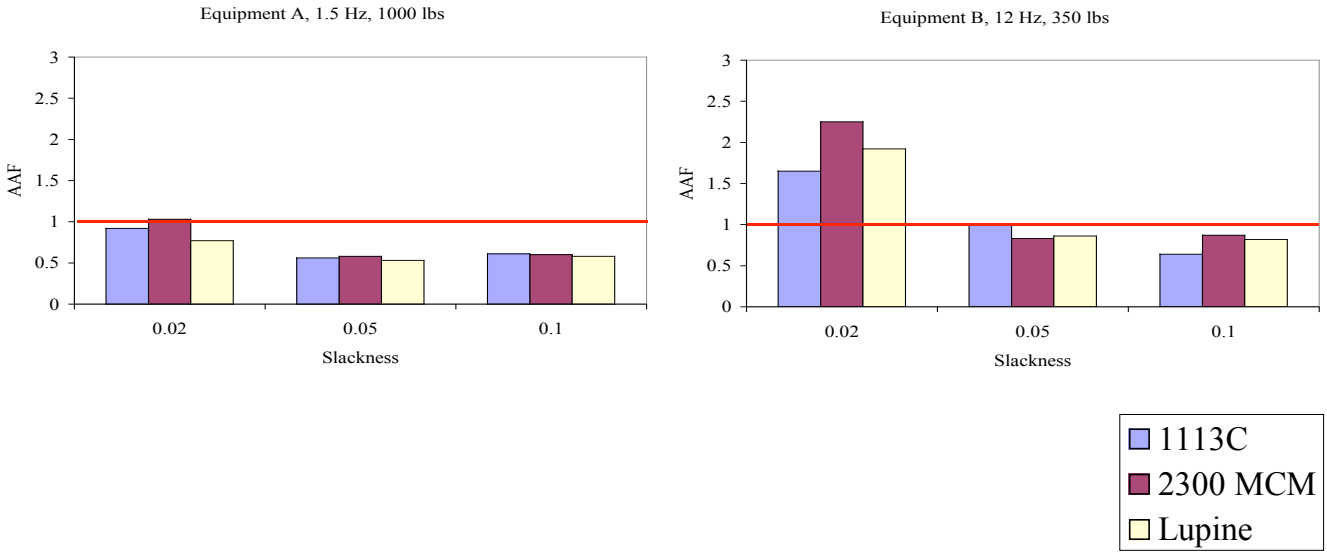

Figure 2.17 Acceleration Amplification Factor (AAF)

Tabas Ground Motion, 50% Span.

Although the presence of the flexible conductors can amplify or reduce the dynamic response of equipment components depending on their dynamic characteristics, slackness of the conductor and the frequency content and intensity of the earthquake ground motion input, the results presented in Figs. 2.12 to 2.17 show several clear trends:

1. For all slackness values, the dynamic response of the flexible equipment A is not affected appreciably by any of the three flexible conductors tested. The DAF and AAF values are less than or equal to unity in most cases.

2. At 5 and 10% slackness, the dynamic response of the rigid equipment B is generally reduced by the presence of the conductor assemblies. The reduction in AAF exceeds the reduction in DAF.

3. At 2% slackness, the dynamic response of the rigid equipment B can be significantly increased once the conductor assemblies become tight and act as tension-only springs. This amplification of the dynamic response increases with the ground motion intensity. The maximum DAF and AAF values measured for the rigid equipment B was over 6 and 2, respectively, for the Equipment Pair 5 under the Tabas ground motion at 50% span.

The maximum horizontal forces in the conductors at the top of each interconnected equipment items recorded for all seismic tests are presented in Tables 2.14 to 2.16 for 10, 5 and 2% slackness, respectively.

Table 2.14 Maximum Horizontal Forces in Conductors from Seismic Tests, 10% Slackness

Pair	Ground Motion-Span (%)	Maximum Force at Top of Equipment A (lbs)			Maximum Force at Top of Equipment B (lbs)		
		1113C	2300 MCM	Lupine	1113C	2300 MCM	Lupine
1	Newhall-30	74	---	---	29	---	---
	Tabas-25	89	---	---	36	---	---
2	Newhall-30	79	105	77	19	76	60
	Tabas-25	110	156	118	48	131	48
	Tabas-50	---	239	183	---	187	170
3	Newhall-30	90	---	---	31	---	---
	Newhall-100	250	---	---	139	---	---
	Tabas-25	76	---	---	41	---	---
	Tabas-50	157	---	---	79	---	---
4	Newhall-30	66	---	---	19	---	---
	Newhall-100	208	---	---	87	---	---
	Tabas-25	73	---	---	40	---	---
	Tabas-50	159	---	---	76	---	---
5	Newhall-30	87	113	85	36	90	43
	Tabas-25	119	138	109	35	113	18
	Tabas-50	184	231	176	59	180	52

Table 2.15 Maximum Horizontal Forces in Conductors from Seismic Tests, 5% Slackness

Pair	Ground Motion-Span (%)	Maximum Force at Top of Equipment A (lbs)			Maximum Force at Top of Equipment B (lbs)		
		1113C	2300 MCM	Lupine	1113C	2300 MCM	Lupine
2	Newhall-30	96	132	106	52	101	37
	Tabas-25	122	181	167	68	145	95
	Tabas-50	201	225	265	92	178	298
5	Newhall-30	91	132	78	45	105	47
	Tabas-25	116	168	79	54	106	79
	Tabas-50	192	201	306	153	170	322

Table 2.16 Maximum Horizontal Forces in Conductors from Seismic Tests, 2% Slackness

Pair	Ground Motion-Span (%)	Maximum Force at Top of Equipment A (lbs)			Maximum Force at Top of Equipment B (lbs)		
		1113C	2300 MCM	Lupine	1113C	2300 MCM	Lupine
2	Newhall-30	266	146	202	340	117	215
	Newhall-100	1240	---	2084	1585	---	2358
	Tabas-25	441	228	206	481	166	216
	Tabas-50	1142	1501	1320	1321	1667	1522
5	Newhall-30	512	129	181	609	100	227
	Newhall-100	1639	2461	2688	2146	2926	2774
	Tabas-25	654	174	258	791	143	363
	Tabas-50	1598	1789	1546	1865	2951	1774

The maximum horizontal forces in the conductors developed at the top of equipment A and equipment B during the seismic tests are presented in Figs. 2.18 to 2.20. Again, the results are presented for Equipment Pairs 2 and 5 and for each ground motion, intensity level, conductor type, and slackness.

At 5 and 10% slackness, the forces generated at the top of the interconnected equipment are small. The maximum measured force was 322 lbs at the top of the stiff equipment B of equipment pair 5 interconnected by the Lupine conductor with 5% slackness and excited by the Tabas ground motion at 50% span. As noted previously, in most cases, the force at the top of the flexible equipment A is larger than the force at the top of the stiff equipment B.

At 2% slackness, the forces generated at the top of the interconnected equipment are an order of magnitude higher that that measured at 5 and 10% slackness. The maximum measured force was 2951 lbs at the top of the stiff equipment B of equipment pair 5 interconnected by the 2300 MCM conductor and excited by the Tabas ground motion. For this slackness, the forces at the top of both interconnected equipment are similar.

Note that the conductor forces shown in the figures were obtained by equation (2.3) and do not reflect the total demands on the equipment items since the inertia forces have been removed.

Equipment Pair 2

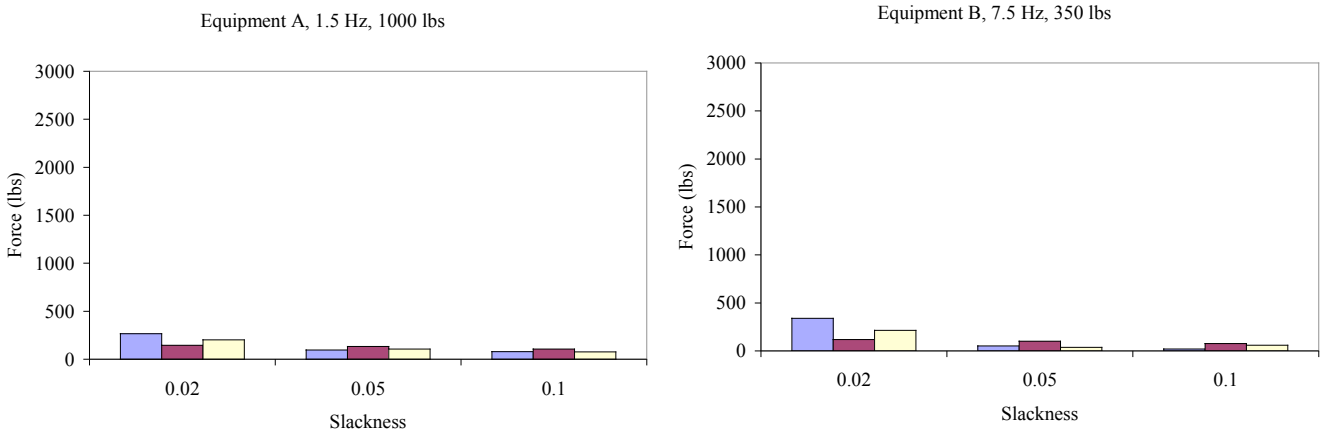

Equipment Pair 5

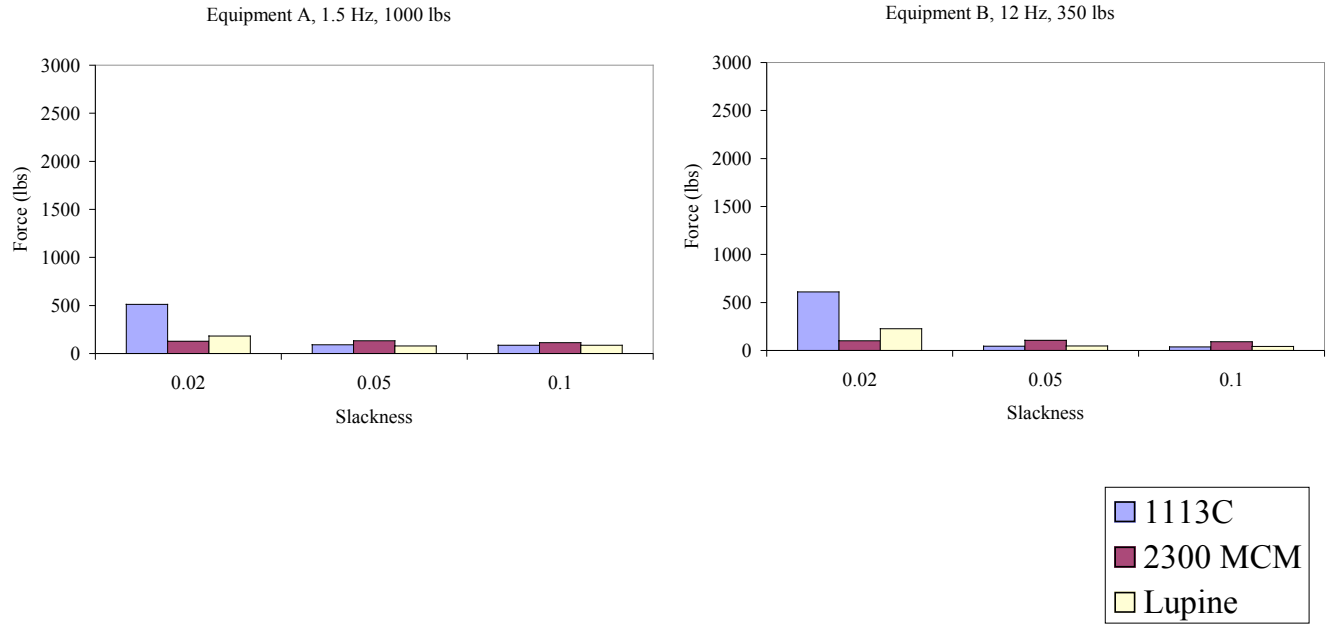

Figure 2.18 Maximum Horizontal Forces Conductors, Newhall Ground Motion, 30% Span.

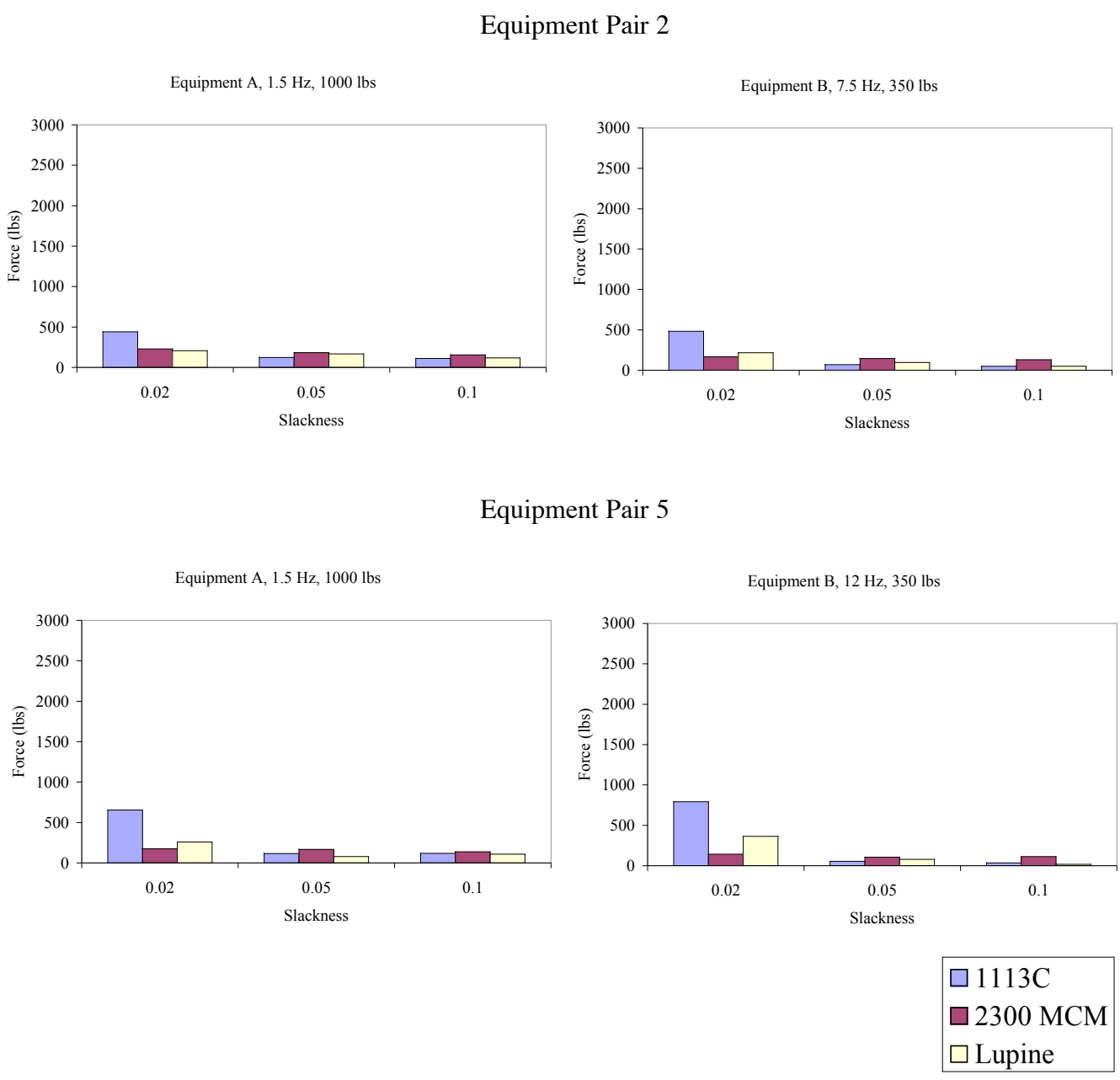

Figure 2.19 Maximum Horizontal Forces Conductors, Tabas Ground Motion, 25% Span.

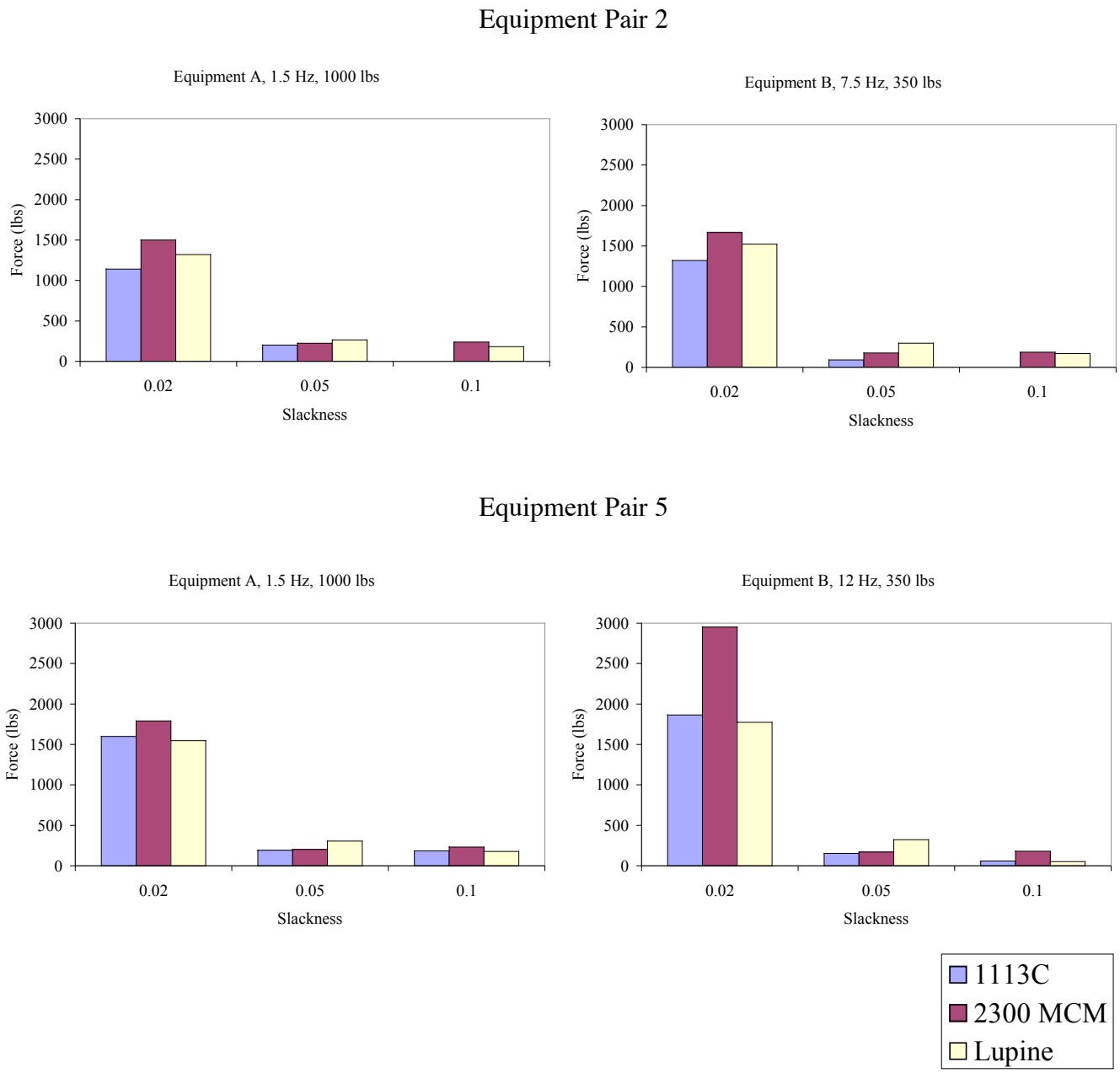

Figure 2.20 Maximum Horizontal Forces Conductors, Tabas Ground Motion, 50% Span.

2.11 Modal Participation Factors of Interconnected Equipment

As discussed in Section 2.1, one of the most important parameters in determining the maximum displacement of an equipment item is its first modal participation factor. In this section, the influence of flexible connections between pairs of equipment is evaluated on the basis of the results of the shake table tests. It is assumed that the connection slackness is sufficient for the individual natural frequencies of the interconnected equipment not to be significantly affected. The influence of flexible connections is characterized by a calibration factor to be applied to the modal participation factor for stand-alone equipment. With this approach, the interaction effect can be taken into account approximately without recourse to a full dynamic analysis of the interconnected equipment.

The generic equipment items used in the shake table tests can be represented by a beam of constant properties, with a lumped mass at the top, as illustrated in Fig. 2.21.

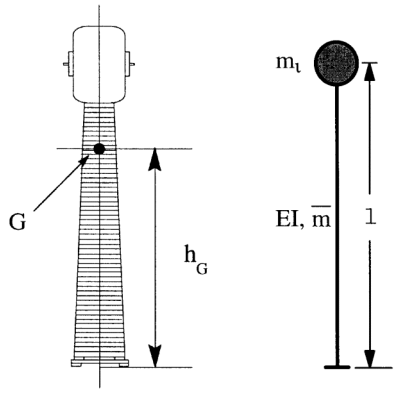

Figure 2.21 Representation of Equipment Item by a Beam of Constant Properties, with a Lumped Mass at the Top (adapted from Dastous et al., 2002).

Using the Bernoulli-Euler beam theory, neglecting axial-force effects, shear deformation and rotary inertia, the mode shapes $\psi(y)$ for such a distributed-parameter system are of the form (Clough and Penzien, 1993):

$$\psi(y) = A_1 \sin(ay) + A_2 \cos(ay) + A_3 \sinh(ay) + A_4 \cosh(ay) \qquad (2.6)$$

where A_i are constants to be determined from the boundary conditions, a is a constant related to the beam properties and y is the coordinate along the beam span.

Using equation (2.6), the fundamental modal participation factor α_1 can be computed (Clough and Penzien, 1993):

$$\alpha_1 = \frac{\psi(y_o)\left[\int_0^l \overline{m}(y)\psi(y)dy + m_t\psi(y_o)\right]}{\int_0^l \overline{m}(y)[\psi(y)]^2 dy + m_t[\psi(y_o)]^2} \qquad (2.7)$$

where $\psi(y_o)$ is the value of the fundamental mode shape at the attachment point y_0 (scaled here to unity) and $\overline{m}(y)$ is the mass per unit length of the beam (assumed constant here) and l is the length of the beam.

From equations (2.7) and (2.6), it can be demonstrated that the fundamental mode shape does not depends on the beam properties but is only a function of the ratio m_t/M, where m_t is the lumped mass at the top of the beam and M is the total mass of the beam.

This result is illustrated in Fig. 2.22, which shows the variation of the first modal participation factor α_1 with the m_t/M ratio. As m_t/M reduces, α_1 converges to the solution for a prismatic beam ($\alpha_1 = 1.566$). As m_t/M increases, α_1 converges to 1, which the solution for a lumped single-degree-of-freedom system.

Table 2.17 compares the first modal participation factor of each stand-alone specimen, as obtained from Fig. 2.22, with the mean value obtained from the shake table tests conducted. The experimental modal participation factors were obtained from equation (2.1), assuming 2% equivalent viscous damping. Good agreement is observed for the first two specimens (low-frequency equipment). For the high-frequency equipment (3,4 and 5), the measured first modal-participation factors are significantly higher than those predicted. This discrepancy between the experimental and analytical results could be caused by the rocking at the base of these stiff cantilevers observed during the tests. This phenomenon was due to the flexibility of the connection between the base of the equipment and the shake table and is not taken into account in the analysis results shown in Fig. 2.22.

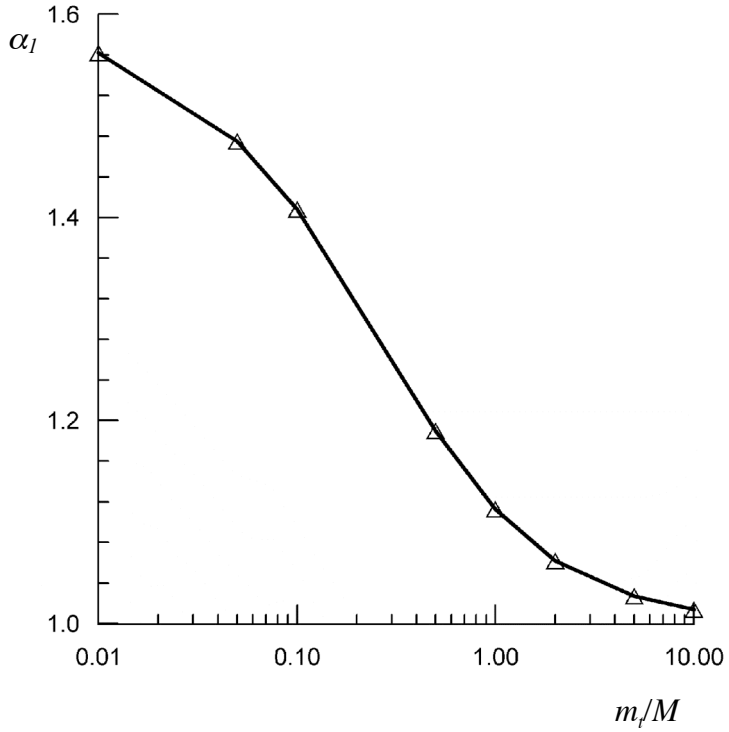

Figure 2.22 First Modal Participation Factor for Beam with Lumped Mass (from Dastous et al., 2002).

Table 2.17 First Modal Participation Factors for Standalone Equipment Specimens

Equipment No.	m_t/M	α_1 (Tests)	α_1 (Fig. 2.22)
1	4.17	1.05	1.03
2	1.20	1.12	1.11
3	0.27	1.70	1.28
4	0.15	1.90	1.36
5	0.15	3.03	1.36

For each shake table test conducted at 5% and 10% slackness, equation (2.1) was used to estimate the first modal participation factor for each interconnected equipment item. A correction factor CF was then computed by normalizing each modal participation factor of interconnected equipment by the corresponding stand-alone first modal-participation factor. The latter was obtained from the shake table tests on the standalone equipment. Note that all spectral values in equation (2.1) were taken at 2% damping.

The resulting correction factors are plotted in Fig. 2.23 for the two connection slackness values considered in the study (5% and 10%). The data for 2% slackness was not included since strong nonlinear interaction occurred at that value and it was not possible to identify the individual natural frequencies of the connected equipment.

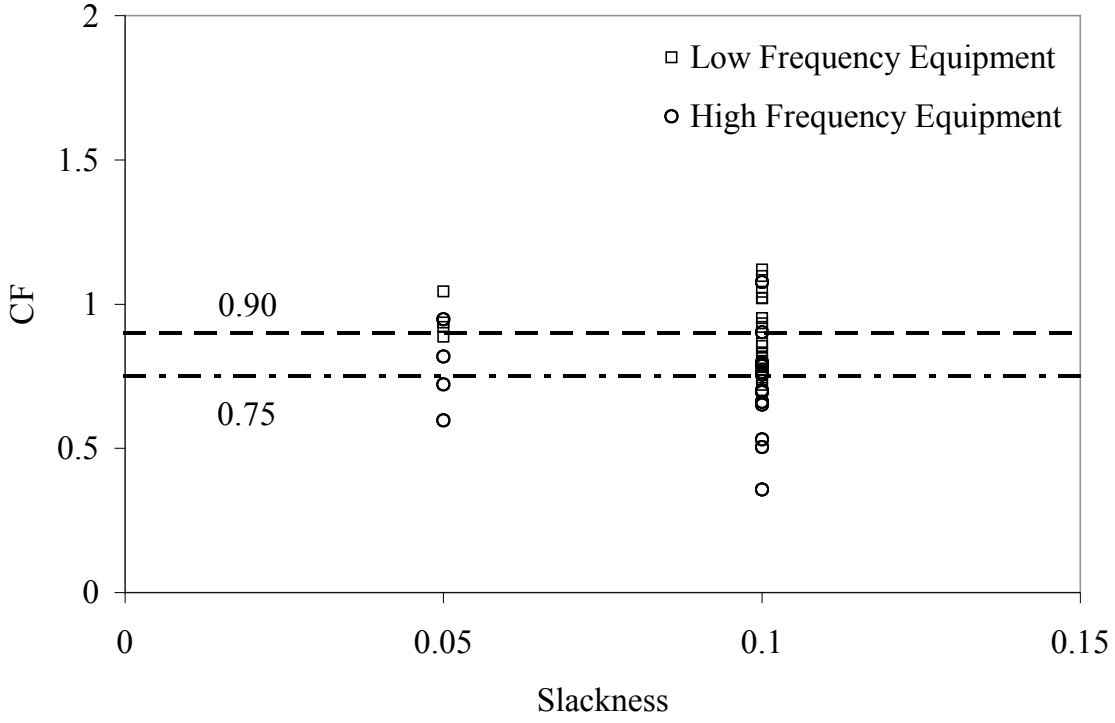

Figure 2.23 Correction Factors for the First Modal Participation Factors of Interconnected Equipment.

The correction factors are slightly higher for the low-frequency equipment (1 and 2) than for the high-frequency equipment (3,4 and 5). Most of the computed CF values are less than unity, indicating that the first modal participation factor of the equipment is reduced by the presence of the connection. This is caused by the added mass of the connection applied at the top of the equipment. This added mass increases the m_t/m ratio, and thereby reduces the modal participation factor (see Fig. 2.22).

Also shown in Fig. 2.23 are the mean values of CF for the low-frequency equipment (0.90) and the high-frequency equipment (0.75). Until more data becomes available, these values could be

used to correct the first modal participation factor obtained for equipment analyzed as stand-alone and account approximately for the interaction effect of flexible connections.

Although these correction factors can be used if sufficient slackness is included so that no significant nonlinear interaction occurs between connected equipment, there is some limitations associated with these factors. The experiments were conducted with a somewhat narrow range of simulated equipment, and there are some assumptions embedded in the selection of masses for the simulated equipment. Also, transformer bushing mounting plate and/or gasket flexibility can lead to rocking of the bushing, which could change significantly its modal participation factor.

CONCLUSIONS

The computerized substation equipment database developed in this project allows centralizing the dynamic characteristics of substation equipment. This database includes in downloadable Excel format all the data collected for the 283 equipment items included at the time of writing. The database is accessible from the Internet at: http://seismic.ucsd.edu/peer/substation.html. The database contains two search tools: a search by equipment category and a search by voltage range. Also, the database allows the insertion of new equipment items.

Based on the data collected in the database, a preliminary correlative study was performed in order to estimate the relationships between the various dynamic characteristics of substation equipment. Based on the results of this study, the following trends were observed:

- The range of natural frequencies for substation equipment (under 1 Hz to above 20 Hz) is large. Also, significant scatters in the data were observed.
- The fundamental frequency of substation equipment tends to reduce with an increase of equipment voltage.
- The lighter transformer bushings exhibit the highest fundamental frequencies for the whole range of voltage. Conversely, the lowest natural frequencies occur for the much heavier circuit breakers.
- The first modal damping ratios of substation equipment did no exhibit any correlation with the voltage range. The mean damping ratio from the available data is 3% of critical.
- The first modal participation factor of substation equipment did no exhibit any correlation with the voltage range. The mean modal participation factor from the available data is 1.3.

The quasi-static tests conducted on two different flexible conductors in this project have provided an opportunity to evaluate the flexural properties of flexible conductors to use for seismic analyses on interconnected substation equipment. Based on the results of these quasi-static tests, the following conclusions can be drawn:

- The global behavior of both conductors was linear-elastic with negligible hysteretic response.

- For most combinations of axial tension and lateral conductor displacement, the flexural stiffness exhibited by both conductors is very small and tends toward the minimum possible flexural stiffness, corresponding to the situation where all the strands are slipping past each other and are unable able to transfer any shear force.
- Only for very large axial tension values (more than 1000 lbs or 100 με) that the flexural stiffness of the conductors approach the maximum possible flexural stiffness, corresponding to the situation where all the strands are able to transfer the longitudinal shear forces over one another and the conductor section acts as a solid cross-section. It is unlikely that such high axial tension values can be mobilized during the seismic response of interconnected substation electrical equipment.
- Based on the experimental results obtained, the value of the effective flexural stiffness of flexible conductor recommended by the IEEE-P1527/D5 Standard (Institute of Electrical and Electronics Engineers, 1998) appears reasonable.

Based on the results of the shake table tests performed on five different pairs of generic equipment connected by three different types of flexible connector assemblies, the following conclusions can be drawn:

- For all tests at 5 and 10% slackness, the fundamental frequencies of the equipment items were not affected significantly by the presence of the flexible conductor assemblies. In fact, the coupled fundamental frequency of each equipment item was reduced slightly when a conductor assembly was introduced. This reduction in fundamental frequency can be attributed to the added mass of the conductors on both interconnected equipment.
- The change in fundamental frequencies was not as consistent for the tests at 2% slackness. For these tests, the behavior of the interconnected equipment was nonlinear and depended heavily on the excitation amplitude of the random white noise input signal. For low amplitudes, the behavior was uncoupled and similar to the 5 and 10% slackness tests. When the amplitudes increased, the slackness in the conductor was taken up, and the conductor became very taut and transmitted axial vibrations between the interconnected equipment.
- The presence of the conductor assemblies increased significantly the damping ratios of interconnected equipment.

- No damage to any of the three flexible conductors was observed during all the seismic tests conducted.
- Two different types of dynamic responses were observed during the seismic tests. The first type involves low interaction between the interconnected equipment due to a large slack (5 and 10%) and/or under low intensity ground motions. For this case, very different frequency contents between the relative displacement, absolute acceleration, and force response of each equipment item was observed. Also, the absolute vertical acceleration at mid-span of the connector was in phase with the absolute horizontal acceleration at the top of the flexible equipment A. This result indicates that the large horizontal movement of the flexible Equipment A was transferred almost entirely into a vertical motion of the conductor with little transmission to the rigid Equipment B.
- The second type of dynamic response involves high interaction between the interconnected equipment due to a small slack (2%) and/or under high intensity ground motions. For this case, large vertical acceleration pulses (above 10 g) were observed at mid-span of the conductor. These pulses induced peak horizontal forces simultaneously at both ends of the conductor.
- For all slackness values, the dynamic response of the flexible Equipment A is not affected very much by any of the three flexible conductors tested.
- At 5 and 10% slackness, the dynamic response of the rigid Equipment B is generally reduced by the presence of the conductor assemblies.
- At 5 and 10% slackness, the forces generated at the top of the interconnected equipment are small. In most cases, the force at the top of the flexible Equipment A is larger than the force at the top of the stiff Equipment B.
- At 2% slackness, the dynamic response of the rigid Equipment B can be significantly increased once the conductor assemblies become tight and act as tension-only springs. This amplification of the dynamic response increases with the intensity of the ground motion.
- At 2% slackness, the forces generated at the top of the interconnected equipment are an order of magnitude higher that that measured at 5 and 10% slackness. For this slackness, the forces at the top of both interconnected equipment specimens are similar.

The influence of flexible connection on the stand-alone modal participation factor was also investigated through the shake table tests. When sufficient slack was provided so that no nonlinear interaction effects occurred, it was observed that, in general, the stand-alone modal-participation factor was lower in the presence of the flexible conductor. It was also found that the equipment's first natural frequency in such conditions was not modified substantially. An average correction factor of 0.90 was obtained for the stand-alone modal-participation factor of the low-frequency equipment of the pair tested, while an average value of 0.75 was obtained for the higher-frequency equipment.

REFERENCES

Abrahamson, N., (1997). Personal Communication.

Applied Technology Council (1992). "Guidelines for Cyclic Seismic Testing of Components of Steel Structures", ATC-24, Redwood City, CA.

Benuska, L., Technical Editor (1990). "Loma Prieta Earthquake Reconnaissance Report", Earthquake Spectra, Supplement to Volume 6, Earthquake Engineering Research Institute, Oakland, CA.

Clough, R.W., and Penzien, J. (1993). "Dynamics of Structures", Second Edition, McGraw-Hill, New York.

Dastous, J-B, Filiatrault, A., and Pierre, J-R. (2002) "Estimation of Displacement at Interconnection Point of Substation Equipment Subjected to Earthquakes", IEEE Transactions on Power Delivery, (under review).

Der Kiureghian, A., Sackman, J.L., and Hong, K.J. (1999). "Interaction in Interconnected Electrical Substation Equipment Subjected to Earthquake Ground Motions", Report PEER 1999/01, Pacific Earthquake Engineering Research Center, University of California, Berkeley, Berkeley, CA.

Experimental Dynamic Investigations. (1993). "U2 & V2 Manual", Vancouver, Canada

Filiatrault, A., Tremblay, R., Thoen, B.K. and Rood, J. (1996). "A Second Generation Earthquake Simulation System in Canada: Description and Performance Evaluation", 11th World Conference on Earthquake Engineering, Acapulco, Mexico, Paper # 1204 on CD ROM.

Filiatrault, A., Kremmidas, S., Elgamal, A. and Seible, F. (1999). "Substation Equipment Interaction – Rigid and Flexible Conductor Studies", Structural Systems Research Project Report No. SSRP-99/09, Department of Structural Engineering, University of California, San Diego, La Jolla, CA, 218 p.

Filiatrault, A. and Kremmidas, S. (2000). "Seismic Interaction Between Components of Electrical Substation Equipment Interconnected by Rigid Bus Conductors", ASCE Journal of Structural Engineering, 126(10), 1140-1149.

Filiatrault, A., Kremmidas, S., Seible, F., Clark, A.J., Nowak, R., and Thoen, B.K. (2000). "Upgrade of First Generation Uniaxial Seismic Simulation System with Second Generation Real-Time Three-Variable Digital Control System", 12th World Conference on Earthquake Engineering, Auckland, New Zealand, Paper No. 1674, on CD-ROM.

Hall, J., Technical Editor (1995). "Northridge Earthquake of January 17, 1994 Reconnaissance Report Volume 1 ", Earthquake Spectra, Supplement to Volume 11, Earthquake Engineering Research Institute, Oakland, CA.

Institute of Electrical and Electronics Engineers. 1997. "Recommended Practices for Seismic Design of Substations", IEEE-693 Standard, IEEE Standards Dept., Piscataway, NJ.

Institute of Electrical and Electronics Engineers. 1998. "Recommended Practice for the Design of Flexible Buswork Located in Seismically Active Area", IEEE-P1527/D5 Standard, IEEE Standards Dept., Piscataway, NJ.

APPENDIX A. SUBSTATION EQUIPMENT DATABASE

APPENDIX B. SHOP DRAWINGS OF GENERIC EQUIPMENT SPECIMENS

APPENDIX C. RESULTS OF FREQUENCY EVALUATION TESTS

APPENDIX D. RESULTS OF DAMPING EVALUATION TESTS

APPENDIX E. RESULTS OF SEISMIC TESTS